PLASMA DYNAMICS

IX. PLASMA DYNAMICS

Academic and Research Staff

Prof. William P. Allis
Prof. Abraham Bers
Prof. George Bekefi
Prof. Sanborn C. Brown
Prof. Sow-Hsin Chen
Prof. Bruno Coppi
Prof. Thomas H. Dupree
Prof. E. Victor George
Prof. Elias P. Gyftopoulos
Prof. Hermann A. Haus
Prof. Lawrence M. Lidsky
Prof. James E. McCune
Prof. Peter A. Politzer
Prof. Dieter J. Sigmar
Prof. Louis D. Smullin
Prof. Robert J. Taylor
Dr. Edward G. Apgar
Dr. Giuseppe F. Bosia
Dr. Philippe Brossier
Dr. Bert C. J. M. De Kock
Dr. Bernard J. Meddens
Dr. D. Bruce Montgomery*
Dr. Lodewyk T. M. Ornstein
Dr. Ronald R. Parker
Dr. Arthur H. M. Ross
Dr. Tiete J. Schep
Dr. Piet van der Laan
John J. McCarthy
William J. Mulligan

Graduate Students

Eugene L. Bernstein
Charles T. Breuer
Leslie Bromberg
Natale M. Ceglio
Frank W. Chambers
Tsi-Pin Choong
Wing-Shek Chow
Paul W. Chrisman, Jr.
Donald L. Cook
David A. Ehst
Nathaniel J. Fisch
Alan R. Forbes
Ricardo M. O. Galvão
Keith C. Garel
Jeffry Golden
Richard J. Hawryluk
Ady Hershcovitch
Steven P. Hirshman
James C. Hsia
Donald P. Hutchinson
Saeed Z. Jabbawy
Charles F. F. Karney
David S. Komm
John L. Kulp, Jr.
Ping Lee
Yongyut Manichaikul
Paul M. Margosian
François Martin
John L. Miller
Paul E. Morgan
Michael R. Murphy
Thaddeus Orzechowski
David O. Overskei
Aniket Pant
Gerald D. Pine
Robert H. Price
Charles A. Primmerman
Donald Prosnitz
Gregory Rewoldt
Paul A. Roth
Mario Simonutti
Miloslav S. Tekula
David J. Tetrault
Alan E. Throop
Marcio L. Vianna
Bruce V. Waddell
Duncan C. Watson
Charles W. Werner
David M. Wildman
Stephen M. Wolfe

*Dr. D. Bruce Montgomery is at the Francis Bitter National Magnet Laboratory.

IX. PLASMA DYNAMICS

A. Laser-Plasma Interactions

1. TWO- AND THREE-DIMENSIONAL STABILITY ANALYSIS FOR SECOND-ORDER LASER-PLASMA INTERACTIONS

National Science Foundation (Grant GK-37979X)

Frank W. Chambers, Abraham Bers

The theory for pinch-point time asymptotic three-dimensional pulse-shape analysis discussed in Quarterly Progress Report No. 111 (pp. 31-37) and also in Section IX-D. 2 has been applied to five different nonlinear interactions with parameters appropriate to the laser-pellet interaction problem. These five interactions are Raman (EM → EM + EP), Brillouin (EM → EM + IA), two-plasmon (EM → EP + EP), plasmon-phonon (EM → EP + IA), and nonoscillatory (EM + EM → EP + EP). The coupling coefficient γ, which would correspond to the maximum growth rate in time with no damping, is given for each interaction in Table IX-1. The interactions have been divided into two groups: transverse, which include one electromagnetic wave in the decay products, and longitudinal, in which both decay waves are electrostatic. The basic derivation of these coefficients has been given elsewhere[1, 2] (see also Sec. IX-D. 3). In Table IX-1 the three-dimensional aspect of the couplings is included in the vector dot and cross products. Calculations were carried out in the two-dimensional plane which maximized the coupling. The laser electric field is assumed to be linearly polarized with $\vec{E}$ along the $\hat{z}$ axis and to propagate in the $\hat{x}$ direction. The coupling is maximum for the transverse interactions when the decay waves are in the x-y plane; for longitudinal interactions the coupling is maximum when the decay waves are in the x-z plane. Our results will be presented as contour plots of the growth rate s_{oi} vs observer velocity $\vec{V}$ in the two-dimensional plane of maximum response (see Quarterly Progress Report No. 111, pp. 31-37, and also Sec. IX-D. 2).

Formulas and references for group velocities and dampings of waves $\vec{v}_{gi}(\vec{k}_i)$ and $\gamma_i(k_i)$ are listed in Table IX-2. The real dispersion relation is used to calculate group velocities and to relate ω and $\vec{k}$ for frequency and wave number matching. The group velocities and dampings are calculated under the assumption that real $\vec{k}$ and ω satisfy the matching conditions.

Calculations were performed for a neodymium laser incident on a deuterium pellet with parameters from Nuckolls, Emmett, and Wood.[3] The plasma density was taken to be some fraction of the critical density for neodymium 1.06 μm light which is $n_c = 10^{21}/cm^3$. The electron temperature was always taken as 1 keV. For laser power the level 10^{15} W/cm^2 was chosen because it is a realistic intensity for a focused neodymium laser. Furthermore, the instabilities considered turn out to be weakly unstable

Table IX-1. Nonlinear interactions with their coupling coefficients.

$$v_{Te} = \frac{K_B T_e}{m_e} \qquad c_s = \frac{K_B T_e + 3K_B T_i}{M_i} \qquad v_L = \frac{eE_L}{m_e \omega_L}$$

Interaction 1 → 2 + 3	Locus	γ^2 = Coupling Coefficient Squared
	Transverse	
EM → EM + EP Raman	$\frac{1}{4}$ Critical	$\gamma^2 = \dfrac{v_L^2 \omega_{pe} k_3^2 \lvert \vec{k}_2 \times \vec{e}_1 \rvert^2}{16\, \omega_2 k_2^2}$
EM → EM + IA Brillouin	Critical	$\gamma^2 = \dfrac{v_L^2 \omega_{pe}^4 \omega_3 c_s^2 \lvert \vec{k}_2 \times \vec{e}_1 \rvert^2}{16\, \omega_{pe}^2 \omega_2 v_{Te}^2 k_2^2}$
	Longitudinal	
EM → EP + EP Two-plasmon	$\frac{1}{4}$ Critical	$\gamma^2 = \dfrac{v_L^2 \omega_{pe}^2}{16} \left\{ \dfrac{(\vec{k}_2 \cdot \vec{e}_1) k_3}{k_2 \omega_3} + \dfrac{(\vec{k}_3 \cdot \vec{e}_1) k_2}{k_3 \omega_2} \right\}^2$
EM → EP + IA Plasmon-Phonon	Critical	$\gamma^2 = \dfrac{v_L^2 \omega_{pe} \omega_3 m_e}{16\, M_i} \left\{ \dfrac{k_2 (\vec{k}_3 \cdot \vec{e}_1)}{\omega_2 k_3} + \dfrac{k_3 (\vec{k}_2 \cdot \vec{e}_1)}{\omega_3 k_2} \right\}^2$
EM + EM → EP + EP Nonoscillatory	Critical	$\gamma_o^2 = \left(\dfrac{v_L^2}{4 v_{Te}^2} \right)^2 \omega_{pe}^2 \left\{ \dfrac{(\vec{k}_2 \cdot \vec{e}_1)(\vec{k}_3 \cdot \vec{e}_1)\, k^2 c_s^2}{k_2 k_3 \left(\omega^2 - k^2 c_s^2 \right)} \right\}^2$ $\omega \equiv (\omega_2 - \omega_3)/2 \qquad \vec{k} \equiv (\vec{k}_2 - \vec{k}_3)/2$

Table IX-2. Dispersion relations used for $\omega, \vec{k}$ matching and wave damping.

Wave	Dispersion Relation	Damping Mechanism	Reference
EM	Electromagnetic Waves $\omega_r^2 = c^2k^2 + \omega_{pe}^2$ $\omega_i = -\nu_{ei} = -\dfrac{(\ln \Lambda/10)\, n_e(cm^{-3})}{3.5\ 10^4\ (T_e(eV))^{3/2}}$	Electron-Ion Collisions	4
EP	Electron Plasma Oscillations $\quad K \equiv k\lambda_D$ $\omega_r^2 = \omega_{pe}^2 + 3k^2v_{Te}^2$ $\omega_i = -\nu_{ei} - \nu_{eld}$ $\nu_{eld} = \begin{cases} \dfrac{\omega_{pe}}{(8\pi)^{1/2}} \dfrac{1}{K^3} \exp\left[\dfrac{-1}{2K^2}(1+3K^2+6K^4+24K^6+180K^8)\right] & K < .28 \\ \text{Use Fried-Conte Z Functions} & K > .28 \end{cases}$	Electron-Ion Collisions + Electron Landau Damping	5 6
IA	Ion-Acoustic Waves $\quad K \equiv k\lambda_D$ $\omega_r = c_s k \qquad c_s^2 = (K_B T_e + 3K_B T_i)/M_i$ $\omega_i = -\nu_{ii}/2 - \nu_{eld} - \nu_{ild}$ $\nu_{ii} = \dfrac{(\ln \Lambda/10)\, n_e(cm^{-3})}{3 \cdot 10^6\ (T_e(eV))^{3/2}}$ $\nu_{eld} = \omega_{pi}\left(\dfrac{\pi}{8}\right)^{1/2}\left(\dfrac{m_e}{M_i}\right)^{1/2} \dfrac{K}{(1+K^2)^2}$ $\nu_{ild} = \omega_{pi}\, e^{-3/2}\left(\dfrac{\pi}{8}\right)^{1/2}\left(\dfrac{T_e}{T_i}\right)^{3/2} \dfrac{K}{(1+K^2)^2} \exp\left\{\dfrac{-T_e}{2T_i} \dfrac{1}{(1+K^2)}\right\}$	Ion-Ion Collisions Electron Landau Damping Ion Landau Damping	4

Table IX-3. Parameters for calculations and results from plots in Figs. IX-1 and IX-2.

(T_e = 1 keV, T_i = 50 eV, P = 10^{15} W/cm^2 except as noted)					
Figure			(i)	(ii)	(iii)
1(a)	EM → EM + EP	n/n_c	.016	.063	.191
	Raman	ω_{pe}/ω_L	.125	.250	.4375
		$s_{oi}^{max}(10^{-3}\ \omega_L)$	1.76	5.63	7.81
		$k\lambda_D$	.657	.296	.126
1(b)	EM → EM + IA	n/n_c	.010	.563	.563
	Brillouin	ω_{pe}/ω_L	.100	.750	.750
		$s_{oi}^{max}(10^{-3}\ \omega_L)$	.029	.236	4.00
		P (W/cm^2)	10^{13}	10^{13}	10^{15}
		T_i (eV)	125.	50.	50.
		$k\lambda_D$	.088	.078	.078
2(a)	EM → EP + EP	n/n_c	.203	.214	.226
	Two-plasmon	ω_{pe}/ω_L	.450	.4625	.475
		$s_{oi}^{max}(10^{-3}\ \omega_L)$	2.08	4.57	5.55
		$k\lambda_D$	.312	.271	.224
2(b)	EM → EP + IA	n/n_c	.810	.856	.951
	Plasmon-Phonon	ω_{pe}/ω_L	.900	.925	.975
		$s_{oi}^{max}\left(10^{-3}\ \omega_L\right)$	5.95	8.27	6.61
		$k\lambda_D$	.280	.227	.125
2(c)	EM + EM → EP + EP	n/n_c	.980	.983	.990
	Nonoscillatory	ω_{pe}/ω_L	.990	.991	.995
		$s_{oi}^{max}\left(10^{-3}\ \omega_L\right)$	–	25.3	25.4
		$k\lambda_D$	.088	.082	.062

at this power level so that this theory gives meaningful results. The results can be scaled approximately to other laser wavelengths and densities, provided (n/n_c) and $k_l\lambda_d$ are held constant. This scaling is valid for the coupling coefficients and Landau dampings, but not for collisional damping, which is usually unimportant.

The calculated pulse response shape depends primarily on three variables; the laser polarization, the coupling coefficient, and the wave dampings.

We consider first the transverse interactions, Raman and Brillouin scattering, illustrated in Fig. IX-1. Note that the V_x-V_y plane is displayed and the maximum observer velocity is c, which is necessary because of the electromagnetic decay products. Parameters and numerical results for the plots in Figs. IX-1 and IX-2 are given in

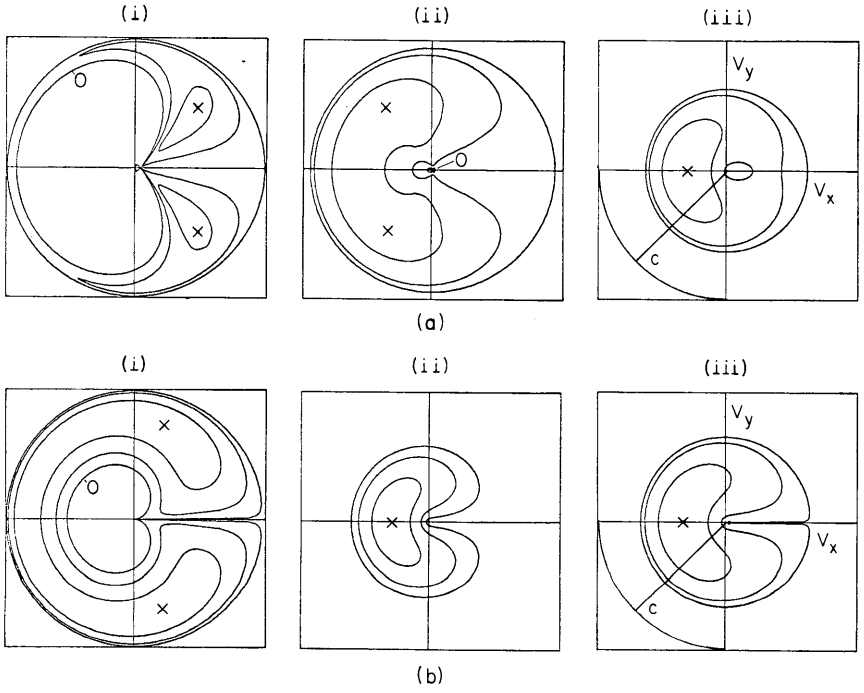

Fig. IX-1. Two-dimensional contour plots of the pulse response in the V_x-V_y plane vs observer velocity for transverse interactions. The laser pump is incident in the x direction and plane polarized in the z direction. (a) Raman EM → EM + EP. (b) Brillouin EM → EM + IA.

Table IX-3. In (iii) of Fig. IX-1a we have plotted contours of 0, 40%, and 80% of the maximum growth s_{oi}^{max}, which is 7.81×10^{-3} times the laser frequency and occurs at the velocity marked "X". The outermost contour represents marginal stability. The next concentric contour and the contour that encircles the origin are 40% contours, the closed kidney-shaped contour is the 80% contour. From Table IX-3, for this case

$k\lambda_D = .126$ and Landau damping is negligible; the pulse response is essentially that for the undamped case. Here the response is determined primarily by the coupling coefficient, which depends on the magnitude of the plasma oscillation wavevector k_3. This vector is a maximum when the second electromagnetic wave is at 180° with respect to the laser, hence the maximum scatter in the backward direction. As the density is increased the $\vec{k}_2$ wavevector of the electromagnetic decay wave decreases. This causes the maximum velocity of the pulse response to decrease. Furthermore, since $k_3 = k_1 \mp k_2$ in forward and backward scattering, as k_2 becomes small the forward and backward coupling coefficients for the pulse response nearly become equal. In fact, as we near 1/4 critical density the pattern shown in (iii) in Fig. IX-1a will become nearly circularly symmetric.

As we decrease the density, λ_D increases and Landau damping becomes important. In (i) and (ii) in Fig. IX-1a backscattering is being suppressed by Landau damping so that primary scatter occurs at the sides or in the forward direction. Note from Table IX-3 that there is a corresponding decrease in the maximum growth rate.

The Brillouin interaction, Fig. IX-1b, is similar to the Raman interaction in the undamped case, since the coupling coefficient goes as $k_3^{1/2}$. (Note in Table IX-1 that $\gamma^2 \sim \omega_3 \sim k_3 c_s$.) In (iii) in Fig. IX-1b the instability is absolute, the origin in the V_x-V_y plane is enclosed by the zero growth-rate contour and has a finite growth rate. In (ii) in Fig. IX-1b the power has been reduced by a factor of 100; now the origin is no longer enclosed, and the instability is convective. Finally, at low power and far out in density the effects of damping are apparent in (i) in Fig. IX-1b; again the damping has the largest effect in the backward direction where k_3 is largest.

Next, we consider the longitudinal interactions in Fig. IX-2, which displays the V_x-V_z plane, and the maximum observer velocity is v_{Te}. The two-plasmon instability is illustrated in Fig. IX-2a. In (iii) in Fig. IX-2a where the effects of damping are unimportant ($k_3\lambda_D < .25$), the shape of the pulse is entirely determined by the angular dependence of the coupling coefficient (see Table IX-1). The zeros along V_x occur because there is no coupling in the case of collinear wavevectors; this is true of all longitudinal interactions. There is also a zero where $\vec{k}_2$ and $\vec{k}_3$ form an equilateral triangle with $\vec{k}_1$. In this case where damping is negligible the maximum growth for any direction of $\vec{v}_{g2}$ occurs at observer velocity $\vec{V} = (\vec{v}_{g2}+\vec{v}_{g3})/2$ (Quarterly Progress Report No. 111, see Eq. 15, p. 34), for plasma oscillations $\vec{v}_g \simeq 3\vec{k}\lambda_D v_{Te}$. Consequently, $\vec{V} = 3\lambda_D v_{Te}(\vec{k}_2+\vec{k}_3)/2 = 3\vec{k}_1\lambda_D v_{Te}/2$. This velocity corresponds to the group velocity of a plasma oscillation with a wavevector $\vec{k}_1/2$. Thus the cloverleaf pattern is centered about this velocity, and it is here that the maximum growth occurs. In fact, the growth rate at this velocity is multivalued, since the response for any direction of $\vec{k}_2$ will include this point. Moving slightly away from 1/4 critical density ((i) and (ii) in

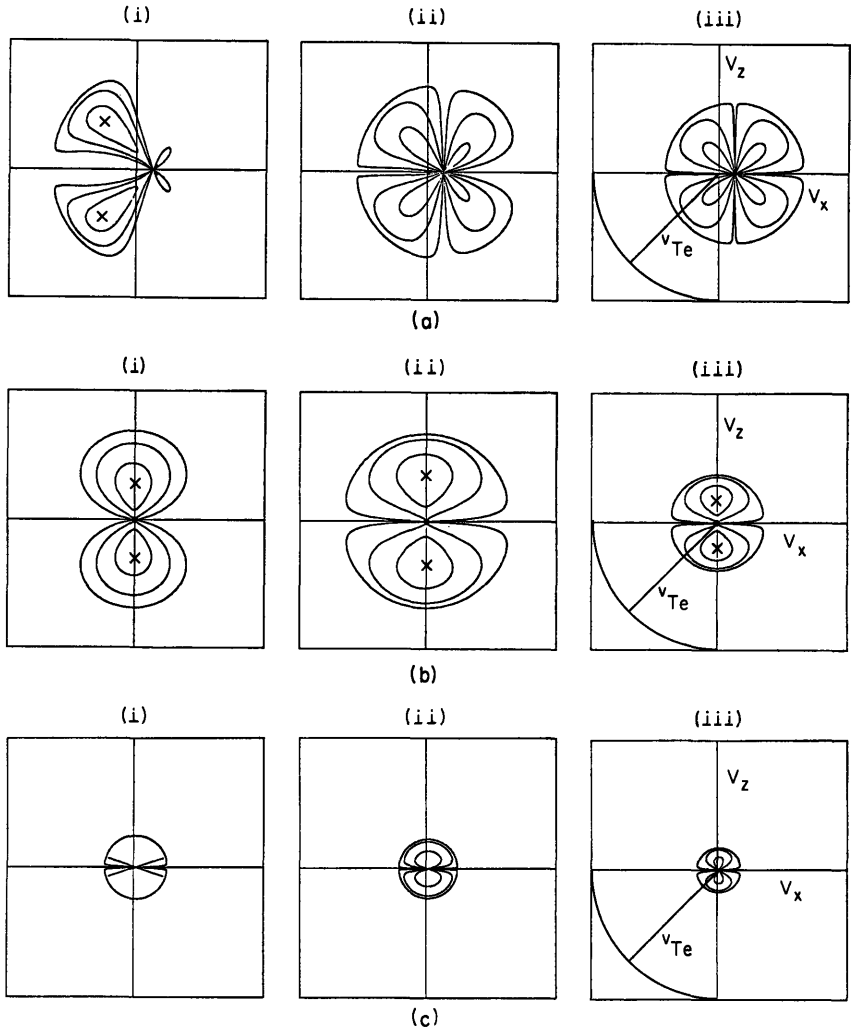

Fig. IX-2. Two-dimensional contour plots of the pulse response in the V_x-V_z plane vs observer velocity for longitudinal interactions. The laser pump is incident in the x direction and plane polarized in the z direction. (a) Two-plasmon EM → EM + EP. (b) Plasmon-phonon EM → EP + IA. (c) Nonoscillatory EM + EM → EP + EP.

Fig. IX-2a) results in a large increase in the $\vec{k}_{2,3}$ vectors to achieve matching, hence Landau damping becomes important. Since the forward-going wave always has the slightly longer wavevector, it is suppressed first, and the result is the lopsided pattern shown in (i) in Fig. IX-2a.

Similarly the plasmon-phonon instability pulse response (Fig. IX-2b) illustrates the effects of coupling coefficient and damping. As ω_{pe} decreases in order to ω match, $\vec{k}_3$ must be increased. At first as the coupling coefficient that goes as $\omega_3 = c_s k_3$ (see Table IX-I) increases the growth rate increases (see (ii) in Fig. IX-2b). As one

moves further from the critical surface, however, the longitudinal wavevector magnitudes further increase and Landau damping becomes important. Then, as seen in (i) in Fig. IX-2b and in Table IX-3, the growth rate again decreases.

Finally, we have included the nonoscillatory instability in Fig. IX-2c. This is actually a four-wave coupling and it requires the inclusion of third-order conductivity, hence the v_L^4 in the coupling coefficient. To look at it another way, the pump enters twice, thereby coupling the two plasma waves (see Watson and Bers, Sec. IX-D. 3).

This coupling relies on the proximity of the ion-acoustic resonance as seen from the $\omega^2 - k^2 c_s^2$ term in the denominator of the coupling coefficient. All calculations for this instability have been carried out very near the critical surface. The two-dimensional response has a zero in the collinear case and is maximum at nearly 90°. From similar arguments, as with the two-plasmon interaction, the maximum growth is on the V_x axis at $V_x = v_{gEP}(k_1)$. Note the large growth rates, which clearly exceed the acoustic frequency, which indicates that our weak-coupling assumption is not valid. Note also in (i) in Fig. IX-2c that the ion-acoustic wave comes exactly into resonance for $\phi = 20°$. The theory has broken down dramatically because we have used only the real parts of ω and $\vec{k}$ in calculating the ion-acoustic dispersion relation. This instability requires a more accurate treatment, as discussed in Section IX-A. 2.

Thus far, results have been presented in two dimensions. The extension to three dimensions is straightforward but not trivial. The three-dimensional response differs markedly for the longitudinal and transverse interactions. The longitudinal interactions rely on the laser electric field to drive the electric field of the decay product; hence, when the component of $\vec{E}_1$ along, say, $\vec{k}_2$ vanishes there is no interaction. Thus in Fig. IX-2 the growth rate along V_x is always zero. For these interactions we have illustrated the V_x-V_z plane where the interaction is maximum. In the V_x-V_y plane the coupling coefficient vanishes. As β, the angle between the k plane under consideration and $\vec{E}_1$, is rotated (see Fig. IX-3) the coupling varies as $\cos^2 \beta$ and the pulse response in three dimensions is simply a figure of rotation about the V_x axis with the coupling coefficient reduced by $\cos^2 \beta$ for the various β. This is illustrated in Fig. IX-4a. For transverse interactions we must again have $\vec{E}_1 \cdot \vec{E}_2 \neq 0$, but now the situation is not so simple. The coupling depends not only on the β orientation of the plane in which we are calculating with respect to $\vec{E}_1$ but also on the angle ϕ of the $\vec{k}_2$ in this plane with respect to the $\vec{k}_1$. The angular dependence cannot be separated into a simple dependence on β times a dependence on ϕ, as was possible for the longitudinal case. The general description of transverse interactions in three dimensions is not a simple figure of rotation; however, we can simplify matters in certain planes where ϕ and θ, the angle in the vector cross product, are simply related. Specifically, we can calculate in the Cartesian planes:

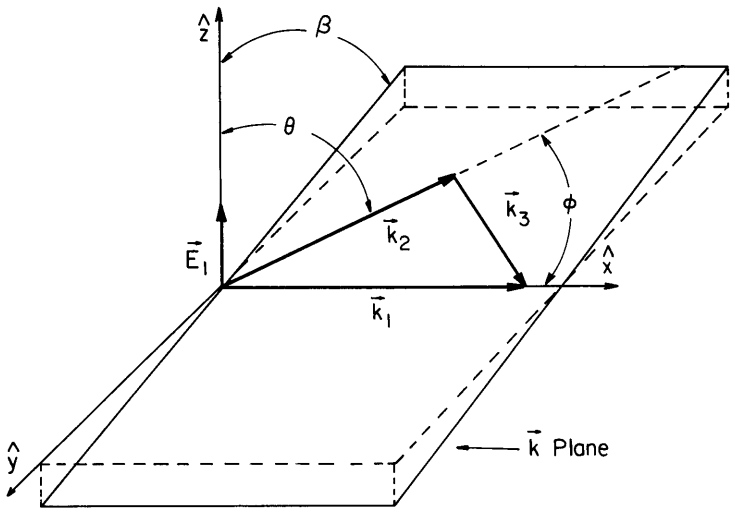

Fig. IX-3. Illustration of the important angles in the three-dimensional problem. β is the angle between $\vec{E}_1$ and a vector common to both the k and y-z planes; ϕ is the angle between $\vec{k}_2$ and $\vec{k}_1$ in the k plane; θ is the angle between $\vec{k}_2$ and $\vec{E}_1$. Only two of these angles are independent but in general they are not simply related.

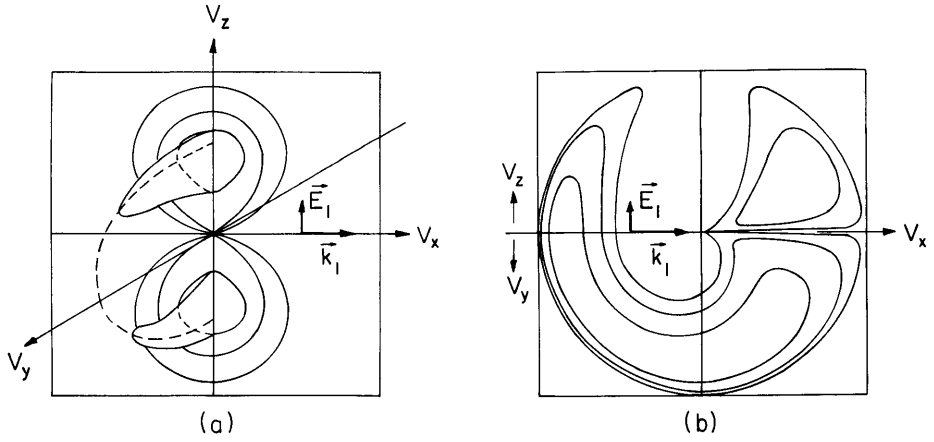

Fig. IX-4. Pulse response in three dimensions for (a) longitudinal and (b) transverse interaction.

V_y-V_z $\quad \phi \cong 90°$, θ varies

V_x-V_z $\quad \phi = 90° - \theta$

V_x-V_y $\quad \phi$ varies, $\theta = 90°$

Figure IX-4b gives the response in the V_x-V_y and V_x-V_z planes for the parameters in (i) in Fig. IX-1b. The lower half of Fig. IX-4b is the V_x-V_y plane response, the upper half the V_x-V_z plane; to visualize the interaction in three dimensions, we can fold this figure at right angles along the V_x axis.

There are several important limitations on the results that we have presented. Some concern the accuracy of the theory and others the applicability of this model to the finite, inhomogeneous laser-pellet plasma. In solving the homogeneous problem we have used second-order conductivity (except in the case of the nonoscillatory instability) and we have approximated the dispersion relations of the decay products as straight lines. In finding pinch points for the inverse Fourier-Laplace transform this is equivalent to assuming a perturbation about ω_r and k_r for the intersecting dispersion relations; hence, our theory is probably only valid for small growth rates. For example, in the nonoscillatory instability we have calculated growth rates that clearly exceed the acoustic frequency, hence these results violate the small growth-rate assumption. This particular instability has been investigated in greater detail (see Sec. IX-A. 2). Investigations of the other four instabilities including third-order conductivity and more accurate approximations to the dispersion relations have shown that at the power of 10^{15} W/cm^2 they are adequately described by this linearized theory.

We must also examine the applicability of this theory to the laser-pellet plasma. Our approach thus far has been to calculate the pulse response locally at different points along the density gradient. We must investigate the criteria for this localization to be valid. There are several effects to be considered. A mismatch in $\vec{k}$ or ω can be introduced by density variations or by a temperature variation; this mismatch will occur over characteristic lengths. Damping may limit an interaction to a finite region of still another scale length. We may also be limited by the finite width of the laser beam. We can calculate which of these lengths is the limiting factor for a given interaction. Knowing the pulse propagation velocity, we can determine the length of time the pulse spends in this region. Then, knowing the homogeneous growth rate, we can calculate the number of e-foldings that the pulse undergoes in this region. The condition for localization is simply that the pulse e-folds several times before propagating out of the interaction region. Note that for the transverse interactions whose pulse velocities are fractions of c this criterion is more severe than for longitudinal interactions where velocities are closer to v_{Te}. This condition on the growth rate can be related in turn to a condition on the power, thereby giving a localization threshold. Considering the

Raman instability, mismatch will be introduced by the changing plasma frequency. This will limit the growth of the instability. The case in which mismatch is the important factor has been solved by Rosenbluth.[7] For the two-plasmon interaction, mismatch is no longer important, the oppositely propagating plasmons cancel the mismatch that they introduce. The damping increases dramatically, however, as we move away from 1/4 critical density, hence there must be significant growth before the pulse propagates into the highly damped regions. In the parametric interaction the maximum scattering is at 90° where the density gradient has little effect. But the finite laser beamwidth and spherical shape of the pellet can become the limiting factors.

In conclusion, at the power level 10^{15} W/cm^2 the assumption of localization is good for gaining an understanding of the three-dimensional three-wave interactions, but more accurate models for the interaction and plasma may be required to account for effects that thus far we have ignored. Finally, it must be remarked that the detailed consequences of these interactions, with regard to both backscattering and plasma heating, must be determined from the nonlinear and/or turbulent evolution of these instabilities.

References

1. A. Bers, Notes on Lectures: Linear Waves and Instabilities, given at Ecole d'Eté de Physique Théorique, Les Houches, France, July 1972 (Gordon and Breach, New York, in press).
2. F. W. Chambers, R. J. Hawryluk, and A. Bers, Quarterly Progress Report No. 110, Research Laboratory of Electronics, M. I. T., July 15, 1973, pp. 45-55.
3. J. Nuckolls, J. Emmett, and L. Wood, "Laser Induced Thermonuclear Fusion," Phys. Today, Vol. 26, No. 8, p. 46, August 1973.
4. S. I. Braginskii, "Transport Processes in a Plasma," Reviews of Plasma Physics, Vol. 1 (Consultants Bureau, New York, 1965), p. 215.
5. J. Canosa, "Asymptotic Solution of Landau's Dispersion Equation," Phys. Fluids 15, 1536 (1972).
6. M. A. Lieberman, Quarterly Progress Report No. 77, Research Laboratory of Electronics, M. I. T., April 15, 1965, pp. 141-143.
7. M. N. Rosenbluth, R. B. White, and C. S. Liu, "Temporal Evolution of a Three-Wave Parametric Instability," Phys. Rev. Letters 31, 1190 (1973).

2. THREE-DIMENSIONAL DISPERSION RELATIONS FOR THIRD-ORDER LASER-PLASMA INTERACTIONS

National Science Foundation (Grant GK-37979X)

Duncan C. Watson, Abraham Bers

Introduction

We shall use the theory of coherent wave coupling in three dimensions presented in Section IX-D.3 to give a unified description of the following instabilities: plasmon-phonon,[1] modified plasmon-phonon,[2] nonoscillatory,[3] modified nonoscillatory,[4] Raman,[5] modified Raman,[6] Brillouin, modified Brillouin,[6] two-plasmon,[7] coalesced Raman and plasmon-plasmon,[8] and coalesced plasmon-phonon and nonoscillatory. The stability analysis for the unmodified interactions is discussed in Section IX-A.1 and has also been reported elsewhere.[9] The stability analysis for modified instabilities is carried out to the extent of finding one-dimensional cross sections of the corresponding pulse shapes. These cross sections are taken in directions for which the unmodified instabilities have the maximum growth rates and the effect of modification on the pulse shape is most pronounced. We shall show that at high pump powers the plasmon-phonon and nonoscillatory instabilities lead to a single coalesced unstable pulse.

Three-Dimensional Dispersion Relations

Consider the unmodified plasmon-phonon instability, which occurs when $(K)_S$ and $(K_-)_S$ are small (see Sec. IX-D.3, Eq. 28). From Section IX-D.3, Eq. 29, taking only the electron contributions to the nonlinear currents, we find

$$\left(1-\frac{\omega_{pe}^2}{\omega^2-\gamma_e k^2 v_{Te}^2}-\frac{\omega_{pi}^2}{\omega^2-\gamma_i k^2 v_{Ti}^2}\right)\left(1-\frac{\omega_{pe}^2}{\omega_-^2-\gamma_e k_-^2 v_{Te}^2}-\frac{\omega_{pi}^2}{\omega_-^2-\gamma_i k_-^2 v_{Ti}^2}\right)$$

$$=\frac{|v_{Le}^2|}{v_{Te}^2}\,\omega_{pe}^4\left[\frac{(\vec{e}_{s-}\cdot\vec{e}_L)\omega_- kv_{Te}+k_- v_{Te}\omega(\vec{e}_s\cdot\vec{e}_L)}{\left(\omega^2-\gamma_e k^2 v_{Te}^2\right)\left(\omega_-^2-\gamma_e k_-^2 v_{Te}^2\right)}\right]^2 \qquad (1)$$

Consider the neighborhood of a point $(\vec{k},\omega)\equiv(\vec{k}_{IA},\omega_{IA})$ where the hypersurfaces $(K)_S = 0$, $(K_-)_S = 0$ intersect and so the corresponding $(\vec{k}_-,\omega_-)\equiv(\vec{k}_{BG},-\omega_{BG})$. Choose the values of γ_e, γ_i in (1) to agree with the results of Vlasov theory and use the fact that $|\omega_{BG}/k_{BG}| \gg v_{Te} \gg |\omega_{IA}/k_{IA}|$. Then

$$\frac{1}{k^2\lambda_{De}^2}\left(1-\frac{k^2c_s^2}{\omega^2}\right)\left(1-\frac{\omega_p^2}{\omega_-^2-3k_-^2v_T^2}\right)\cong\frac{|v_L^2|}{v_T^2}\,\frac{\omega_p^4\omega_-^2k^2v_T^2(\vec{e}_{s-}\cdot\vec{e}_L)^2}{k^4v_T^4\left(\omega_-^2-3k_-^2v_T^2\right)^2}. \tag{2}$$

Expanding about $(\vec{k}_{IA}, \omega_{IA})$ to first order in $\Delta\vec{k}, \Delta\omega$, we have

Three-dimensional Unmodified Plasmon-Phonon Instability:

$$\left(\Delta\omega-\vec{v}_g^{IA}\cdot\Delta\vec{k}\right)\left(\Delta\omega+\vec{v}_g^{BG}\cdot\Delta\vec{k}\right)\cong-\frac{v_{LASER}^2}{16\,v_T^2}\,\omega_{BG}\omega_{IA}(\vec{e}_{BG}\cdot\vec{e}_L)^2, \tag{3}$$

where

$$v_o\equiv v_L\exp(ik_Lz-i\omega_Lt)+\text{complex conjugate}$$

$$\equiv v_{LASER}\cos(k_Lz-\omega_Lt+\phi) \qquad \therefore\ v_{LASER}=2|v_L|. \tag{4}$$

Equation 1 is also appropriate for the unmodified plasmon-plasmon instability. Consider the neighborhood of a point $(\vec{k}, \omega) \equiv (\vec{k}_{BG'}, \omega_{BG'})$ where the hypersurfaces $(K)_S = 0$, $(K_-)_S = 0$ intersect, and let the corresponding $(\vec{k}_-, \omega_-) \equiv (\vec{k}_{BG}, -\omega_{BG})$. Use the fact that $|\omega_{BG}/k_{BG}|$, $|\omega_{BG'}/k_{BG'}| \gg v_{Te}$. Then

$$\left(1-\frac{\omega_p^2}{\omega^2-3k^2v_T^2}\right)\left(1-\frac{\omega_p^2}{\omega_-^2-3k_-^2v_T^2}\right)=\frac{|v_L^2|}{v_T^2}\cdot\omega_p^4\,\frac{\left[(\vec{e}_{s-}\cdot\vec{e}_L)\omega_-k+k_-\omega(\vec{e}_s\cdot\vec{e}_L)\right]^2}{\left(\omega^2-3k^2v_T^2\right)^2\left(\omega_-^2-3k_-^2v_T^2\right)^2}\,v_T^2. \tag{5}$$

Expanding about $(\vec{k}_{BG'}, \omega_{BG'})$ to first order in $\Delta\vec{k}, \Delta\omega$, we have

Three-dimensional Plasmon-Plasmon Instability:

$$\left(\Delta\omega-\vec{v}_g^{BG'}\cdot\Delta\vec{k}\right)\left(\Delta\omega+\vec{v}_g^{BG}\cdot\Delta\vec{k}\right)\cong-\frac{v_{LASER}^2}{16}\left[-\frac{(\vec{e}_{BG}\cdot\vec{e}_L)}{v_{ph}^{BG'}}+\frac{(\vec{e}_{BG'}\cdot\vec{e}_L)}{v_{ph}^{BG}}\right]^2\omega_{BG}\omega_{BG'}, \tag{6}$$

where $\frac{1}{v_{ph}^{BG'}}$ is the scalar $\frac{k_{BG'}}{\omega_{BG'}}$, $\frac{1}{v_{ph}^{BG}}$ is the scalar $\frac{k_{BG}}{\omega_{BG}}$.

From Section IX-D.3, Eq. 32, taking only the electron contributions to the nonlinear currents, we get

$$\left(1-\frac{\omega_{pe}^2}{\omega^2-\gamma_e k^2 v_{Te}^2}-\frac{\omega_{pi}^2}{\omega^2-\gamma_i k^2 v_{Ti}^2}\right)\left(-\frac{k_-^2c^2}{\omega_-^2}+1-\frac{\omega_{pe}^2}{\omega_-^2}-\frac{\omega_{pi}^2}{\omega_-^2}\right)$$

$$=\frac{|v_{Le}^2|}{v_{Te}^2}\,\omega_{pe}^4\left[\frac{(\vec{e}_{M-}\cdot\vec{e}_L)\omega_- kv_T}{\omega_-^2\left(\omega^2-\gamma k^2 v_T^2\right)}\right]^2. \tag{7}$$

Using (7) for the unmodified Brillouin instability, consider the neighborhood of a point $(\vec{k},\omega)\equiv(\vec{k}_{IA},\omega_{IA})$ where the hypersurfaces $(K)_S=0$, $(K_-)_M=0$ intersect and the corresponding point $(\vec{k}_-,\omega_-)\equiv(\vec{k}_{EM'},-\omega_{EM'})$.

$$\frac{1}{k^2\lambda_{De}^2}\left(1-\frac{k^2c_s^2}{\omega^2}\right)\left(\frac{\omega_-^2-\omega_{pe}^2-k_-^2c^2}{\omega_-^2}\right)\cong\frac{|v_L^2|}{v_T^2}\,\frac{\omega_p^4k^2v_T^2\omega_-^2(\vec{e}_{M-}\cdot\vec{e}_L)^2}{\omega_-^4\left(\omega^2-\gamma k^2v_T^2\right)^2}. \tag{8}$$

Expanding about $(\vec{k}_{IA},\omega_{IA})$ to first order in $\Delta\vec{k}$, $\Delta\omega$, we have

Three-dimensional Unmodified Brillouin Instability:

$$\left(\Delta\omega-\vec{v}_g^{IA}\cdot\Delta\vec{k}\right)\left(\Delta\omega+\vec{v}_g^{EM'}\cdot\Delta\vec{k}\right)\cong-\frac{v_{LASER}^2}{16}\,\omega_{EM'}\omega_{IA}(\vec{e}_{EM'}\cdot\vec{e}_L)^2\,\frac{\omega_p^2}{\omega_{EM'}^2}. \tag{9}$$

Using (7) for the unmodified Raman instability, consider the neighborhood of a point $(\vec{k},\omega)\equiv(\vec{k}_{BG},\omega_{BG})$ where the hypersurfaces $(K)_S=0$, $(K_-)_M=0$ intersect and so the corresponding point $(\vec{k}_-,\omega_-)\equiv(\vec{k}_{EM'},-\omega_{EM'})$. Then

$$\left(1-\frac{\omega_p^2}{\omega^2-3k^2v_T^2}\right)\left(\frac{\omega_-^2-\omega_{pe}^2-k_-^2c^2}{\omega_-^2}\right)\cong\frac{|v_L|}{v_T^2}\,\frac{\omega_p^4k^2v_T^2\omega_-^2(\vec{e}_{M-}\cdot\vec{e}_L)^2}{\omega_-^4\left(\omega^2-3k^2v_T^2\right)^2}. \tag{10}$$

Expanding about $(\vec{k}_{BG},\omega_{BG})$ to first order in $\Delta\vec{k}$, $\Delta\omega$, we have

Three-dimensional Unmodified Raman Instability:

$$\left(\Delta\omega-\vec{v}_g^{BG}\cdot\Delta\vec{k}\right)\left(\Delta\omega+\vec{v}_g^{EM'}\cdot\Delta\vec{k}\right)\cong-\frac{v_{LASER}^2}{16}\,\frac{\omega_p^2}{\omega_{EM'}\omega_{BG}}\,k_{BG}^2(\vec{e}_{EM'}\cdot\vec{e}_L)^2. \tag{11}$$

From Section IX-D. 3, Eq. 33, taking only the electron contributions to the nonlinear currents, we find

$$\left(1 - \frac{\omega_{pe}^2}{\omega^2 - \gamma_e k^2 v_{Te}^2} - \frac{\omega_{pi}^2}{\omega^2 - \gamma_i k^2 v_{Ti}^2}\right)$$

$$= \frac{|v_{Le}^2|}{v_{Te}^2}\,\omega_{pe}^4\left[\frac{(\vec{e}_{M-}\cdot\vec{e}_L)\omega_- kv_{Te}}{\omega_-^2\left(\omega^2-\gamma_e k^2 v_{Te}^2\right)}\right]^2 \Bigg/ \left(-\frac{k_-^2c^2}{\omega_-^2} + 1 - \frac{\omega_{pe}^2}{\omega_-^2} - \frac{\omega_{pi}^2}{\omega_-^2}\right)$$

$$+ \frac{|v_{Le}^2|}{v_{Te}^2}\,\omega_{pe}^4\left[\frac{(\vec{e}_{S-}\cdot\vec{e}_L)\omega_- kv_{Te} + k_- v_{Te}\omega(\vec{e}_S\cdot\vec{e}_L)}{\left(\omega^2-\gamma_e k^2 v_{Te}^2\right)\left(\omega_-^2-\gamma_e k_-^2 v_{Te}^2\right)}\right]^2 \Bigg/ \left(1 - \frac{\omega_{pe}^2}{\omega_-^2-\gamma_e k_-^2 v_{Te}^2} - \frac{\omega_{pi}^2}{\omega_-^2-\gamma_i k_-^2 v_{Ti}^2}\right). \tag{12}$$

Using (12) for coalescing Raman and plasmon-plasmon instabilities, take

$$\left|\frac{kv_T}{\omega}\right| \ll 1, \qquad \left|\frac{k_- v_T}{\omega_-}\right| \ll 1, \qquad \omega^2 - \gamma_e k^2 v_{Te}^2 = \omega_{pe}^2. \tag{13}$$

Set

$$(\vec{k}, \omega) \equiv (\vec{k}_2, \omega_2), (\vec{k}_-, \omega_-) \equiv (-\vec{k}_1, -\omega_1), |v_L| = v_o/2 \tag{14}$$

and approximate $\omega_1 = \omega_2 = \omega_p$ except in terms involving their difference:

Three-dimensional Coalesced Raman and Plasmon-Plasmon instability: (This is a form used by Langdon, Lasinski, and Kruer.[8])

$$4\left(\frac{\omega_2^2 - \omega_{pe}^2}{\omega_{pe}^2}\right) = \frac{k_2^2}{k_1^2}\,\frac{|\vec{k}_1\times\vec{v}_o|^2}{\left(-k_1^2c^2+\omega_1^2-\omega_p^2\right)} + \frac{(\vec{k}_1\cdot\vec{v}_o)^2\left(k_1^2-k_2^2\right)^2}{k_1^2k_2^2\left(\omega_1^2-\omega_p^2\right)}. \tag{15}$$

From Section IX-D.3, Eq. 30, taking only the electron contributions to the nonlinear currents, we get

$$\left(1 - \frac{\omega_{pe}^2}{\omega_-^2 - \gamma_e k_-^2 v_{Te}^2} - \frac{\omega_{pi}^2}{\omega_-^2 - \gamma_i k_-^2 v_{Ti}^2}\right)$$

$$= \frac{|v_{Le}^2|}{v_{Te}^2}\,\omega_{pe}^4 \left[\frac{(\vec{e}_{S-}\cdot\vec{e}_L)\omega_- k v_{Te} + k_- v_{Te}\omega(\vec{e}_S\cdot\vec{e}_L)}{\left(\omega^2-\gamma_e k^2 v_{Te}^2\right)\left(\omega_-^2-\gamma_e k_-^2 v_{Te}^2\right)}\right]^2 \Bigg/ \left(1 - \frac{\omega_{pe}^2}{\omega^2 - \gamma_e k^2 v_{Te}^2} - \frac{\omega_{pi}^2}{\omega^2 - \gamma k^2 v_{Ti}^2}\right)$$

$$+ \frac{|v_{Le}^2|}{v_{Te}^2}\,\omega_{pe}^4 \left[\frac{k_- v_{Te}\omega(\vec{e}_M\cdot\vec{e}_L)}{\left(\omega_-^2-\gamma_e k_-^2 v_{Te}^2\right)\omega^2}\right]^2 \Bigg/ \left(-\frac{k^2c^2}{\omega^2} + 1 - \frac{\omega_{pe}^2}{\omega^2} - \frac{\omega_{pi}^2}{\omega^2}\right)$$

$$+ \frac{|v_{Le}^2|}{v_{Te}^2}\,\omega_{pe}^2 \Big[(\vec{e}_{S-}\cdot\vec{e}_L)\,\omega_- k^2 v_{Te}^2 \omega_-(\vec{e}_{S-}\cdot\vec{e}_L) + (\vec{e}_{S-}\cdot\vec{e}_L)\,\omega_-(\vec{e}_S\cdot\vec{e}_L)\,\omega k v_{Te} k_- v_{Te}$$

$$+ k_- v_{Te}(\vec{e}_S\cdot\vec{e}_L)\,\omega k v_{Te}\omega_-(\vec{e}_{S-}\cdot\vec{e}_L) + k_- v_{Te}(\vec{e}_S\cdot\vec{e}_L)^2\,\gamma k^2 v_{Te}^2 k_- v_{Te}\Big] \Big/$$

$$\left[\left(\omega_-^2-\gamma_e k_-^2 v_{Te}^2\right)^2\left(\omega^2-\gamma_e k^2 v_{Te}^2\right)\right]$$

$$+ \frac{|v_{Le}^2|}{v_{Te}^2}\,\omega_{pe}^2 \Big[(\vec{e}_{S-}\cdot\vec{e}_L)\,\omega_- k_{--}^2 v_{Te}^2 \omega_-(\vec{e}_{S-}\cdot\vec{e}_L) + (\vec{e}_{S-}\cdot\vec{e}_L)\,\omega_-(\vec{e}_{S--}\cdot\vec{e}_L)\,\omega_- k_{--} v_{Te} k_- v_{Te}$$

$$+ k_- v_{Te}(\vec{e}_{S--}\cdot\vec{e}_L)\,\omega_{--} k_- v_{Te}\omega_-(\vec{e}_{S-}\cdot\vec{e}_L) + k_- v_{Te}(\vec{e}_{S--}\cdot\vec{e}_L)^2\,\gamma k_{--}^2 v_{Te}^2 k_- v_{Te}\Big] \Big/$$

$$\left[\left(\omega_-^2-\gamma_e k_-^2 v_{Te}^2\right)^2\left(\omega_{--}^2-\gamma_e k_{--}^2 v_{Te}^2\right)\right]. \qquad (16)$$

Using (16) for the modified plasmon-phonon instability, we consider the neighborhood of a point $(\vec{k}, \omega) \equiv (\vec{k}_{IA}, \omega_{IA})$ where the hypersurfaces $(K)_S = 0$, $(K_-)_S = 0$ intersect, and let the corresponding $(\vec{k}_-, \omega_-) \equiv (\vec{k}_{BG}, -\omega_{BG})$. But let the neighborhood of $(\vec{k}_{IA}, \omega_{IA})$ extend over a frequency span of several ω_{IA}. Use the facts that $|\omega_{--}/k_{--}| > |\omega_-/k_-| \gg v_{Te} \gg |\omega/k|$. Then the second and fourth of the four terms on the right-hand side of (16) may be neglected. In the first term, that part of the numerator enclosed in brackets may itself be approximated by its first term. Similarly, in the the third term that part of the numerator enclosed in brackets may itself be approximated by its first term. Making these approximations we obtain

$$\left(1 - \frac{\omega_p^2}{\omega_-^2 - 3k_-^2 v_T^2}\right) \cong \frac{|v_L^2|}{v_T^2} \frac{\omega_-^2}{k^2 v_T^2} (\vec{e}_{S-} \cdot \vec{e}_L)^2 \Bigg/ \frac{1}{k^2 \lambda_D^2} \left(1 - \frac{k^2 c_s^2}{\omega^2}\right)$$

$$- \frac{|v_L^2|}{v_T^2} \omega_-^2 \frac{(\vec{e}_{S-} \cdot \vec{e}_L)^2}{\omega_p^2}. \tag{17}$$

Expand the left-hand side about $(\vec{k}_{BG}, -\omega_{BG})$, thereby linearizing the Bohm-Gross dispersion function but leaving the ion-acoustic dispersion function in unlinearized form, and noting that $(\vec{k}_- - \vec{k}_{BG}, \omega_- - (-\omega_{BG})) \equiv (\vec{k}-\vec{k}_{IA}, \omega-\omega_{IA})$, we get

Three-dimensional Modified Plasmon-Phonon Instability:

$$(\omega-\omega_{IA}) + \vec{v}_g^{BG} \cdot (\vec{k}-\vec{k}_{IA}) \cong - \frac{v_{LASER}^2}{8v_T^2} \omega_{BG} \left[\frac{k^2 c_s^2}{\omega^2 - k^2 c_s^2}\right] (\vec{e}_{BG} \cdot \vec{e}_L)^2. \tag{18}$$

From Section IX-D. 3, Eq. 34, taking only the electron contributions to the nonlinear currents, we have

$$\left(-\frac{k_-^2 c^2}{\omega_-^2} + 1 - \frac{\omega_{pe}^2}{\omega_-^2} - \frac{\omega_{pi}^2}{\omega_-^2}\right)$$

$$= \frac{|v_{Le}^2|}{v_{Te}^2} \omega_{pe}^4 \left[\frac{(\vec{e}_{M-} \cdot \vec{e}_L)\omega_- k v_T}{\omega_-^2\left(\omega^2 - \gamma_e k^2 v_{Te}^2\right)}\right]^2 \Bigg/ \left(1 - \frac{\omega_{pe}^2}{\omega^2 - \gamma_e k^2 v_{Te}^2} - \frac{\omega_{pi}^2}{\omega^2 - \gamma_i k^2 v_{Ti}^2}\right)$$

$$+ \frac{|v_{Le}^2|}{v_{Te}^2} \omega_{pe}^2 \frac{(\vec{e}_{M-} \cdot \vec{e}_L)^2 \omega_-^2 k^2 v_{Te}^2}{\omega_-^4\left(\omega^2 - \gamma_e k^2 v_{Te}^2\right)}$$

$$+ \frac{|v_{Le}^2|}{v_{Te}^2} \omega_{pe}^2 \frac{(\vec{e}_{M-} \cdot \vec{e}_L)^2 \omega_-^2 k_{--}^2 v_{Te}^2}{\omega_-^4\left(\omega_{--}^2 - \gamma_e k_{--}^2 v_{Te}^2\right)}. \tag{19}$$

Using (19) for the modified Brillouin instability, consider the neighborhood of a point $(\vec{k}, \omega) \equiv (\vec{k}_{IA}, \omega_{IA})$ where the hypersurfaces $(K)_S = 0$, $(K_-)_M = 0$ intersect, and let the corresponding $(\vec{k}_-, \omega_-) \equiv (\vec{k}_{EM'}, -\omega_{EM'})$. But let this neighborhood of $(\vec{k}_{IA}, \omega_{IA})$ extend

over a frequency span of several times ω_{IA}. Use the facts that $|\omega_{--}/k_{--}| > |\omega_{-}/k_{-}| \gg v_{Te} \gg |\omega/k|$. Then the third of the three terms on the right-hand side of (19) may be neglected. With these approximations,

$$\left(-\frac{k_{-}^2c^2}{\omega_{-}^2}+1-\frac{\omega_p^2}{\omega_{-}^2}\right)\cong\frac{|v_L^2|}{v_T^2}\,\frac{\omega_p^4(\vec{e}_{M-}\cdot\vec{e}_L)^2}{\omega_{-}^2k^2v_T^2}\Bigg/\frac{1}{k^2\lambda_D^2}\left(1-\frac{k^2c_s^2}{\omega^2}\right)-\frac{|v_L^2|}{v_T^2}\,\frac{\omega_p^2}{\omega_{-}^2}(\vec{e}_{M-}\cdot\vec{e}_L)^2. \tag{20}$$

Expanding the left-hand side about $(\vec{k}_{EM'}, -\omega_{EM'})$, thereby linearizing the electromagnetic dispersion function but leaving the ion-acoustic dispersion relation in unlinearized form, and noting that $(\vec{k}_{-}-\vec{k}_{EM'}, \omega_{-}-(-\omega_{EM'})) \equiv (\vec{k}-\vec{k}_{IA}, \omega-\omega_{IA})$, we get

Three-dimensional Modified Brillouin Instability:

$$(\omega-\omega_{IA})+\vec{v}_g^{EM'}\cdot(\vec{k}-\vec{k}_{IA})\cong-\frac{v_{LASER}^2}{8v_T^2}\,\frac{\omega_p^2}{\omega_{EM'}}\left[\frac{k^2c_s^2}{\omega^2-k^2c_s^2}\right](\vec{e}_{EM'}\cdot\vec{e}_L)^2. \tag{21}$$

Using (19) for the form of modified Raman instability in extremely underdense plasma, we consider the neighborhood of a point $(\vec{k}, \omega) \equiv (\vec{k}_{BG}, \omega_{BG})$ where the hypersurfaces $(K)_S = 0$, $(K_{-})_M = 0$ intersect, and let the corresponding $(\vec{k}_{-}, \omega_{-}) \equiv (\vec{k}_{EM'}, -\omega_{EM'})$. But let this neighborhood of $(\vec{k}_{BG}, \omega_{BG})$ extend over a frequency span of several times ω_{BG}. Use the facts that $|\omega_{--}/k_{--}| > |\omega_{-}/k_{-}| \gg |\omega/k| \gg v_{Te}$. Then the third of the three terms on the right-hand side of (19) may be neglected. With these approximations,

$$\left(-\frac{k_{-}^2c^2}{\omega_{-}^2}+1-\frac{\omega_p^2}{\omega_{-}^2}\right)\cong\frac{|v_L^2|}{v_T^2}\,\frac{\omega_p^4(\vec{e}_{M-}\cdot\vec{e}_L)^2\,k^2v_T^2}{\omega_{-}^2\omega^4}\Bigg/\left(1-\frac{\omega_p^2}{\omega^2}\right)$$

$$+\frac{|v_L^2|}{v_T^2}\,\frac{\omega_p^2(\vec{e}_{M-}\cdot\vec{e}_L)^2\,k^2v_T^2}{\omega_{-}^2\omega^2}.$$

Expand the left-hand side about $(\vec{k}_{EM'}, -\omega_{EM'})$, thereby linearizing the electromagnetic dispersion function, but leave the Bohm-Gross dispersion relation in unlinearized form. Note that

$$(\vec{k}_{-}-\vec{k}_{EM'}, \omega_{-}-(-\omega_{EM'})) \equiv (\vec{k}-\vec{k}_{BG}, \omega-\omega_{BG}).$$

Three-dimensional Modified Raman Instability:
(An extremely underdense plasma. See Forslund, Kindel, and Lindman.[6])

$$(\omega-\omega_{BG}) + \vec{v}_g^{EM'} \cdot (\vec{k}-\vec{k}_{BG}) = -\frac{v_{LASER}^2}{8v_T^2} \frac{k^2 v_T^2 (\vec{e}_{EM'} \cdot \vec{e}_L)^2}{\omega_{EM'}} \left(\frac{\omega_p^2}{\omega^2 - \omega_p^2}\right). \tag{23}$$

From Section IX-D.3, Eq. 35, taking only the electron contributions to the nonlinear currents, we get

$$\left(1 - \frac{\omega_{pe}^2}{\omega^2 - \gamma_e k^2 v_{Te}^2} - \frac{\omega_{pi}^2}{\omega^2 - \gamma_i k^2 v_{Ti}^2}\right)$$

$$= \frac{|v_{Le}^2|}{v_{Te}^2} \omega_{pe}^4 \left[\frac{(\vec{e}_{M-} \cdot \vec{e}_L)\omega_- k v_{Te}}{\omega_-^2 (\omega^2 - \gamma_e k^2 v_{Te}^2)}\right]^2 \Bigg/ \left(-\frac{k_-^2 c^2}{\omega_-^2} + 1 - \frac{\omega_{pe}^2}{\omega_-^2} - \frac{\omega_{pi}^2}{\omega_-^2}\right)$$

$$+ \frac{|v_{Le}^2|}{v_{Te}^2} \omega_{pe}^4 \left[\frac{(\vec{e}_{S-} \cdot \vec{e}_L)\omega_- k v_{Te} + k_- v_{Te} \omega (\vec{e}_S \cdot \vec{e}_L)}{(\omega^2 - \gamma_e k^2 v_{Te}^2)(\omega_-^2 - \gamma_e k_-^2 v_{Te}^2)}\right]^2 \Bigg/ \left(1 - \frac{\omega_{pe}^2}{\omega_-^2 - \gamma_e k_-^2 v_{Te}^2} - \frac{\omega_{pi}^2}{\omega_-^2 - \gamma_i k_-^2 v_{Ti}^2}\right)$$

$$+ \frac{|v_{Le}^2|}{v_{Te}^2} \omega_{pe}^2 \frac{\left[(\vec{e}_S \cdot \vec{e}_L)^2 \omega^2 k_+^2 v_{Te}^2 + 2(\vec{e}_S \cdot \vec{e}_L)(\vec{e}_{S+} \cdot \vec{e}_L)\, \omega\omega_+ k k_+ v_{Te}^2 + (\vec{e}_{S+} \cdot \vec{e}_L)^2 \gamma_e k^2 k_+^2 v_{Te}^4\right]}{(\omega^2 - \gamma_e k^2 v_{Te}^2)^2 (\omega_+^2 - \gamma_e k_+^2 v_{Te}^2)}$$

$$+ \frac{|v_{Le}^2|}{v_{Te}^2} \omega_{pe}^2 \frac{\left[(\vec{e}_S \cdot \vec{e}_L)^2 \omega^2 k_-^2 v_{Te}^2 + 2(\vec{e}_S \cdot \vec{e}_L)(\vec{e}_{S-} \cdot \vec{e}_L)\, \omega\omega_- k k_- v_{Te}^2 + (\vec{e}_{S-} \cdot \vec{e}_L)^2 \gamma_e k^2 k_-^2 v_{Te}^4\right]}{(\omega^2 - \gamma_e k^2 v_{Te}^2)^2 (\omega_-^2 - \gamma_e k_-^2 v_{Te}^2)}. \tag{24}$$

Using (24) for modified Raman instability near the quarter critical surface, $|\omega_+| \sim 3\omega_{pe}$ so the third of the four terms on the right-hand side of (24) may be neglected. As for the coalescing Raman and plasmon-plasmon instability, take

$$\left|\frac{k v_T}{\omega}\right| \ll 1, \qquad \left|\frac{k_- v_T}{\omega_-}\right| \ll 1, \qquad \begin{aligned} \omega^2 - \gamma_e k^2 v_{Te}^2 &\cong \omega_{pe}^2 \\ \omega_-^2 - \gamma_e k_-^2 v_{Te}^2 &\cong \omega_-^2 \end{aligned} \tag{25}$$

Now approximate $\omega_1 = \omega_2 = \omega_p$ except in terms involving their difference,

Three-dimensional Raman Instability Modified by Δk Shift, with the Δk Shift Remaining Small. The effect is that of coalescence of the Raman and Plasmon-Plasmon instabilities.

$$4\left(\frac{\omega_2^2-\omega_p^2}{\omega_2^2}\right) \approx \frac{k_2^2}{k_1^2}\,\frac{|\vec{k}_1\times\vec{v}_o|^2}{\left(-k_1^2c^2+\omega_1^2-\omega_p^2\right)} + \frac{(\vec{k}_1\cdot\vec{v}_o)^2}{k_1^2k_2^2}\,\frac{\left(k_1^2-k_2^2\right)^2}{\left(\omega_1^2-\omega_p^2\right)}. \tag{26}$$

From Section IX-D.3, Eq. 36, taking only the electron contributions to the nonlinear conductivity, we get

$$\left(1-\frac{\omega_{pe}^2}{\omega_+^2-\gamma_e k_+^2 v_{Te}^2}-\frac{\omega_{pi}^2}{\omega_+^2-\gamma_i k_+^2 v_{Te}^2}\right)\left(1-\frac{\omega_{pe}^2}{\omega_-^2-\gamma_e k_-^2 v_{Te}^2}-\frac{\omega_{pi}^2}{\omega_-^2-\gamma_i k_-^2 v_{Ti}^2}\right)$$

$$= \left(1-\frac{\omega_{pe}^2}{\omega_+^2-\gamma_e k_+^2 v_{Te}^2}-\frac{\omega_{pi}^2}{\omega_+^2-\gamma_i k_+^2 v_{Te}^2}\right)|E_L|^2\,G_-$$

$$+ \left(1-\frac{\omega_{pe}^2}{\omega_-^2-\gamma_e k_-^2 v_{Te}^2}-\frac{\omega_{pi}^2}{\omega_-^2-\gamma_i k_-^2 v_{Ti}^2}\right)|E_L|^2\,G_+$$

$$-|E_L|^4\,G_-G_+ + |E_L|^4\,H_-H_+. \tag{27}$$

Using (27) for nonoscillatory instability, we consider the neighborhood of a point $(\vec{k},\omega) \equiv (\vec{k}_{NO}, \omega_{NO})$ where the hypersurfaces $(K_+)_S = 0$, $(K_-)_S = 0$ intersect, and let the corresponding $(\vec{k}_+, \omega_+) \equiv (\vec{k}_{BG'}, \omega_{BG'})$, $(\vec{k}_-, \omega) \equiv (\vec{k}_{BG}, -\omega_{BG})$. Use the facts that $|\omega_{++}/k_{++}|$, $|\omega_{--}/k_{--}| > |\omega_+/k_+|$, $|\omega_-/k_-| \gg v_{Te} \gg |\omega/k|$. Then from Section IX-D.3, Eqs. 30, 31, 37, and 38, we have

$$|E_L|^2\,G_- \cong \frac{|v_L|^2}{v_T^2}\,\frac{\omega_{BG}^2}{\omega_p^2}\left[\frac{k^2c_s^2}{\omega^2-k^2c_s^2}\right](\vec{e}_{BG}\cdot\vec{e}_L)^2 \tag{28}$$

$$|E_L|^2 G_+ \cong \frac{|v_L|^2}{v_T^2} \frac{\omega_{BG'}^2}{\omega_p^2} \left[\frac{k^2 c_s^2}{\omega^2 - k^2 c_s^2}\right] (\vec{e}_{BG'} \cdot \vec{e}_L)^2 \tag{29}$$

$$E_L^{*2} H_- \cong \frac{v_L^{*2}}{v_T^2} \frac{\omega_{BG}\omega_{BG'}}{\omega_p^2} \left[\frac{k^2 c_s^2}{\omega^2 - k^2 c_s^2}\right] (\vec{e}_{BG} \cdot \vec{e}_L)(\vec{e}_{BG'} \cdot \vec{e}_L) \tag{30}$$

$$E_L^2 H_+ \cong \frac{v_L^2}{v_T^2} \frac{\omega_{BG}\omega_{BG'}}{\omega_p^2} \left[\frac{k^2 c_s^2}{\omega^2 - k^2 c_s^2}\right] (\vec{e}_{BG} \cdot \vec{e}_L)(\vec{e}_{BG'} \cdot \vec{e}_L). \tag{31}$$

Linearize both Bohm-Gross dispersion relations, and note that to this approximation

$$|E_L|^4 G_- G_+ = |E_L|^4 H_- H_+. \tag{32}$$

Then (27) becomes

Three-dimensional Nonoscillatory Instability:

$$\{(\omega-\omega_{NO}) - (\vec{k}-\vec{k}_{NO}) \cdot \vec{v}_g^{BG'}\}\{(\omega-\omega_{NO}) + (\vec{k}-\vec{k}_{NO}) \cdot \vec{v}_g^{BG}\}$$

$$= \frac{v_{LASER}^2}{4v_T^2} \left\{ \frac{\omega_{BG}}{2} \left((\omega-\omega_{NO}) - (\vec{k}-\vec{k}_{NO}) \cdot \vec{v}_g^{BG'}\right)(\vec{e}_{BG} \cdot \vec{e}_L)^2 \right.$$

$$\left. - \frac{\omega_{BG'}}{2} \left((\omega-\omega_{NO}) + (\vec{k}-\vec{k}_{NO}) \cdot \vec{v}_g^{BG}\right)(\vec{e}_{BG'} \cdot \vec{e}_L)^2 \right\} \left[\frac{k^2 c_s^2}{k^2 c_s^2 - \omega^2}\right] \tag{33}$$

(for the three-dimensional unmodified nonoscillatory instability, replace $(\vec{k}, \omega)$ with $(\vec{k}_{NO}, \omega_{NO})$ in the final square bracket).

One-Dimensional Cross Sections of Asymptotic Modified Pulse Shapes

We shall now apply the stability analysis of Bers and Chambers (Sec. IX-D. 2) to the specific modified dispersion relations that we have just derived. In the cross section of maximum growth rate we obtain the time-asymptotic form of an evolving unstable pulse resulting from an initially localized excitation. We do this for the modified Brillouin, the modified decay, and the modified nonoscillatory instabilities.

Unmodified stimulated Brillouin scattering yields a time-asymptotic pulse shape

(see Sec. IX-A. 1) with the peak lying on the x axis. We investigate the effect of modification on the one-dimensional cross section through the peak as follows. We write the modified Brillouin dispersion relation in the form

$$\omega + \vec{v}_g^{EM'} \cdot (\vec{k}-\vec{k}_{INT}) = -\frac{v_{LASER}^2}{8v_T^2}\frac{\omega_p^2}{\omega_{EM'}}\left[\frac{k^2c_s^2}{\omega^2 - k^2c_s^2}\right](\vec{e}_{EM'}\cdot\vec{e}_L)^2, \tag{34}$$

where $(\vec{k}, \omega) = (\vec{k}_{INT}, 0)$ defines a point on the intersection of the hypersurfaces $(K_-)_m = 0$, $\omega = 0$. We assume that for frame velocities in the x direction the absolute instability occurs at a value $\vec{k} = \vec{k}_o$ which also lies in the x direction. Then we may take $\vec{k}_{INT}$ to lie in the x direction. Then $\vec{k}_- \equiv \vec{k}_{EM'}$ and $\vec{v}_g^{EM'}$ also lie in the x direction and (34) becomes

$$\omega + v_g^{EM'}(k_x-k_{INT}) = -\frac{v_{LASER}^2}{8v_T^2}\frac{\omega_p^2}{\omega_{EM'}}\left[\frac{k^2c_s^2}{\omega^2 - k^2c_s^2}\right]. \tag{35}$$

We introduce normalized quantities as follows. Define

$$\frac{k}{k_{INT}} \equiv K \qquad \frac{\omega}{k_{INT}c_s} \equiv \Omega \qquad \frac{c_s}{v_g^{EM'}} \equiv C \qquad \frac{v_{LASER}^2}{8v_T^2}\frac{\omega_p^2}{\omega_{EM'}k_{INT}v_g^{EM'}} \equiv A. \tag{36}$$

Then (35) becomes

$$(C\Omega+K_x-1)\left(\Omega^2-K_x^2\right) = -AK_x^2. \tag{37}$$

The absolute instability in a frame moving in the x direction with normalized velocity $V_x = v_{x(frame)}/c_s$ then satisfies

$$\left.\begin{aligned} &D_v \equiv (C(\Omega+K_xV_x)+K_x-1)\left((\Omega+K_xV_x)^2-K_x^2\right) + AK_x^2 = 0 \\ &\partial D_v/\partial K_x = 0 \end{aligned}\right\} \tag{38}$$

The pair (K_{ox}, Ω_o) corresponding to absolute instability is used to plot ω_{oi} as a function of V_x. The resulting pulse-shape cross section is displayed in Fig. IX-5. The parameters entering the calculation are chosen for a neodymium laser delivering 10^{15} W/cm^{-2} onto a deuterium plasma of electron temperature 1 keV and ion temperature 50 eV.

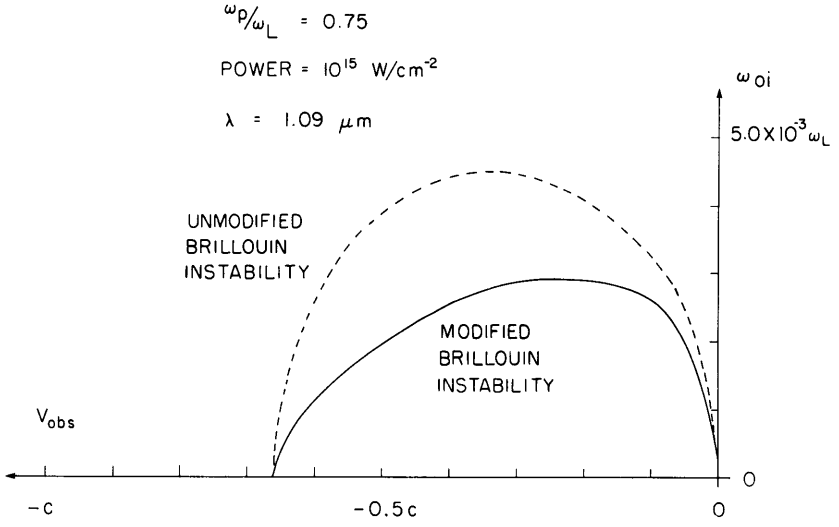

Fig. IX-5. Modified Brillouin instability.

Unmodified plasmon-phonon instability yields a time-asymptotic pulse shape (see Sec. IX-A.1) with peaks very near the z axis. We investigate the effect of modification on a one-dimensional cross section along the z axis as follows. We write the modified decay dispersion relation in the form

$$\omega + \vec{v}_g^{BG} \cdot (\vec{k}-\vec{k}_{INT}) = -\frac{v_{LASER}^2}{8v_T^2}\,\omega_{BG}\left[\frac{k^2c_s^2}{\omega^2-k^2c_s^2}\right](\vec{e}_{BG}\cdot\vec{e}_L)^2, \tag{39}$$

where $(\vec{k}, \omega) = (\vec{k}_{INT}, 0)$ defines a point on the intersection of the hypersurfaces $(K_-)_s = 0$, $\omega = 0$. We assume that for frame velocities in the z direction the absolute instability occurs at values of $\vec{k} = \vec{k}_o$ so that $\vec{k}_{-o} \equiv \vec{k}_o - \vec{k}_L$ lies nearly in the z direction. Then $\vec{v}_g^{BG}$ may be taken to lie in the z direction and (14) becomes

$$\omega + v_g^{BG}(k_z - k_{INT\,z}) = -\frac{v_{LASER}^2}{8v_T^2}\,\omega_{BG}\left[\frac{k^2c_s^2}{\omega^2-k^2c_s^2}\right] \tag{40}$$

with the proviso that the $\vec{k}$ resulting from any calculation using (40) must be such that $\vec{k}-\vec{k}_L$ lies within a narrow angle from the x axis. That is,

$$|k_x - k_L| \ll |k_z|, \qquad |k_y| \ll |k_z|. \tag{41}$$

We introduce normalized quantities as follows. Define

$$\frac{k}{k_{INT\,z}} \equiv K \qquad \frac{\omega}{k_{INT\,z}c_s} \equiv \Omega \qquad \frac{c_s}{v_g^{BG}} \equiv C \qquad \frac{v_{LASER}^2}{8v_T^2}\,\frac{\omega_{BG}}{k_{INT\,z}v_g^{BG}} \equiv A. \tag{42}$$

Then (40) becomes

$$(C\Omega+k_z-1)\left(\Omega^2-K_z^2\right) = -AK_z^2. \tag{43}$$

The absolute instability in a frame moving in the z direction with normalized velocity $V_z \equiv v_{z(\text{frame})}/c_s$ then satisfies

$$\left.\begin{aligned} &D_v \equiv (C(\Omega+K_zV_z)+K_z-1)\left((\Omega+K_zV_z)^2-K_z^2\right) + AK_z^2 = 0 \\ &\partial D_v/\partial K_z = 0. \end{aligned}\right\} \tag{44}$$

The values $k_z = k_{oz}(v_z)$ of the wave numbers at which absolute instability occurs must satisfy (41). This provides an a posteriori check on the validity of the approximation

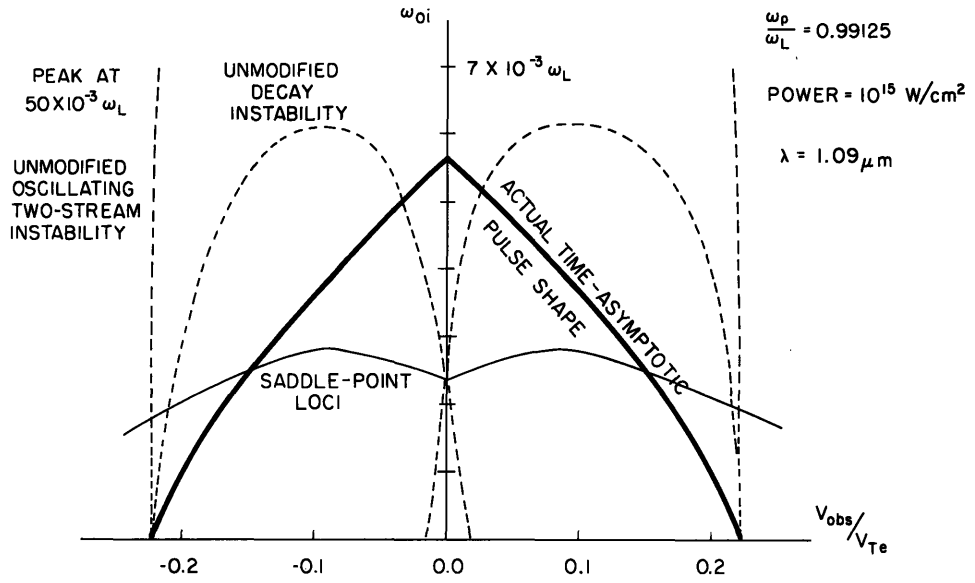

Fig. IX-6. Modified plasmon-phonon instability with nonoscillatory instability neglected.

(40). The resulting pulse-shape cross section is displayed in Fig. IX-6. Again, the parameters entering the calculation are chosen to describe a neodymium laser delivering 10^{15} W/cm^{-2} onto a deuterium plasma of electron temperature 1 keV and ion temperature 50 eV.

Unmodified "nonoscillatory" instability yields a time-asymptotic pulse shape (see Sec. IX-A. 1) with peaks very near the z axis. We investigate the effect of modification on a one-dimensional cross section along the z axis as follows. We write the modified "nonoscillatory" dispersion relation

$$\left\{(\omega-\omega_{NO})-(\vec{k}-\vec{k}_{NO})\cdot\vec{v}_g^{BG'}\right\}\left\{(\omega-\omega_{NO})+(\vec{k}-\vec{k}_{NO})\cdot\vec{v}_g^{BG}\right\}$$

$$=\frac{v_{LASER}^2}{8v_T^2}\left[\omega_{BG}\left\{(\omega-\omega_{NO})-(\vec{k}-\vec{k}_{NO})\cdot\vec{v}_g^{BG'}\right\}(\vec{e}_{BG}\cdot\vec{e}_L)^2\right.$$

$$\left.-\omega_{BG'}\left\{(\omega-\omega_{NO})+(\vec{k}-\vec{k}_{NO})\cdot\vec{v}_g^{BG}\right\}(\vec{e}_{BG'}\cdot\vec{e}_L)^2\right]\left\{\frac{k^2c_s^2}{k^2c_s^2-\omega^2}\right\}, \tag{45}$$

where $(\vec{k},\omega)=(\vec{k}_{NO},\omega_{NO})$ defines a point on the intersection of the hypersurfaces $(K_+)_s=0$, $(K_-)_s=0$. Note that this dispersion relation describes the interaction of two plasmons and two phonons, as well as the original pump wave. It includes the modified plasmon-phonon instability, and describes how the modified plasmon-phonon instability and the modified nonoscillatory instability affect each other. This mutual distortion will be seen to become a coalescence at the power level considered. Assume that for frame velocities in the x direction the absolute instability occurs at values of $\vec{k}=\vec{k}_o$ so that $\vec{k}_{\pm o}\equiv\vec{k}_o\pm\vec{k}_L$ lie almost along the z axis. Then $\vec{v}_g^{BG}$, $\vec{v}_g^{BG'}$, $\vec{e}_{BG}$, $\vec{e}_{BG'}$ may be taken to lie in the z direction, and correspondingly

$$\left.\begin{aligned}&\vec{v}_g^{BG}=\vec{v}_g^{BG'}\qquad\omega_{BG}=\omega_{BG'}\\&(\vec{k}_{NO},\omega_{NO})=(\vec{k}_{INT},0)\end{aligned}\right\}. \tag{46}$$

Then (44) becomes

$$\omega^2-(k_z-k_{INT\,z})^2\,v_g^{BG\,2}=-\frac{v_{LASER}^2}{4v_T^2}\,\omega_{BG}(k_z-k_{INT\,z})\,v_g^{BG}\left(\frac{k^2c_s^2}{k^2c_s^2-\omega^2}\right), \tag{47}$$

with the proviso that the $\vec{k}$ resulting from any calculation using (47) must be such that $\vec{k}\pm\vec{k}_L$ lie within a narrow angle about the z axis. That is,

$$|k_x-k_L|\ll|k_z|,\qquad|k_y|\ll|k_z|. \tag{48}$$

We introduce normalized quantities as follows. Define

$$\frac{k}{k_{INT\,z}}\equiv K\qquad\frac{\omega}{k_{INT\,z}\,c_s}\equiv\Omega\qquad\frac{c_s}{v_g^{BG}}\equiv C\qquad\frac{v_{LASER}^2}{8v_T^2}\,\frac{\omega_{BG}}{k_{INT\,z}v_g^{BG}}\equiv A. \tag{49}$$

Then (47) becomes

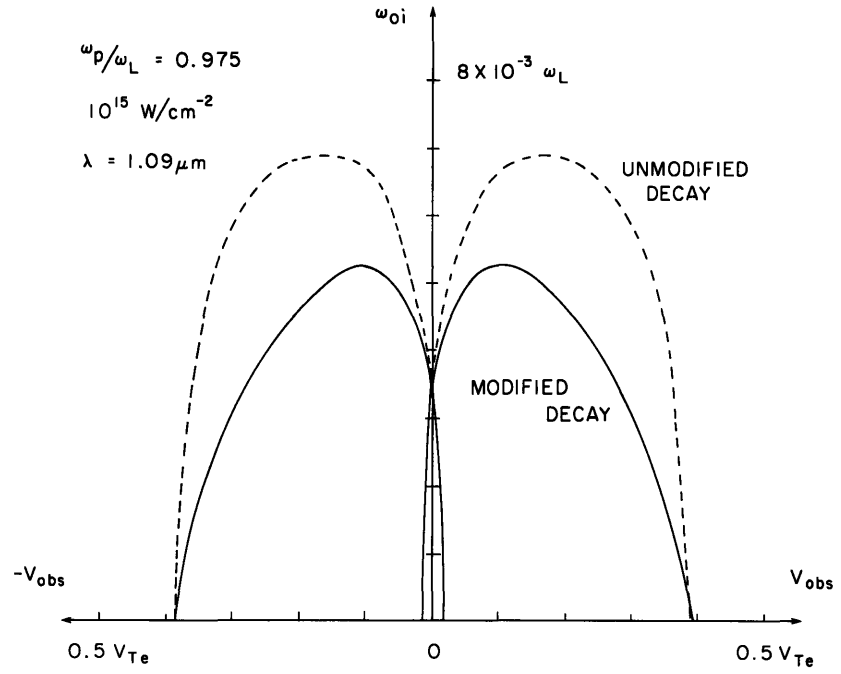

Fig. IX-7. Domination of modified plasmon-phonon instability by modified nonoscillatory instability.

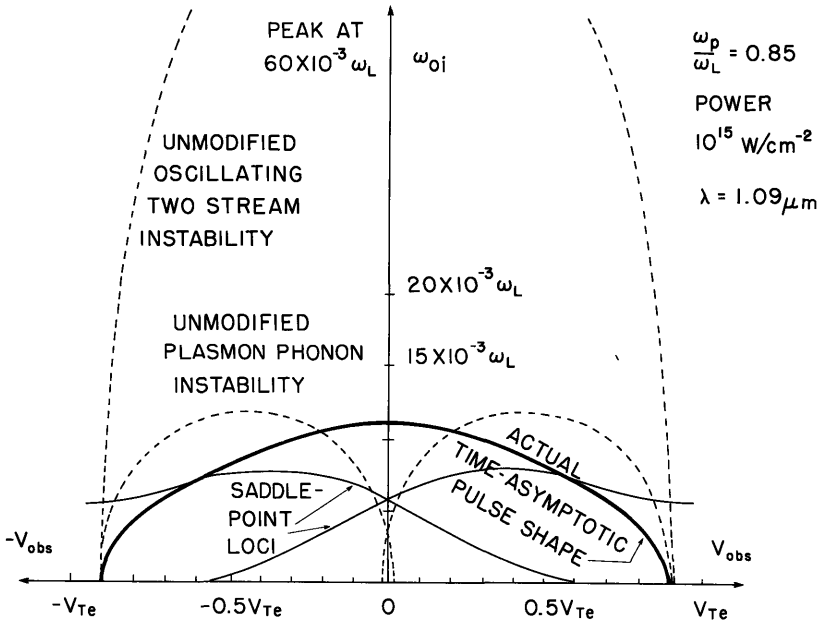

Fig. IX-8. Coalescence of modified plasmon-phonon instability and modified nonoscillatory instability.

$$\left\{C^2\Omega^2-(K_z-1)^2\right\}\left(K_z^2-\Omega^2\right) = -2A(K_z-1)\,K_z^2. \tag{50}$$

The absolute instability in a frame moving in the z direction with normalized velocity $V_z = v_{z(\text{frame})}/c_s$ then satisfies

$$D_v \equiv \left\{C^2(\Omega+K_zV_z)^2-(K_z-1)^2\right\}\left(K_z^2-\Omega^2\right) + 2A(K_z-1)\,K_z^2 = 0$$
$$\partial D_v/\partial K_z = 0. \tag{51}$$

The values $k_z = k_{oz}(v_z)$ of the wave numbers at which absolute instability occurs must satisfy (48). This provides an a posteriori check on the validity of the approximation (47). The resulting pulse-shape cross sections are displayed in Figs. IX-7 and IX-8 for two plasma densities. Again the calculation is for a neodymium laser delivering 10^{15} W/cm^{-2} onto a deuterium plasma of electron temperature 1 keV and ion temperature 50 eV. We note that, at this power-level, very near the critical density (Fig. IX-7) the modified nonoscillatory instability completely defines the pulse shape, while at somewhat lower densities (Fig. IX-8) the pulse shape is formed by a coalescence of the modified plasmon-phonon and the modified nonoscillatory instabilities.

References

1. D. DuBois and M. V. Goldman, Phys. Rev. Letters 14, 544 (1965).
2. V. P. Silin, Sov. Phys. – JETP 21, 1127 (1965).
3. K. Nishikawa, Phys. Soc. Japan 24, 916 and 1152 (1968).
4. S. Jorna, Private communication, KMS Fusion, Inc., Ann Arbor, Michigan, August 1973.
5. G. G. Comisar, Phys. Rev. 141, 200 (1966).
6. D. W. Forslund, J. M. Kindel, and E. L. Lindman, Los Alamos Report LA-UR 73-500 (1973) (unpublished).
7. D. DuBois and V. Gilinsky, Phys. Rev. 135, A 1519 (1964).
8. A. B. Langdon, B. F. Lasinski, and W. L. Kruer, Report UCRL-75018 (1973), University of California Lawrence Radiation Laboratory Livermore, California.
9. F. W. Chambers, R. J. Hawryluk, and A. Bers, Bull. Am. Phys. Soc. 18, 1336 (1973).
10. D. DuBois and M. V. Goldman, op. cit., see Equation (29).

IX. PLASMA DYNAMICS

B. Intense Relativistic Beam-Plasma Interactions

1. STRUCTURE OF PLASMA GENERATED BY IRRADIATION OF A SOLID TARGET FROM A PULSED CO_2 LASER

National Science Foundation (Grant GK-37979X)

Thaddeus J. Orzechowski, George Bekefi, Jeffry Golden,
Ivan Mastovsky, David P. Bacon

Relatively little work has been reported on the production of plasma by CO_2 lasers focused on large solid targets. In this report we describe observations made under two conditions. In the first, the plasma expands freely into vacuum, and in the second it expands against a strong mirror magnetic field. This plasma will be used eventually as a target for our relativistic beam experiments.

Figure IX-9 shows the experimental arrangement. Light from a double-discharge laser, one meter long, is focused by a germanium lens on the surface of a polished

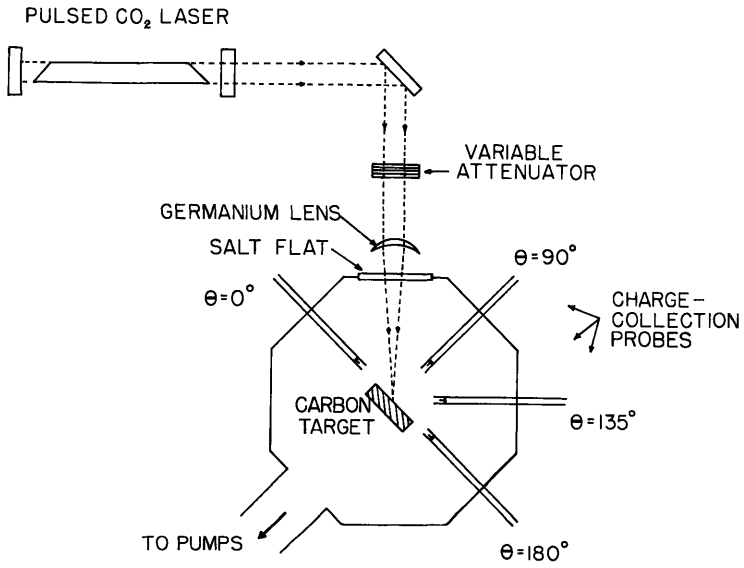

Fig. IX-9. Experimental apparatus. Mirror coils (not shown) are located above and below the vacuum chamber.

carbon block situated in vacuum. The laser beam is incident at a 45° angle to the target normal. Radially movable charge-collection probes are used to monitor the plasma density as a function of both time and position. The polyethylene attenuators shown in Fig. IX-9 are used in studying the production of plasma as a function of laser energy energy.

When the mirror magnetic field is used, it is provided by two pulsed coils situated above and below the vacuum chamber so that the magnetic field lines point out of the

plane of the paper. In this manner, magnetic fields in excess of 9 kG can be made to act on the expanding plasma.

The focused laser spot diameter was measured by using a heat-sensitive film at the focus of the germanium lens and attenuating the laser beam to prevent burning the film.

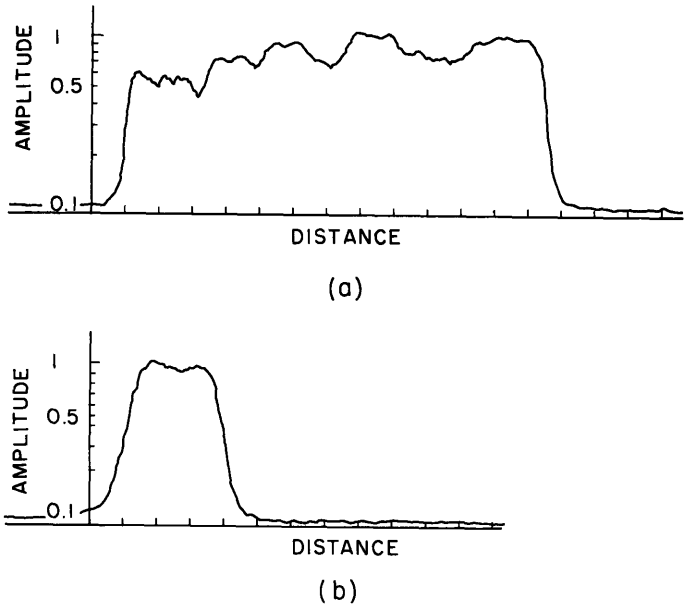

Fig. IX-10. Microdensitometer tracings of the laser pulse profile. (One horizontal division = 67 μm.) (a) Height of pulse. (b) Width of pulse.

The image dimensions were then measured on a microdensitometer. Figure IX-10 shows tracings of the height and width of the image. By converting the area of the rectangle to an effective circular area, we found a spot diameter of 420 μm. From the densitometer tracings it was also possible to determine that the dominant mode of the laser beam is TEM_{41}. The experimental parameters of the laser beam are as follows.

Energy	1.3 J
Spot Diameter	420 μm
Laser Flux	4×10^9 W/cm^2
Ablated Atoms	3×10^{16}/pulse

The laser pulse has a sharp 100-ns peak producing approximately 0.6 J of energy and a long tail (~500 ns) containing an equal amount of energy (Fig. IX-11a). By using the effective spot diameter, we found that the laser flux is approximately 4 GW/cm^2. The ablation of matter (Fig. IX-11b) was deduced from careful weighing measurements

before laser irradiation and after irradiation by 1000 successive pulses. Assuming that all the ablated matter is ionized, and using the spot diameter as an estimate of the initial plasma size, we found that the plasma density is greater than the critical density for penetration of 10.6 μm laser radiation.

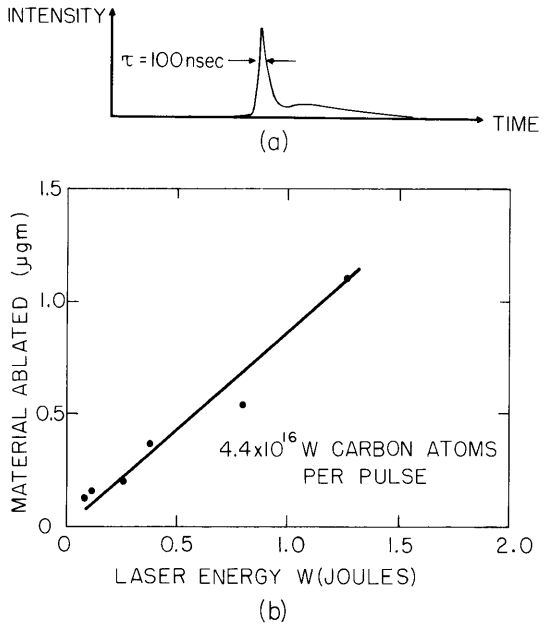

Fig. IX-11. (a) Laser pulse shape. (b) Ablated matter vs energy.

We shall now describe our observations of a freely expanding plasma in the absence of magnetic field. Figure IX-12 illustrates the spatial and temporal evolution of the plasma. Each curve is a plot of density as a function of radial position (along the target normal) for various times during the expansion. (Note that the density is in arbitrary

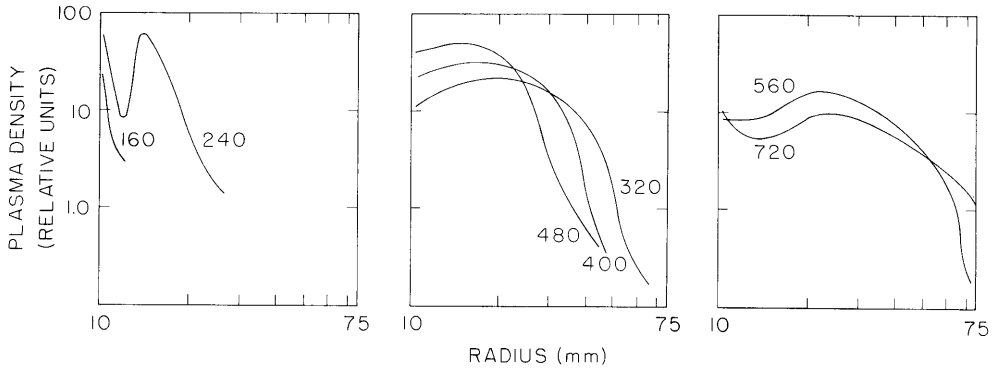

Fig. IX-12. Plasma profiles (density vs position) for various times (in ns) in the expansion normal to the target surface.

units.) The peak density at 240 ns is of the order of 10^{16} particles per cubic centimeter. At early times in the expansion, the plasma is well differentiated into a sharp, rapidly moving shock and a more sluggish inner core. The shock thickness increases with time and the density falls at a rate shown in Fig. IX-13. Both the peak shock density and the

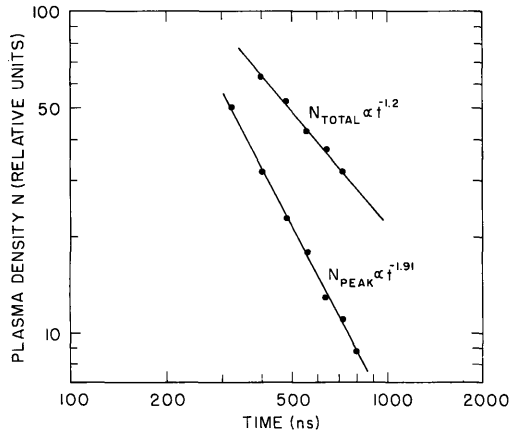

Fig. IX-13. Plasma density (peak and integrated) as a function of time.

integrated shock density follow power laws. The exponents in these laws are not in agreement with a three-dimensional hydrodynamic model of the shock expansion. The observations of Rumsby and Beaulieu[1] differ from ours. They used a ruby laser of approximately 1 J energy and found agreement with the three-dimensional shell model. We believe that the breakdown of the three-dimensional analysis results from the strong spatial anisotropy of our plasma.

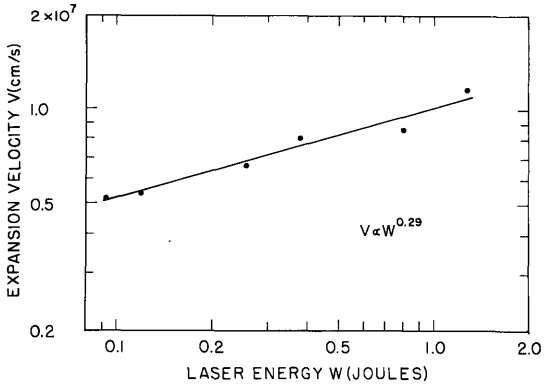

Fig. IX-14. Expansion velocity normal to the target surface as a function of laser energy.

Figure IX-14 illustrates the dependence of the plasma expansion on laser energy. The value of the exponent (0.29), which relates the velocity to the energy, is of some importance. Its value is close to 0.33, which is characteristic of a regime in which the initial plasma density is of the order of the critical density for laser light penetration. Dyer,

Pert, and their co-workers,[2, 3] find an exponent of 0.12 in a regime of laser fluxes that overlap our own. The discrepancy between the two sets of observations is not understood.

The spatial anisotropy of our plasma is evident: for example, the plasma density at a fixed radial distance from the focal spot along the tangent to the target surface is at least an order of magnitude lower than the density normal to the surface. An equally pronounced anisotropy exists in the expansion velocities of the fast shock and the plasma core. The fast shock exists primarily in a cone about the target normal, whereas the

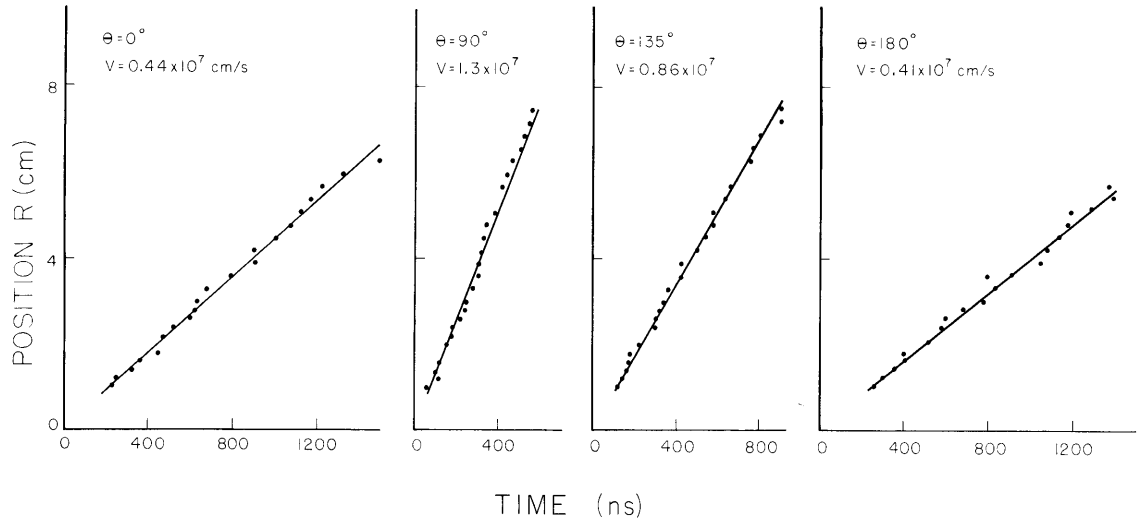

Fig. IX-15. Expansion velocities for various angular orientations illustrating the anisotropy of the plasma.

slow plasma core predominates along the target surface. Figure IX-15 shows the position of the plasma boundary as a function of time for four different angular orientations. Angles $\theta = 0°$ and $\theta = 180°$ describe the behavior of the slowly expanding core, which expands along the target surface. The two remaining angles refer to the expansion of the fast shock, which is normal to the target surface and 45° off the normal. The constancy of the velocity over the entire duration of the observed expansion is indicative of negligible momentum coupling to the background gas.

We have also studied the plasma expansion in magnetic fields in the range 3-9 kG, with a fixed 3:1 mirror ratio. We summarize our observations as follows: The central plasma core decelerates with time and stops where we believe the plasma energy corresponds to $\beta = 1$. In contrast, the fast shock exhibits no deceleration, as shown in Fig. IX-16, where we show the shock position vs time for three different values of magnetic field. Note that the velocity is constant in time and virtually independent of

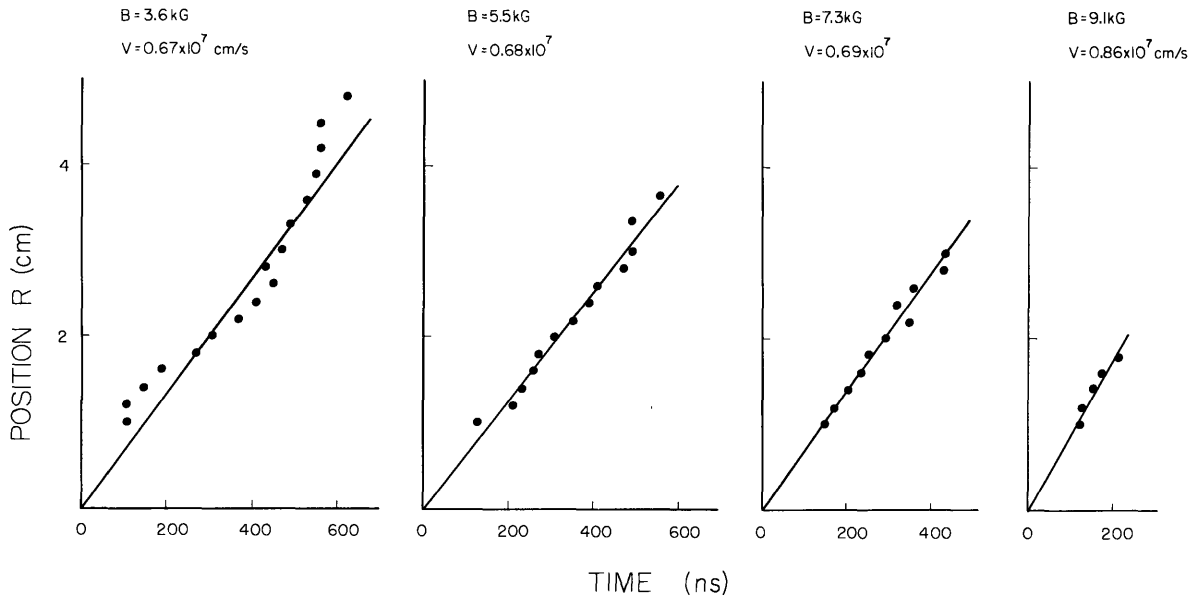

Fig. IX-16. Expansion velocities normal to the target surface for various applied magnetic field intensities.

the strength of B. The velocities are somewhat slower than for the freely expanding plasma. Figure IX-17 illustrates the time evolution of the plasma along the normal to the target surface. The plasma is still differentiated into a shock and core, but the core stops at a position 20 mm from the focal spot. Also, the shock density falls off more rapidly. This decrease in density is shown in Fig. IX-18. Here the peak shock density is plotted as a function of radius for different magnetic field strengths. When the shock reaches certain critical positions, its density is rapidly

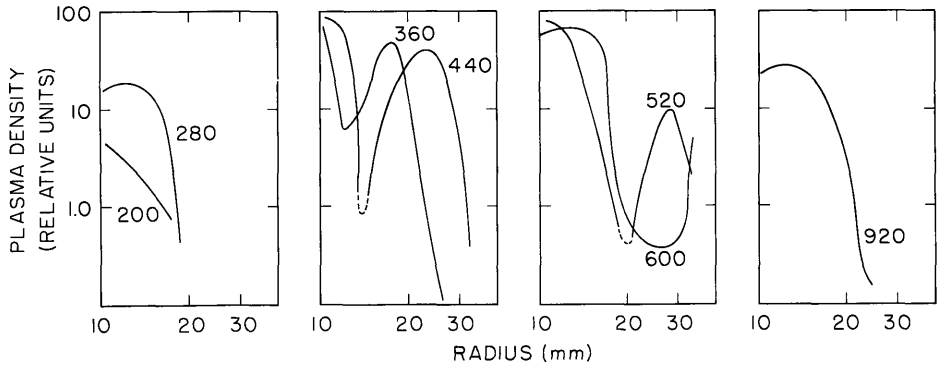

Fig. IX-17. Plasma profile (density vs position) for various times (in ns) in the expansion against a 7.3 kG applied magnetic field.

depleted, but it progresses with undiminished speed. Before these critical radii are reached, the scaling of density with position is the same as for the freely expanding

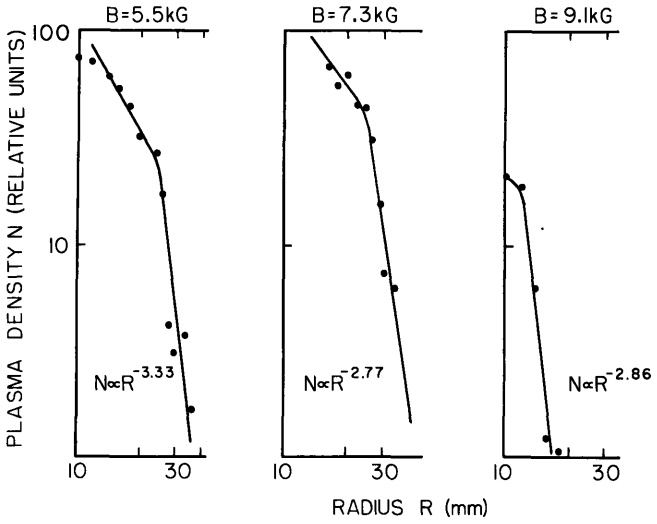

Fig. IX-18.

Peak plasma density as a function of position normal to the target surface for various applied magnetic fields.

plasma in the absence of magnetic field, $n \propto r^{-2}$. We believe that this similarity to the freely expanding plasma is due to the large kinetic energy density in the shock compared with the magnetic energy density for these radii. Beyond these points, the power laws are as shown in Fig. IX-18; that is, $n \propto r^{-3}$.

We plan to measure the electron temperature as a function of time and position, using spectroscopy and diamagnetic probes. We feel that only after the temperature behavior is understood will we be able to undertake a detailed theoretical analysis of the behavior of the plasma in a magnetic field.

References

1. P. T. Rumsby and J. Beaulieu, "Expansion of a Laser-Produced Plasma," Proc. V European Conference on Controlled Fusion and Plasma Physics, Grenoble, 1972.
2. P. E. Dyer et al., "Interaction of High-Power CO_2 Lasers with Solid Targets" (unpublished).
3. G. E. Pert et al., "Interaction of High-Power CO_2 Laser with Solid Targets" (unpublished).

2. MAGNETIC INSULATION OF AN INTENSE RELATIVISTIC ELECTRON BEAM

National Science Foundation (Grant GK-37979X)

Jeffry Golden, Thaddeus J. Orzechowski, George Bekefi

It is often desired to reduce, or altogether prevent, electron flow from occurring in a vacuum gap between two electrodes subjected to intense voltage differences.[1] Such needs arise, for example, in the design of ion diodes[2, 3] in which one of the basic and still unsolved problems is the suppression of the electrons that are field-emitted from the cathode. One scheme that has been proposed[4] is to apply a sufficiently strong magnetic field oriented at right angles to the electric field of the diode.

The insulating effect of a magnetic field has been demonstrated[5] satisfactorily at low diode voltages, but inconclusively at high diode voltages.[6] In this report we limit ourselves to the latter regime, with voltages in the range 100-250 kV. The experimental arrangement is illustrated in Fig. IX-19. The cylindrical diode consists of an outer thin-walled stainless-steel 4.84 cm ID cathode connected via a cathode shank to the inner conductor of the water-filled coaxial capacitor that serves as the transmission line of our 2.5 Ω COGEN III high-voltage facility.[7] A stainless-steel inner stem supports the anode made of graphite (POCO Graphite T. M.). A set of anodes with 4.38-3.77 cm diameters is used, which provides diodes with 2.3-5.4 mm spacings. The anode is connected to the outer grounded terminal of the water-filled capacitor via a return current can, as shown in Fig. IX-19. The diode current I_D is monitored with a rapidly responding current-viewing probe (T & M Research Products Inc.), and the diode voltage V_D is obtained from a measurement of the transmission-line voltage and knowledge of its impedance (the presence of an 18.5 Ω copper sulphate shunt impedance in parallel with the diode is properly accounted for in the derivation of V_D). The magnetic field B_o acting on the diode is generated in a solenoid energized by a capacitor bank, and is timed in such a way that B_o remains virtually constant over the duration of the ~50-ns voltage pulse applied across the diode. The thin-walled stainless-steel diode construction ensures good penetration of the pulsed magnetic field into the diode interior. The diode is evacuated and maintained at pressures better than 5×10^{-5} Torr. The burn marks observed on the anode indicate that electron emission from the cathode occurs over its entire curved surface, and not merely from isolated regions. The cylindrical diode

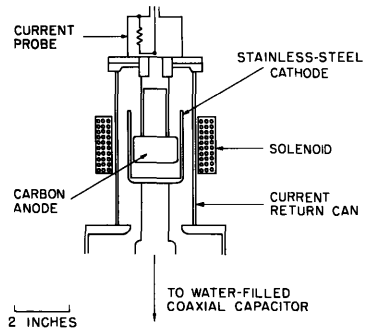

Fig. IX-19.
Cylindrical diode schematic.

geometry has the advantage[4] that any diamagnetic currents (azimuthal currents) can flow freely; thus, undesirable space-charge gradients caused by charge accumulation are avoided.

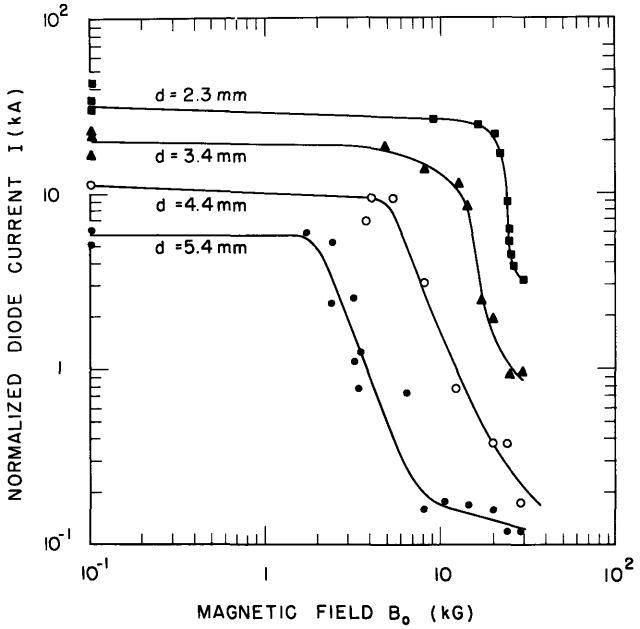

Fig. IX-20. Diode current as a function of applied magnetic field for four diode spacings d. Current is normalized in accordance with Eq. 1.

The results of the experiments are shown in Fig. IX-20. The applied axial magnetic field is plotted on the abscissa and the normalized diode current I on the ordinate. Since the diode voltage varies somewhat from shot to shot, and also with gap spacing, the diode current, for convenience of presentation, is normalized to a "standard" voltage of 160 kV, which is the mean voltage of these experiments. The normalization is accomplished by invoking the Child-Langmuir law and writing

$$I = I_D[160/V_D(kV)]^{3/2}, \tag{1}$$

where I_D is the true measured diode current. From Fig. IX-20 we see that for a given cathode-anode spacing d the magnetic field has little effect on the electron emission until a critical magnetic field $B_o = B_o^*$ is reached, beyond which the current falls precipitously. We also see that B_o^* is a function of the spacing d.

Theory shows[1, 4, 5] that magnetic insulation will occur, provided that

$$[eB_o d_{eff}/m_o c]^2 > \left[2eV_D/m_o c^2\right] + \left[eV_d/m_o c^2\right]^2. \quad (2)$$

Here d_{eff} is the true anode-cathode spacing in planar geometry, but for cylindrical geometry it is defined as

$$d_{eff} = \left(r_b^2 - r_a^2\right)/2r_a$$

$$= d[1 + (d/2r_a)], \quad (3)$$

where r_b is the radius of the outer cathode, and r_a is the radius of the inner anode ($r_a < r_b$). For our diode voltages, the relativistic correction given by the second term of Eq. 2 is negligible, and the formula for the critical magnetic field takes on the simple form

$$B_o^* d_{eff}/V_D^{1/2} = 1.07, \quad (4)$$

now with B_o^* in kilogauss, V_D in kilovolts and d_{eff} in millimeters. Table IX-4 lists the experimentally determined critical fields for the different diode spacings. We see

Table IX-4. Critical magnetic field as a function of diode spacing.

d_{eff} (mm)	B_o^* (kG)	$B_o^* d_{eff}/V_D^{1/2}$
2.45	22	4.3
3.62	12.5	3.6
4.83	5.0	1.9
6.10	1.9	0.9

that the ratio $B_o^* d_{eff}/V_D^{1/2}$ takes on values not too different from the value of 1.07 required by theory. The measured ratio, however, exhibits a systematic variation as d_{eff} is changed, which does not agree with the statement of Eq. 4. Part of this discrepancy, but probably not all of it, may be the result of diode "closure." It is known that plasma formed at the cathode travels across the gap with the result that d becomes a function of time.[8] With velocities[8] typically of the order of 3×10^6 cm/s, the plasma moves ~1 mm during the 50-ns pulse. The reduced d then requires a larger magnetic field to achieve insulation, in conformity with the results of Table IX-4. It is clear that the effect of closure becomes less important for the larger gap spacings.

At magnetic fields well beyond the critical field a weak residual current remains (see Fig. IX-20) whose magnitude appears not to be greatly influenced by the size of B_o. We do not yet know the origin of this current. It could be an ion current flowing from anode to cathode (the ions coming from a plasma residing at the anode surface); or it may be the result of an instability[1] which drives electrons across the gap. Alternatively, it could be a current of electrons flowing along magnetic field lines in the direction of the current probe. For example, a slight tilt of the cathode relative to the anode produces a component of the diode electric field which is collinear with B_o and thus causes electrons to be accelerated in that direction. This effect is similar to what occurs in a magnetron injection gun.[9, 10]

In conclusion, we have demonstrated the insulating effect of a strong magnetic field acting on a high-voltage diode. And while currents have been reduced by almost 2 orders of magnitude, a small residual current remains whose origin must still be studied in detail.

We wish to thank I. Mastovsky and D. Bacon for their assistance in running the experiment.

References

1. R. V. Lovelace and E. Ott, Laboratory of Plasma Studies Report No. LPS 133, Cornell University, August 1933.
2. M. Friedman, IEEE Trans. Nucl. Sci. 19, No. 2, 184 (1972).
3. S. Humphries, Jr., Laboratory of Plasma Studies Report No. LPS 136, Cornell University, October 1973.
4. R. N. Sudan and R. V. Lovelace, Phys. Rev. Letters 31, 1174 (1973); I. Nebenzahl, Laboratory of Plasma Studies Report No. LPS 76, Cornell University, July 1971.
5. A. W. Hull, Phys. Rev. 18, 31 (1921).
6. R. Miller, N. Rostoker, and I. Nebenzahl, Bull. Am. Phys. Soc. 17, 1007 (1972).
7. J. Golden, Quarterly Progress Report No. 103, Research Laboratory of Electronics, M. I. T., October 15, 1971, p. 103; also S. M. Thesis, Department of Aeronautics and Astronautics, M. I. T., 1972.
8. R. K. Parker, Ph. D. Thesis, University of New Mexico, 1973 (unpublished); K. B. Prestwich and G. Yonas, Bull. Am. Phys. Soc. 17, 981 (1972).
9. G. S. Kino and N. Taylor, Trans. IEEE, Vol. ED-9, No. 1, pp. 1-11, January 1962.
10. M. Friedman and M. Ury, Rev. Sci. Instr. 41, 1334 (1970).

3. BEAM-PLASMA INTERACTION IN A LONGITUDINAL DENSITY GRADIENT

National Science Foundation (Grant GK-37979X)

Abraham Bers, Marcio L. Vianna

In this report we show that plasma density gradients in the direction of beam flow strongly modify the time-space evolution of the two-stream instability. The theory is supported by computer experiments, and is applied to determine lower bounds to the interaction length of relativistic electron beams with small plasma targets.

For a homogeneous plasma, the beam-plasma interaction (nonresonant electron-electron two-stream) evolves essentially as an absolute instability with very large growth rate. We are considering the strongest hydrodynamic interaction, that is, in the absence of such effects as temperature, collisions, or finite transverse dimensions, all of which diminish the growth rate in a way that is well known.[1] In the nonlinear regime the instability is quenched by particle overtaking and trapping, and can lead to appreciable heating of the plasma electrons.[2] We wish to point out that a plasma density gradient in the beam flow direction changes the evolution of this instability in an important way. We show this by determining the Green's function solution for the problem. We also show that this is confirmed by computer simulations, and that we can determine the onset of the nonlinear regime with respect to the beam injection boundary. The variation of plasma density along the beam flow direction is inherent in beam-plasma experiments, for example, where the plasma is confined by a mirror magnetic field. Recent developments in high-current relativistic beams, and their intense beam-plasma interactions,[3] have made it possible to use such beams to heat the plasma around a pellet.[4] Such plasmas, again, are inherently inhomogeneous. We apply our results to such examples and determine the beam characteristics required for a strong interaction.

The simplest model equations for the problem are the linearized hydrodynamic equations in one space dimension for cold-beam and cold-plasma electrons, combined with Maxwell's current equation. The Green's function equation for the current density may then be written in normalized variables as

$$\left[g(y) + \frac{\partial^2}{\partial\tau^2}\right]\frac{\partial^2}{\partial y^2} j + \frac{\partial^2}{\partial\tau^2} j = \delta(y)\,\delta(\tau), \tag{1}$$

where $y = \omega_b x/v_o$, $\tau = \omega_p(t-x/v_o)$, ω_p is the maximum plasma frequency of interest, $\omega_b^2 = 4\pi n_b e^2/m\gamma^3$ is the beam plasma frequency for relativistic electrons, $\gamma = \left(1-v_o^2/c^2\right)^{-1/2}$,

and $g(y) = \omega_p^2(y)/\omega_p^2 = n_p(y)/n_p$ represents the density profile. The perturbed beam current density $J(x,t)$ is related to $j(y,\tau)$ by $J(x,t) = j[y(x), \tau(t,x)]$. To specify the problem completely, the boundary conditions are $j(y,\tau) = 0$ for $y \leq 0$, and $j(y,\tau) = 0$ for $\tau \leq 0$. We choose a linearly increasing density profile for our model of the inhomogeneous plasma, such that $g(y) = \epsilon y + g_o$, where $\epsilon = (1-g_o)(\omega_b L/v_o)^{-1}$, $g_o = n_p(0)/n_p = \omega_p^2(0)/\omega_p^2$, and $L/(1-g_o)$ is the scale length of the density gradient. We can solve this problem exactly in terms of a contour integral representation:

$$j(y,\tau) = \frac{1}{2\epsilon}\int_\Gamma d\alpha \left[\frac{\alpha^2-g}{\alpha^2-g_o}\right]^{1/2} e^{i\alpha\tau}\left\{J_1\left[\frac{2\alpha}{\epsilon}(\alpha^2-g)^{1/2}\right]\right.$$

$$\left. \cdot\, Y_1\left[\frac{2\alpha}{\epsilon}\left(\alpha^2-g_o\right)^{1/2}\right] - J_1\left[\frac{2\alpha}{\epsilon}\left(\alpha^2-g_o\right)^{1/2}\right] Y_1\left[\frac{2\alpha}{\epsilon}(\alpha^2-g)^{1/2}\right]\right\}. \tag{2}$$

Here J_1 and Y_1 are Bessel functions of order 1 and Γ is a Laplace contour below all singularities. The representation is also valid in the homogeneous plasma limit, which can be recovered from (2) by making $g_o \to 1$ and expanding the asymptotic result in a power series in ϵy.

A more convenient representation can be derived by carrying out the contour integration in (2) around the branch cuts and poles, which leads to the real integral representation

$$j(y,\tau) = -\frac{2}{\epsilon}\int_{g_o^{1/2}}^{g^{1/2}} ds \left[\frac{g-s^2}{s^2-g_o}\right]^{1/2} \sin s\tau\, J_1\left[\frac{2s}{\epsilon}\left(s^2-g_o\right)^{1/2}\right] I_1\left[\frac{2s}{\epsilon}(g-s^2)^{1/2}\right]$$

$$+ \frac{(g-g_o)^{1/2}}{g_o} I_1\left[\frac{2}{\epsilon} g_o^{1/2}(g-g_o)^{1/2}\right] \sin g_o^{1/2}\tau. \tag{3}$$

The first term is a pulselike solution. The second term arises from the localized excitation of plasma oscillations that persist into a steady state because our plasma model has neither collisions nor thermal diffusion, either of which would damp it out. Hence we ignore this term in describing the pulse response. We focus our interest on the inhomogeneous plasma and consider $g_o \ll 1$. Then for $\epsilon\tau^2/8 > 1$ and $\epsilon\tau^2/16y < 1$ we are able to get a stationary phase approximation to the integral in (3), which is

$$j(y,\tau) \sim \left[\frac{2y}{\epsilon}\right]^{1/2} (1-\epsilon\tau^2/16y)^{1/2}\, I_1[(\tau/2)(\epsilon y)^{1/2}(1-\epsilon\tau^2/16y)^{1/2}] \cos(\epsilon\tau^2/8)/(\epsilon\tau^2/8). \tag{4}$$

In Fig. IX-21a we compare the numerically calculated j from formula (3) (with the

omission of the second term) taking $g_o = 0$ with (4) for a small y, where the approximation should be only fair. In Fig. IX-21b we show a picture of the perturbed current waveform. The amplitude maximum computed from (4) can easily be retrieved. Its locus is given by $j_{max} = (g-g_o)^{-1/2} I_1(y)$. The position and time of arrival of the maximum are related by $y_m = \epsilon\tau_m^2/8$, and hence fall within the validity of (4). The velocity of the pulse maximum as a function of time is $v_m = v_o\left[1 - \left(1+\omega_p^2 v_o t/2L\omega_b^2\right)^{-1/2}\right]$, and the time taken for the pulse maximum to arrive at a point x is $t = v_o^{-1}\left[x + 2\omega_b(2Lx)^{1/2}\omega_p^{-1}\right]$.

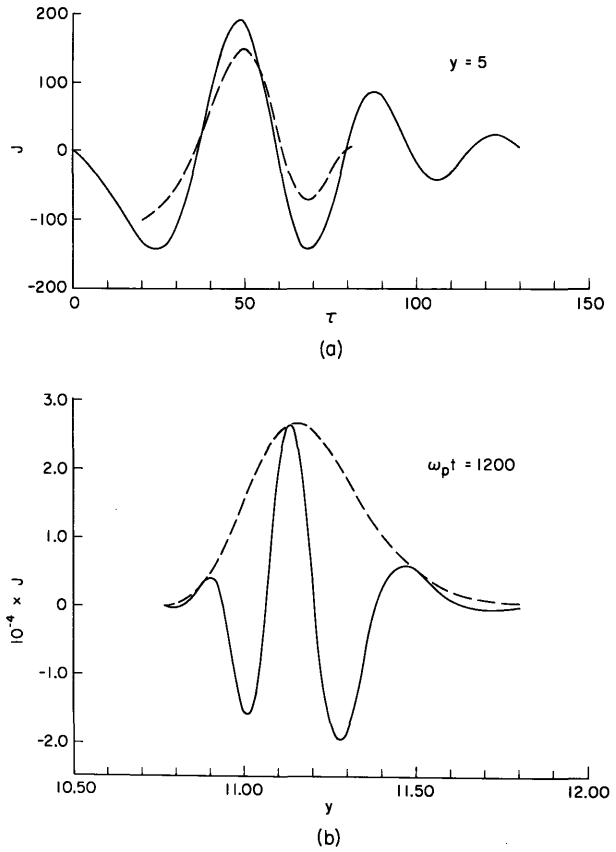

Fig. IX-21. Pulse evolution in space and time for $\epsilon = (\omega_b L/v_o)^{-1} = 10^{-2}$.

(a) Current pulse waveform for a fixed point in space (y = 5) and $n_p(0) = g_o = 0$ as a function of τ. The solid line was calculated numerically from the exact solution, Eq. 3, omitting the steady-state term; the dashed curve was calculated from the approximate Eq. 4. The accuracy of Eq. 4 increases for larger y.

(b) Picture of the current pulse waveform calculated from Eq. 4, where $\omega_p\tau = 1200$, and $\omega_b^2/\omega_p^2 = 10^{-4}$. Dashed line indicates the pulse envelope.

The steady-state amplitude of a sinusoidal excitation $\delta(y)\cos \alpha\tau$ can be written immediately from (2); for $\alpha > g^{1/2}$ it is just 2π times the integrand of (2). For $\alpha = g_o^{1/2} < g^{1/2}$, by analytic continuation, and ignoring the plasma resonance solution,[5] we get

$$j(y,\tau) = \frac{\pi}{\epsilon^2} g_o^{1/2}(g-g_o)^{1/2} I_1\left[\frac{2}{\epsilon} g_o^{1/2}(g-g_o)^{1/2}\right] \sin g_o^{1/2}\tau. \tag{5}$$

The plasma resonance solution is again related to the second term in Eq. 3 and is singular at the origin. This singularity, however, is removed by the inclusion of either plasma collisions or temperature. In Fig. IX-22 we reproduce the results of the computer experiments done by Davis and Bers,[6] where the beam is velocity modulated at the origin. Equation 5 is the steady-state current density resulting from a unit current density modulation at the origin; this can easily be related to a velocity modulation amplitude at the origin v(0, 0) to give

$$J(x,t) = ev(0,0)(n_p n_b)^{1/2}\left[\gamma^3(1-g_o)\, x/L\right]^{1/2} I_1\left[2(\omega_b/v_o)\left(\frac{g_o x L}{1-g_o}\right)^{1/2}\right] \sin \omega_{po}(t-x/v_o). \tag{6}$$

The locus of amplitude maxima for the transient can then be found approximately from (4):

$$j_m \sim ev(0,0)(\epsilon^2/\pi)\left[\gamma^3 n_b n_p/g_o\right]^{1/2} (L/x)^{1/2} I_1(\omega_b x/v_o). \tag{7}$$

Comparing (7) with (6), we find that at any position the steady-state current density is always larger than the maximum transient current density at the same position. This, together with Fig. IX-22, shows that the steady state prevails near where the beam is injected, and determines the onset of the nonlinear regime. We find this to occur at the position where the steady-state perturbed current density becomes equal to the dc current density $en_b v_o$.

We now consider the case in which the waves grow from the noise level in the plasma. From the equipartition theorem for plasmas,[7] we can make an estimate of the amplitude of the fluctuating electric field near the beam entrance. This gives $E_o \sim (12\pi)^{1/2} \times e(n_{po}/\lambda_{Do})^{1/2}$, where λ_{Do} is the Debye length at y = 0, and e is the electronic charge. Using this as the amplitude of a driving electric field on the beam at y = 0, we find the steady-state current density to be (5) multiplied by $(\epsilon/\pi g_o^{1/2})(\omega_b \lambda_{Do} \omega_p E_o/4\pi v_o)$. By equating this current density to $en_b v_o$ we then arrive at

$$N_{Do}^{-1/2}(\gamma n_p/n_b)^{3/2}\, g_o(\omega_b\lambda_{Do}/v_o)^2\, [(1-g_o)\, x/L]^{1/2}\, I_1[2(\omega_b L/v_o)(g_o/1-g_o)^{1/2}\, (x/L)^{1/2}] = 1, \tag{8}$$

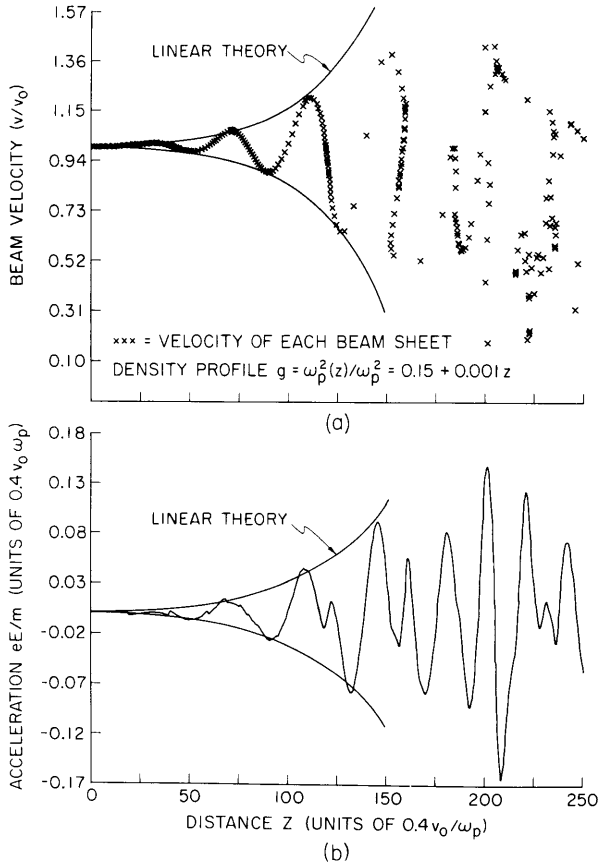

Fig. IX-22. Results of computer experiments.[6] In this experiment $g_o = 0.15$, $\epsilon = 35.4 \times 10^{-3}$, $v(0,0)/v_o = 10^{-3}$, and $\omega_b^2/\omega_p^2 = 5 \times 10^{-3}$. The pictures were taken at $\tau = 300/\omega_p$ and a steady state seemed to be achieved up to a distance of 150. The beam is velocity modulated at the origin, and the frequency is ω_{po}. (a) Beam sheet velocity; envelope calculated from linear theory. (b) Acceleration of a test particle, eE/m; envelope calculated from linear theory. We note that the nonlinear regime sets in around z = 110. This is found to correspond to the point $J \sim en_b v_o$ in the steady state, whereas the peak amplitude of the transient at the same position is only $0.2\ en_b v_o$.

where $N_{Do} = (4/3)\pi\lambda_{Do}^3 n_{po}$, which gives an equation for the distance x at which nonlinear effects will set in. Since strong energy transfer from the beam to the plasma must occur in the nonlinear regime, Eq. 8 gives a lower bound for a plasma target thickness that may be heated by the two-stream instability. In Fig. IX-23 we show the locus of this lower bound for two extreme types of beam-plasma interaction. The solid curves are typical of a long plasma column, and show how the critical x increases with increasing plasma density gradient. The dashed curves are typical of a small pellet plasma;[8] here the plasma density gradient is fixed, and along each curve we see how the critical x may be reduced by increasing beam density.

In conclusion, we have shown that in the presence of a plasma density gradient in the direction of beam flow the beam-plasma interaction is convectively unstable and the entire unstable pulse propagates essentially with the beam velocity; the nonlinear regime along the beam path is reached where the oscillating beam current density

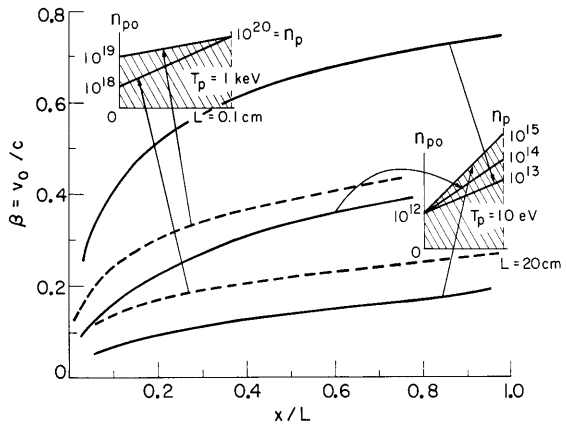

Fig. IX-23. Solution to Eq. 8 giving the locus of the normalized distance x/L, at which the nonlinear regime sets in, vs $\beta = v_o/c$. Solid curves refer to a plasma such that T_e = 10 eV, L = 20 cm, $n_b = n_{po} = 10^{12}/cm^3$. Each curve corresponds to a different maximum plasma density n_p, as indicated, and correspondingly different plasma density gradient. Dashed curves refer to a plasma presumed to result from a laser exploded pellet interacting with an electron beam with a current density of 10 MA/cm^2. The outer region of the plasma has a temperature $T_e = 10^3$ eV, L = 0.1 cm, and a maximum plasma density $n_p = 10^{20}/cm^3$. Each dashed curve refers to a different n_{po}. For the beam velocity range shown the beam density is in the range 10^{15}-$10^{16}/cm^3$.

amplitude equals the dc beam current density. This, coupled with the results of steady-state noise amplification in the presence of the plasma density gradient, can be used to estimate the constraints among plasma length and beam-plasma parameters that need be satisfied for transferring energy from the beam to the plasma. One of the examples in Fig. IX-23 shows that heating of small (0.1 cm) dense ($10^{19}/cm^3$) plasma targets by intense beams (10^7 A/cm^2) requires that these beams be of high density ($10^{16}/cm^3$).

References

1. See R. J. Briggs, in A. Simon and W. B. Thompson (Eds.), Advances in Plasma Physics, Vol. 4 (John Wiley and Sons, Inc., 1971). For relativistic beams, see E. A. Frieman, M. L. Goldberger, K. M. Watson, S. Weinberg, and M. N. Rosenbluth, Phys. Fluids 5, 196 (1962); G. Dorman, J. Plasma Phys. 2, 557 (1968); L. E. Thode and R. N. Sudan, Phys. Rev. Letters 30, 732 (1973).

2. J. A. Davis and A. Bers, in J. Fox (Ed.), Proceedings of the Symposium on Turbulence of Fluids and Plasmas (Polytechnic Press of the Polytechnic Institute of Brooklyn, New York, 1969), pp. 87-108; T. M. O'Neil and J. H. Winfrey, Phys. Fluids 15, 1514 (1972); A. K. Berezin et al., Zh. Eksp. Teor. Fiz. 63, 861 (1972) [Sov. Phys. – JETP 36, 453 (1973)].

3. A. T. Altyntsev, B. N. Breizman, A. G. Es'kov, O. A. Zolotovskii, V. I. Koroteev, P. Kh. Kurtmullaev, V. L. Masalov, D. D. Ryutov, and V. N. Semenov, in Proceedings of the Fourth International Conference on Plasma Physics and Controlled Nuclear Fusion Research, Madison, Wisconsin, 1971 (International Atomic Energy Agency, Vienna, 1972), Vol. 2, p. 309; P. A. Miller and G. W. Kuswa, Phys. Rev. Letters 30, 958 (1973); C. A. Kapetanakos and D. A. Hammer, Appl. Phys. Letters 23, 17 (1973).

4. For a recent descriptive review see Phys. Today, Vol. 26, No. 4, p. 17, April 1973.

5. See H. M. Schneider, Sc.D. Thesis, Department of Electrical Engineering, M.I.T., October 1968 (unpublished).

6. J. A. Davis and A. Bers, in Symposium on Computer Simulation of Plasma and Many-Body Problems, NASA Report SP-153, Washington, D.C., 1967, p. 217; J. A. Davis, Ph.D. Thesis, Department of Electrical Engineering, M.I.T., June 1968 (unpublished).

7. G. Bekefi, Radiation Processes in Plasmas (John Wiley and Sons, Inc., New York, 1966), p. 125.

8. As an example we chose parameters of a plasma surrounding a laser-heated compressing pellet; see J. Nuckolls, J. Emmet, and L. Wood, Phys. Today, Vol. 26, No. 8, August 1973, see Figure 4, p. 51.

IX. PLASMA DYNAMICS

C. Experimental Studies — Waves, Turbulence, and Radiation

1. WAVE CONVERSION NEAR LOWER HYBRID RESONANCE

National Science Foundation (Grant GK-37979X)

Mario Simonutti, Ronald R. Parker

Introduction

The theory of linear wave conversion near lower hybrid resonance in an inhomogeneous plasma, a process first noted by Stix,[1] is being studied in the framework of a self-consistent small-signal linear theory based on the moment equations with an isotropic pressure law. Despite the long period of interest in the mode conversion process in a plasma, an interest resulting from its possible application to plasma heating with radio-frequency power, there is no direct evidence confirming the existence of that process in a plasma. We feel that the reason for this is the lack of an adequate understanding of the complete problem. Our objective is to study sufficiently the theory of mode conversion near lower hybrid resonance (LHR) to determine conditions on the plasma parameters and driving source configuration to be used in the design of an experiment in which mode conversion might best be observed. Only after direct evidence of this process is obtained will it be possible to consider seriously the design of a well-understood RF heating scheme based on that process. Progress and plans toward achieving this goal are reported here.

Moment Equation Theory

The full theory represented by the linearized moment equations with an isotropic pressure law can be cast in the form of a linear dynamic system in physical variables, particle densities and velocities, and electromagnetic fields. We show that the system exhibits the mode conversion process. The form of a linear system presented here allows us to include proper zero-order effects and consider small-signal power and its conservation. This treatment differs markedly from the usual method of dealing with the problem through a differential equation in a single dependent variable that has no direct relation to any of the physical variables and whose coefficients are approximate.[1,2] These coefficients are taken generally from the homogeneous plasma dispersion relation polynomial and must be made linear in the independent variable, since an asymptotic method of solution is usually applied.

The moment equations upon which this report is based are, for each species, the continuity equation and the momentum equation without collisions

$$\frac{\partial \rho_s}{\partial t} + \nabla \cdot \rho_s \bar{v}_s = 0 \tag{1}$$

$$\rho_s m_s \left(\frac{\partial \bar{v}_s}{\partial t} + \bar{v}_s \cdot \nabla \bar{v}_s \right) = \rho_s q_s (\bar{E} + \bar{v}_s \times \bar{B}) - \nabla P_s, \tag{2}$$

where the subscript s indicates particle species. We consider an electron e and single ion species i plasma. Maxwell's equations and a relation between pressure P_s and density ρ_s complete the system. Since collisions are not included, the system is lossless. The equations are solved in the zero order and then linearized in the dependent variables to derive the first-order system. We assume the absence of zero-order drifts parallel to the magnetic field, and the absence of a zero-order electric field.

The zero-order relation between pressure and density is taken as $P_{s,o} = \rho_{s,o} K T_s$, where the species temperature T_s need not be independent of position in the method, but for convenience it will be taken as constant. For a homogeneous plasma, the zero-order solution is trivial; however, for a plasma with a nonuniform density profile zero-order diamagnetic drifts with an associated variation in the zero-order magnetic field $\bar{B}_o$ are predicted. These effects would normally be considered sufficiently small for a low beta plasma so that they should have little effect on the basics of the first-order wave propagation process. In order that the solution satisfy small-signal power conservation, it is essential that they be included, as we shall show. In previous treatments of the problem[1,2] it was impossible to include these zero-order effects, since the equations were derived from considerations of a purely homogeneous plasma.

The diamagnetic drifts are given by the expression

$$\bar{v}_{s,o} = \frac{\bar{B}_o \times \nabla P_{s,o}}{\rho_{s,o} q_s B_o^2} \tag{3}$$

and the associated zero-order magnetic field is given by

$$\frac{1}{2} \frac{B_o^2}{\mu_o} + \sum_s \rho_{s,o} K T_s = \text{constant}, \tag{4}$$

where $\rho_{s,o}$ depends on position according to the imposed density profile. The subscripts zero and one indicate the order of the variables, except in the term μ_o.

A rectangular coordinate system is chosen (see Fig. IX-24) in which $\rho_{s,o}$ and $\bar{B}_o$ vary only in the x direction; $\bar{B}_o$ is in the z direction; y and z are directions of zero-order uniformity. Diamagnetic drifts are then only in the y direction.

The electrostatic approximation $E_1 = -\nabla \phi_1$ is made for the first-order system. The dynamic equations are linearized while taking into account proper zero-order conditions. In order to obtain the driven linear response of the plasma to a fixed frequency source, all first-order variables are taken to have $\exp(i\omega t)$ time variation and complex amplitude.

The y and z spatial dependence is transformed as $\exp(-i(k_y y + k_z z))$ and each k_y, k_z spectrum component of the solution is considered separately. Responses with y and z dependence other than sinusoidal may be determined by Fourier synthesis. Since a

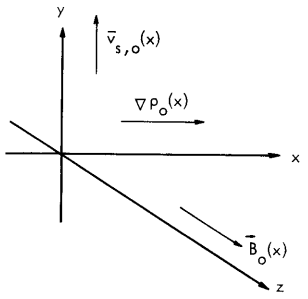

Fig. IX-24.
Coordinate system for the problem.

boundary-value problem is considered in which the boundary conditions are actually radiation conditions, no source term appears explicitly. The relation between the first-order density and pressure is taken as the linearized form of

$$\frac{P_s}{\rho_s^\gamma} = \text{constant} \tag{5}$$

which is $P_{1,s} = \gamma\rho_{1,s} KT_s$.

The linear system obtained under these conditions is

$$\frac{d}{d(k_o x)} \bar{\bar{Y}}(k_o x) = \bar{\bar{A}}(k_o x)\, \bar{\bar{Y}}(k_o x), \tag{6}$$

where the components of $\bar{\bar{Y}}(k_o x)$ are

$$\bar{\bar{Y}}(k_o x) = \begin{bmatrix} \sqrt{\frac{1}{2}\rho_{i,o_{LHR}} m_i}\, v_{i,1_x} \\ \sqrt{\frac{1}{2}\rho_{e,o_{LHR}} m_e}\, v_{e,1_x} \\ \sqrt{\frac{\gamma KT_i}{2\rho_{i,o_{LHR}}}}\, n_{i,1} \\ \sqrt{\frac{\gamma KT_e}{2\rho_{e,o_{LHR}}}}\, n_{e,1} \\ \sqrt{\frac{1}{2}\epsilon_o}\, \phi_1' \\ \sqrt{\frac{1}{2}\epsilon_o k_o^2}\, \phi_1 \end{bmatrix} \equiv \begin{bmatrix} V_i \\ V_e \\ N_i \\ N_e \\ \Phi' \\ \Phi \end{bmatrix} \tag{7}$$

$$
\overline{\overline{A}} = \begin{bmatrix}
\dfrac{-\rho_o'(k_o x)}{k_o \rho_o(k_o x)} & 0 & \dfrac{ic}{\sqrt{\frac{\gamma}{3}} V_{Ti}} \dfrac{\rho_{o_{LHR}}}{\rho_o(k_o x)} \left(\dfrac{\gamma}{3} \dfrac{v_{Ti}^2}{c^2} n_z^2 - 1 \right) & 0 & \dfrac{i\omega_{pi_{LHR}}}{\omega} n_z^2 & 0 \\
0 & \dfrac{-\rho_o'(k_o x)}{k_o \rho_o(k_o x)} & 0 & \dfrac{ic}{\sqrt{\frac{\gamma}{3}} v_{Te}} \dfrac{\rho_{o_{LHR}}}{\rho_o(k_o x)} \left(\dfrac{\gamma}{3} \dfrac{v_{Te}^2}{c^2} n_z^2 - 1 \right) & \dfrac{-i\omega_{pe_{LHR}}}{\omega} n_z^2 & 0 \\
\dfrac{ic}{\sqrt{\frac{\gamma}{3}} V_{Ti}} \dfrac{\rho_o(k_o x)}{\rho_{o_{LHR}}} \left(\dfrac{\omega_{ce_{LHR}}^2}{\omega^2} - 1 + \dfrac{1}{3} \dfrac{v_{Ti}^2}{c^2} M(k_o x) \right) & 0 & \dfrac{1}{\gamma} \dfrac{\rho_o'(k_o x)}{k_o \rho_o(k_o x)} & 0 & 0 & \dfrac{-c}{\sqrt{\frac{\gamma}{3}} v_{Ti}} \dfrac{\omega_{pi_{LHR}}}{\omega} \dfrac{\rho_o(k_o x)}{\rho_{o_{LHR}}} \\
0 & \dfrac{ic}{\sqrt{\frac{\gamma}{3}} V_{Te}} \dfrac{\rho_o(k_o x)}{\rho_{o_{LHR}}} \left(\dfrac{\omega_{ce_{LHR}}^2}{\omega^2} - 1 + \dfrac{1}{3} \dfrac{v_{Te}^2}{c^2} M(k_o x) \right) & 0 & \dfrac{1}{\gamma} \dfrac{\rho_o'(k_o x)}{k_o \rho_o(k_o x)} & 0 & \dfrac{c}{\sqrt{\frac{\gamma}{3}} V_{Te}} \dfrac{\omega_{pe_{LHR}}}{\omega} \dfrac{\rho_o(k_o x)}{\rho_{o_{LHR}}} \\
0 & 0 & 0 & 0 & 0 & 1 \\
0 & 0 & \dfrac{-\omega_{pi_{LHR}}}{\omega} \dfrac{c}{\sqrt{\frac{\gamma}{3}} V_{Ti}} & \dfrac{\omega_{pe_{LHR}}}{\omega} \dfrac{c}{\sqrt{\frac{\gamma}{3}} V_{Te}} & n_z^2 & 0
\end{bmatrix}
$$

where $M(k_o x) = \dfrac{\rho_o''(k_o x)}{k_o^2 \rho_o(k_o x)} + \left(\dfrac{\rho_o'(k_o x)}{k_o \rho_o(k_o x)} \right)^2 \left(N \dfrac{\rho_o(k_o x)}{\rho_{o_{LHR}}} \dfrac{\omega^2}{\omega_{ce_{LHR}}^2} - 1 \right)$

where $N = \left(\dfrac{m_i}{Z m_e} \right)^2 \dfrac{v_{Ti}^2}{3c^2} \dfrac{\omega_{pe_{LHR}}^2}{\omega^2} + \dfrac{v_{Te}^2}{3c^2} \dfrac{\omega_{pe_{LHR}}^2}{\omega^2}$

and $\dfrac{1}{2} m_s v_{Ts}^2 = \dfrac{3}{2} K T_s$

Fig. IX-25. Matrix $\overline{\overline{A}}(k_o x)$ of the linear dynamic system.

and $\bar{\bar{A}}(k_o x)$ is given in Fig. IX-25 for the case $n_y = 0$. For parameters and modes of interest, n_y would be negligibly small and the dependence of the results on k_y is weak.

All dependent variables have the units of energy density to the 1/2 power. The x distance coordinate is normalized to $k_o x$ by the free-space wave number $k_o = \frac{\omega}{c}$. We did this because published work on this problem deals generally with the indices of refraction $n_x = k_x/k_o$, n_y, and n_z, rather than wave numbers k_x, etc. In turn, thermal velocities are normalized to c, the speed of light. The elements of $\bar{\bar{A}}$ are dimensionless.

The wave-conversion condition generally exists at a density near the cold-plasma LHR density, which is determined by ω, B_o, ion-to-electron mass ratio, and ion charge, and is independent of n_z and temperature. Therefore the density $\rho_{o_{LHR}}$ is convenient for normalization. Of course, with finite plasma temperature the actual physics of the cold-plasma LHR is replaced by warm-plasma (moment equation) theory. An important dimensionless parameter describing the plasma is ω_{pe}/ω_{ce}, determined by $\rho_{o_{LHR}}$, which might correspond to the maximum plasma density, and the steady magnetic field $\bar{B}_o$.

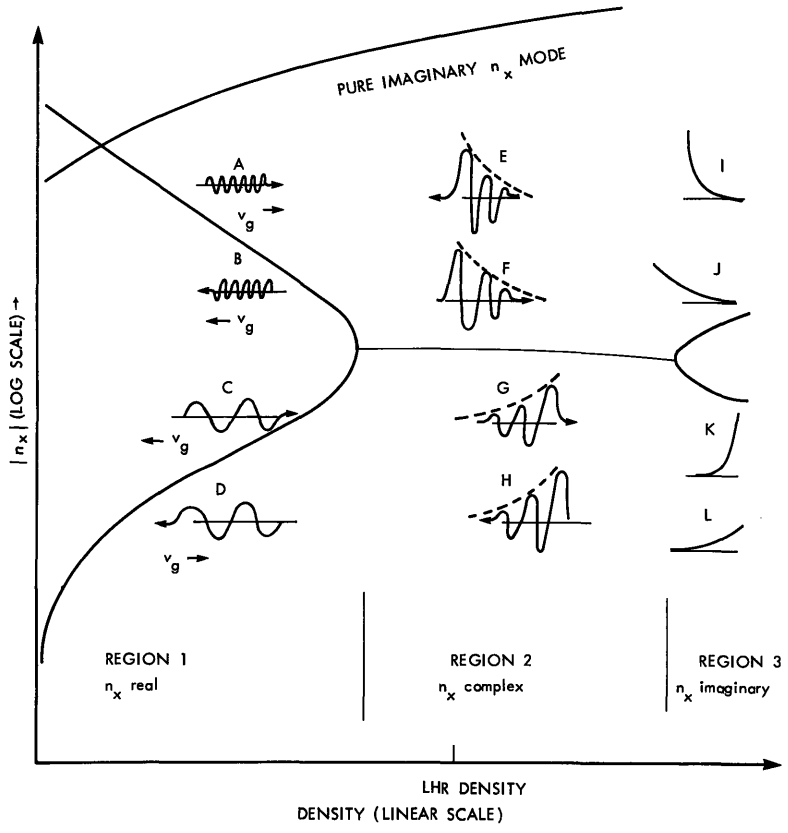

Fig. IX-26. Typical wave number (n_x) vs density around conditions of wave conversion.

In regions of constant plasma density, the matrix $\overline{\overline{A}}(k_o x)$ is constant and the eigenvalues λ of $\overline{\overline{A}}$ are directly related to the wave numbers n_x of the exact modes of oscillation of the system in the uniform region by $\lambda = -in_x$. The dependence of these wave numbers on plasma density and the parameters n_z, T_e, and T_i has been discussed in a previous report.[4] Figure IX-26 represents such a plot of the magnitude of the wave numbers vs plasma density. Since the wave numbers appear in plus and minus pairs, only three branches are shown. The density profile scale lengths for this problem are much larger than the inverse of the wave numbers; therefore, these diagrams are useful for describing the local characteristics of possible waves in different plasma density regions.

We made a check on the validity of the electrostatic approximation for the parameters of this problem. Through formulation of a similar matrix eigenvalue problem from the same moment equation theory, together with the full set of Maxwell's equations, plots of wave number against density were obtained. This is an eighth-order system. Essentially, we found that when the accessibility condition[3] is well satisfied, the results in the electrostatic approximation are in excellent agreement for the modes of interest.

The linear system here is of sixth order where two of the wave numbers are pure imaginary with magnitude generally much greater than that of the remaining four. For such densities, the magnitude of those two imaginary wave numbers can be given approximately by

$$|n_x|^2 = \frac{\omega_{ce}^2}{\omega^2}\left(\frac{c^2}{v_{Te}^2} - n_z^2\right).$$

No physical significance is attached to these modes, and we shall neglect them for the moment. When we find the mathematical solution to the system, they must be dealt with appropriately.

The density dependence of the four wave numbers of interest is characteristic of a system displaying the mode conversion process in the sense that two separate branches of pure real n_z merge at some density. In Fig. IX-26 diagrams indicate the nature of the x-dependence of the waves and the signs of their x-directed phase and group velocities for the three density regions where the wave numbers of interest are real, complex, and imaginary.

In his treatment of the problem by applying transform and asymptotic methods, Stix first pointed out that such wave number vs density dependence implies that mode D (A) with group velocity directed toward the conversion density region in an increasing density profile plasma should completely convert to mode B (C) whose x-directed group velocity is opposite to that of the original mode. The absence of a reflected component having its wave number of equal magnitude but with opposite sign of the incident mode

wave number constitutes a complete conversion in the mathematical sense. An attractive RF plasma-heating scheme based on this concept was proposed by Stix.[1] The nature of the wave-number dependence vs density provides for a smooth transition for propagation from long wavelengths at an RF source located at the outside edge of the plasma to short wavelengths at the center of the plasma. With mode conversion the wavelength would continue to decrease until strong damping takes place. This heats the plasma through short wavelength effects that are not included in the moment equation theory.

In the theoretical treatment by Stix, direct connection to a physical sense of power carried by the waves in the plasma cannot be drawn. Also, the asymptotic solution cannot be used to determine the nature of the fields in the plasma in the critical wave conversion region. Our solution does not have these limitations.

Numerical Solution

The linear system that we have derived can be solved numerically as an initial value problem in ordinary differential equations. Various effective routines are readily available; we use an Adams-Moulton multistep method. The plasma density profile chosen for this problem is composed of two half-spaces of uniform and differing density joined by a transition region of smoothly varying density taken to have a half-cycle cosine variation with x (see Fig. IX-27). The two uniform density values are chosen so that

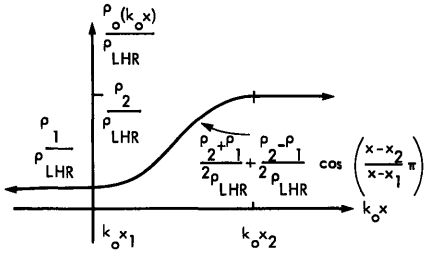

Fig. IX-27.
Density profile of the inhomogeneous plasma.

the wave conversion condition is satisfied somewhere in the transition region, and the greater uniform density value corresponds to one in Regions 2 or 3 in Fig. IX-26. Region 2 will be used in this discussion. The choice of two uniform density regions about the transition allows exact analysis of the solution in those regions in terms of the readily and precisely determined homogeneous plasma modes.

A source of radiation is taken to be located in the lower density region and to radiate power toward Region 2 by mode D. The existence of the shorter wavelength mode A in Region 1 is ruled out on the physical grounds that any radiation source would couple mainly to the longer wavelength mode D which has its wavelength in the lower density region much closer to the free-space wavelength than mode A does. Also, any component of A that may be excited by the source would be strongly damped out very near

the source, since the wavelength is so short.

In Region 2, modes G and H are ruled out because they grow exponentially to unlimited amplitudes with increasing x. Therefore we must find a solution to the linear system in which there is no component of A in Region 1, and no component of G or H in Region 2. The radiation boundary condition problem can be solved by initial value problem methods. Two separate numerical solutions to Eq. 7 have been found where the $\overline{Y}$ initial values at some starting point located in Region 2 are the eigenvectors of the matrix $\overline{\overline{A}}$ corresponding to modes E and F. In general, each of the two solutions will in part yield a component of mode A in Region 1. Based on the linearity of the problem, a linear combination of these two solutions that has no component of mode A in Region 1 is formed. This result satisfies the differential equation and the radiation conditions and, therefore, is taken as the solution to the problem.

Special treatment must be given to the two modes mentioned above which are of no physical interest but have a certain mathematical presence. Round-off error in the computation process quickly brings into the solution a component of the problem mode that grows strongly in the direction of solution. Unattended, the violent growth of this mode would quickly swamp the modes of interest numerically. We periodically analyze the solution as it is generated for the component corresponding to this problem mode, and subtract that component from the solution that is being generated. The justification for this method in a homogeneous plasma is sound. The plasma considered here is inhomogeneous. The problem mode, however, has weak density dependence and its growth scale length is much shorter than the density profile scale length. Therefore the mode is treated locally on a homogeneous plasma basis with apparent success.

In the actual solution of the problem we find that only the partial solution with the eigenvector corresponding to mode E as the initial value in Region 2 is required, since the result is that essentially modes C and A are completely absent in Region 1. Therefore in Region 1 ingoing mode D completely converts to outgoing mode B.

The solutions for variables N_e and Φ, among the 6 variables of the system, are presented in Figs. IX-28 and IX-29 in terms of RF amplitude and phase as a function of $k_o x$. The solutions become exponentially small in Region 2, and give a standing-wave pattern of the interference of two traveling waves of different wavelengths in Region 1. The fields in the wave-conversion region are well-behaved and display a mild maximum consistently in that region. Note that the two variables have different spatial dependence. The phase plot indicates that in Region 1 the variable Φ is mainly the result of mode C, while the variable N_e is mainly the result of mode B.

The parameters of the problem for the solutions presented here correspond to those of a small laboratory type of plasma except that for clarity we have taken a small density profile scale length. Longer scale lengths result in more oscillations in the solution and this is more difficult to present graphically. The general nature of the solution for

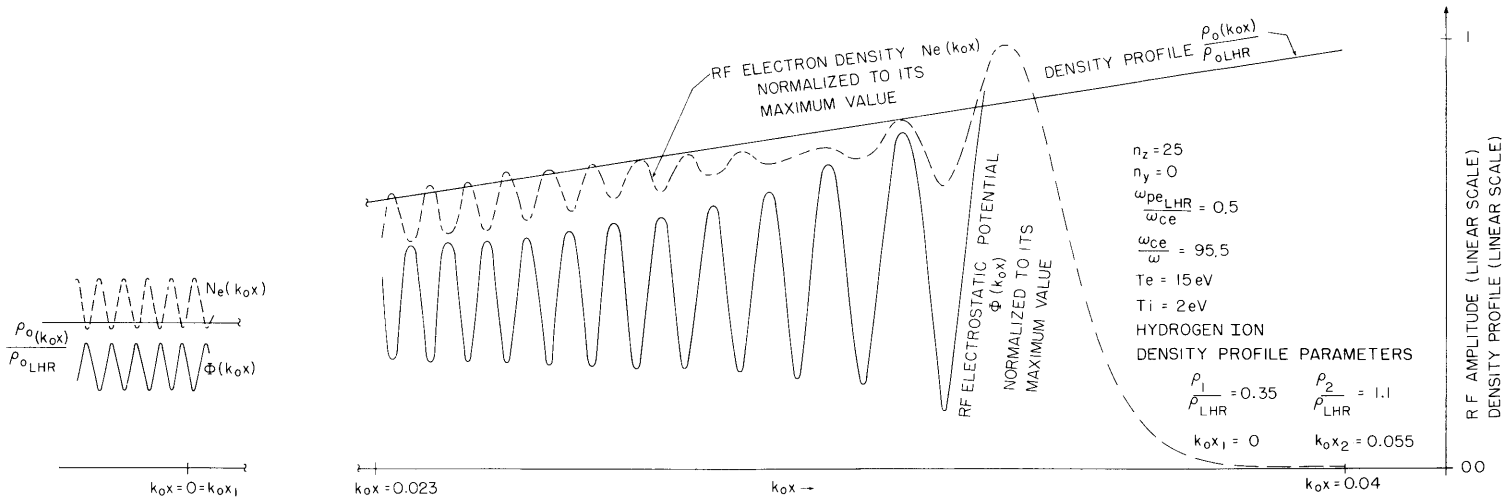

Fig. IX-28. Magnitude of the solution for the variables N_e and Φ.

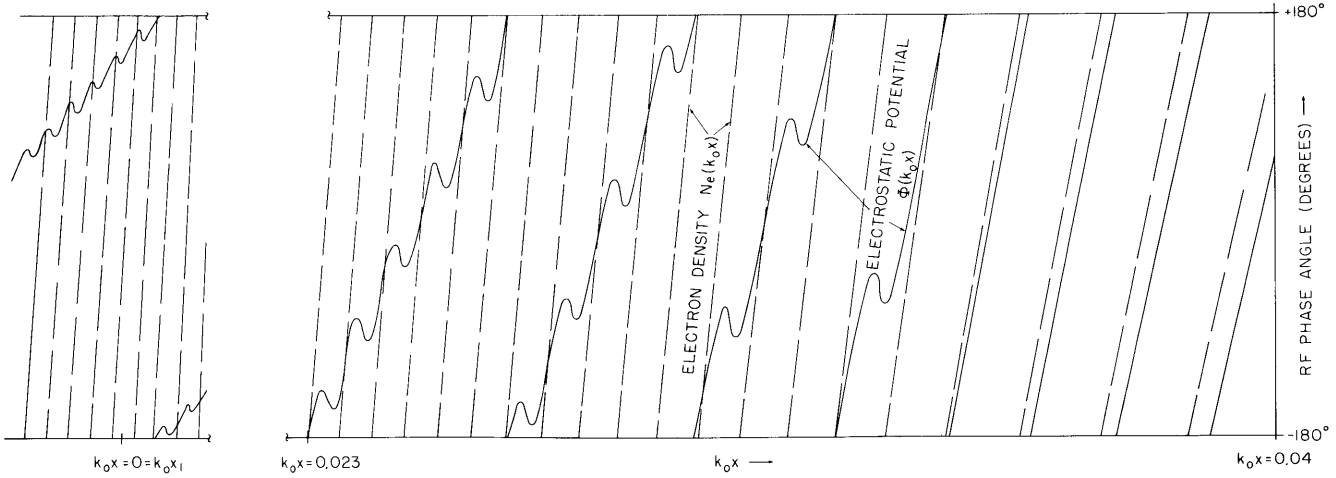

Fig. IX-29. Phase angle of the solution for the variables N_e and Φ.

greater scale lengths is similar and has properties in close correspondence with information from the wave number vs density plots, as the solution here does.

The applicability of this purely numerical method of solution does have the limitation that as the scale lengths are increased and/or the local wavelengths in the plasma are decreased by a change in parameters, the number of cycles of oscillation in the solution may increase to the extent that the accuracy of the numerical solution is poor. Physically meaningful plasma and source configurations that can be treated include lower density laboratory-scale plasmas. It is on such plasmas that the wave conversion might most readily be observed, since diagnostic probes of various types may be inserted directly into such plasmas to measure RF field patterns.

Small-Signal Conservation Theorems

A general small-signal conservation theorem for a set of linear differential equations in nontransformed variables describing a physical system is of the form

$$\nabla \cdot \bar{P}(\bar{r}, t) + \frac{\partial}{\partial t} E(\bar{r}, t) = L(\bar{r}, t), \tag{8}$$

where $\bar{P}$, E, and L are made up of second-order combinations of first-order variables. $\bar{P}$ would have the dimensions of power flux, E of energy density, and L of power per unit volume. We were not successful in obtaining a relation of this form for the warm, inhomogeneous, and anisotropic plasma system treated here, probably because of the degree of complexity involved in such problems. Some results were achieved, however, in the formulation of a complex small-signal conservation theorem in the transformed variables. The theorem provided a means for checking the numerical solution.

To obtain this theorem we take the complex conjugate of the first-order continuity equation, and the first-order momentum equation

$$\left| \frac{\gamma K T_s \rho_{s,1}}{\rho_{s,o}} \right| - i\omega^* \rho^*_{s,1} + \nabla \cdot \rho^*_{s,1} \bar{v}_{s,o} + \nabla \cdot \bar{v}^*_{s,1} \rho_{s,o} = 0 \tag{9}$$

$$\begin{aligned} v^*_{s,1} \cdot \Big| & i\omega \rho_{s,o} m_s \bar{v}_{s,1} + \rho_{s,o} m_s (\bar{v}_{s,o} \cdot \nabla) \bar{v}_{s,1} + \rho_{s,o} m_s (\bar{v}_{s,1} \cdot \nabla) \bar{v}_{s,o} \\ & + \rho_{s,o} q_s \nabla \phi_1 - \rho_{s,o} q_s \bar{v}_{s,1} \times \bar{B}_o - \rho_{s,1} q_s \bar{v}_{s,o} \times \bar{B}_o + \nabla \gamma K T_s \rho_{s,1} = 0. \end{aligned} \tag{10}$$

We perform the indicated scalar multiplication and vector dot product operation, and add together both equations for both species. After some manipulation, we find that for real ω, $\gamma = 1$, and $n_y = 0$,

$$\frac{d}{dx} \mathrm{Re} \left\{ \phi_1 J^*_{\mathrm{tot}, 1_x} + \sum_s \gamma K T_s \rho_{s,1} v^*_{s,1_x} \right\} = 0 \tag{11}$$

or

$$\mathrm{Re}\left\{\phi_1 J^*_{\mathrm{tot},1_x} + \sum_s \gamma K T_s \rho_{s,1} v^*_{s,1_x}\right\} = \text{constant.} \tag{12}$$

The requirement $\gamma = 1$ results, since this is the condition for consistent zero- and first-order pressure-density relations. $\bar{J}_{\mathrm{tot},1}$ is the total small-signal current density that is the sum of the true current and displacement current. The expression in parentheses is interpreted as the small-signal power. Power orthogonality of the homogeneous plasma modes can be proved along similar lines.

The numerical solution agrees with this continuity of small-signal power flux in the sense that in the homogeneous plasma of Region 1 the power associated with the total solution in that region was less than 0.1% of the power carried by the individual homogeneous plasma modes making up that solution. The total power in that region should go to zero because at the starting point in Region 2 the waves are evanescent and the associated small-signal power flux is zero, and the power flux should be constant, zero in this case, for all x. Such close cancellation was obtained only for the conditions $\gamma = 1$ and that the proper zero-order configuration was maintained consistently in the first-order system.

With the same expression for small-signal power, similar conservation was obtained for the case when n_y is nonzero and sufficiently large to influence the solution. We have not yet succeeded in showing analytically that such conservation must exist for that case. This is often a problem in small-signal power theorems, in that a relation is believed to exist but it may be very difficult to prove analytically.

Plans for Future Work

Now that we have developed a technique that can be applied to parameters of laboratory plasmas, we shall make a Fourier synthesis of an n_z spectrum of such solutions in order to calculate the field pattern in the plasma driven from a spatially localized antenna source. This is essentially an extension of the resonance-cone problem[3,5] for the case of a warm inhomogeneous plasma near lower hybrid resonance. We believe that the solution to this problem may provide the key to successful observation of some manifestation of the mode conversion process.

It appears that the single-wave (n_z) analysis is not directly applicable to laboratory arrangements. The nature of the propagation near the mode conversion region puts severe requirements on the degree of definition of the n_z spectrum of a practical antenna structure in an experiment if the single-wave analysis is to apply. Spatial harmonics in the source n_z spectrum will drive several coexisting modes whose individual character may be impossible to isolate. Also, it is known that the group velocity of the waves near the conversion layer has a direction nearly parallel to the magnetic field. This condition

leads to strong finite antenna length (finite n_z linewidth) effects. Both of these effects are explicitly included in the case of a localized source (resonance cone) analysis.

As the local wavelengths in the plasma approach the ion Larmor radius, the moment equation theory may fail. A study of the wave number vs density plots derived from the Vlasov theory for a plasma in a magnetic field could be made which would indicate the limitations of the moment equation theory. An objective in the design of a wave conversion demonstration experiment based on this work will be to minimize the Larmor radius effect. This can be accomplished in part by maintaining a small ω_{pe}/ω_{ce} parameter for the plasma.

References

1. T. H. Stix, "Radiation and Absorption via Mode Conversion in an Inhomogeneous Collision-free Plasma," Phys. Rev. Letters 15, 878 (1965).
2. A. D. Piliya and V. I. Fedorev, "Linear Wave Conversion in an Inhomogeneous Magnetoactive Plasma," Soviet Phys. – JETP 30, 653 (1970).
3. R. R. Parker, "Alcator Lower Hybrid Heating Experiment," Quarterly Progress Report No. 102, Research Laboratory of Electronics, M.I.T., July 15, 1971, pp. 97-111.
4. M. D. Simonutti and R. R. Parker, "Dispersion Relations (Wave Number vs Density) for Warm-Plasma Modes near Lower Hybrid Resonance," Quarterly Progress Report No. 110, Research Laboratory of Electronics, M.I.T., July 15, 1973, pp. 79-86.
5. R. K. Fisher and R. Gould, Phys. Fluids 14, 857 (1971).

IX. PLASMA DYNAMICS

D. General Theory

1. PARAMETRIC EXCITATION OF ION WAVES BY RESONANCE CONE FIELDS NEAR THE LOWER HYBRID FREQUENCY

U. S. Atomic Energy Commission (Contract AT(11-1)-3070)

Charles F. F. Karney, Abraham Bers

Introduction

In previous reports,[1,2] we described the excitation of ion acoustic, electrostatic ion cyclotron, and magnetosonic waves by parametric coupling from waves near the lower hybrid frequency in a highly magnetized plasma. We calculated coupling coefficients for these processes for the case of a homogeneous plasma, but allowed the waves to have various angles with respect to the magnetic field. In order to estimate the usefulness of these interactions for Tokamak plasmas we must now include the effects of finite geometry, inhomogeneity, and the fact that the RF energy of the pump must originate outside the plasma. The linear propagation of the fields near the lower hybrid frequency from the outside to the inside of an inhomogeneous plasma has been studied recently.[3] We adopt these results to describe the pump field inside the plasma. This field, propagating along resonance cones, is of finite spatial extent. Thus its various spatial Fourier components may couple to various low-frequency waves in the plasma. We shall apply our three-dimensional calculation of the possible couplings to describe the parametric down-conversion from a resonance cone pump field. The effect of plasma inhomogeneity on the parametric coupling will also be considered.

Linear Propagation of Pump Fields

To study the problem of an inhomogeneous plasma, we assumed that the pump fields are given by linear theory. Briggs and Parker[3] have studied this problem for a cold plasma in the electrostatic limit, and we use their theory to describe the pump fields in the plasma. We consider a plasma for which ∇n is a constant and perpendicular to $\bar{B}_o$. Such an arrangement is shown in Fig. IX-30.

We assume that a potential $\Phi_o(z)$ is set up at $x = 0$. Then the fields that are set up in the rest of the plasma can be Fourier-transformed in the y and z directions, which are directions of homogeneity. (We shall assume no variation in the y direction, that is, $k_y = 0$.) For any k_z there will be a complicated functional dependence of the fields on the x coordinate, but if the density gradient is weak enough, WKB methods may be used. Under this assumption at any point a local k_x can be identified, which satisfies the local linear dispersion relation. The WKB solution is

$$\Phi(x, k_z) = \Phi_o(k_z) \left[\frac{K_{||}(0)\, K_{\perp}(0)}{K_{||}(x)\, K_{\perp}(x)} \right]^{1/4} \exp\left(i \int_0^x k_x \, dx \right), \tag{1}$$

where $\Phi_o(k_z)$ is the Fourier transform of $\Phi_o(z)$, and

$$k_x(x) = k_z[-K_{||}(x)/K_{\perp}(x)]^{1/2}. \tag{2}$$

$K_{\perp}$ and $K_{||}$ are the x, x and z, z components of the cold-plasma dielectric tensor. In our case we take $\Omega_e^2 \gg \omega^2 \gg \Omega_i^2$. For Tokamak-type plasmas we assume that $\Omega_e^2 \gg \omega_{pe}^2$. Then

$$K_{\perp} \approx 1 - \omega_{pi}^2/\omega^2. \tag{3}$$

$$K_{||} = 1 - \omega_{pe}^2/\omega^2. \tag{4}$$

Note that with these values for $K_{\perp}$ and $K_{||}$ there will be a small region of evanescence in the low-density part of the plasma, where ω exceeds the local electron plasma frequency. This region is usually extremely thin, however, and numerical work by Puri and Tutter[4] shows that fields easily penetrate it. So we shall assume that the fields are given at a point of low density where the waves are propagating. (Note that for calculations of the impedance as seen by the external source this field would have to be calculated with special care because of the external electromagnetic structure that is used. This problem does not concern us here.)

Energy at x = 0 propagates into the plasma along the locus of the group velocity. This is given by the ray path z(x)

$$z(x) = \pm \int^x [-K_{||}/K_{\perp}]^{1/2} \, dx. \tag{5}$$

For $K_{\perp}$ and $K_{||}$ as given by Eqs. 3 and 4 this path is shown in Fig. IX-30. (Notice the greatly distorted scale of this figure.) The ray path, in fact, spends most of the time traveling very nearly parallel to $\bar{B}_o$ (see Fig. IX-31). Note that the trajectory given in Eq. 5 is independent of k_z. This means that if $\Phi_o(z)$ is confined to a region of width w_o, w_o will be the width measured in the z direction of the fields inside the plasma; so the width measured perpendicular to the ray will be $w \sim w_o(m_e/m_i)^{1/2}$ (see Fig. IX-31).

The ray stops penetrating and travels only along the magnetic field when it reaches the lower hybrid resonance layer $x = x_o$ at which point $\omega = \omega_{lh} \approx \omega_{pi}$. The cold-plasma assumption breaks down before this point is reached because the wavelength $(1/k_x)$ becomes comparable to the ion-cyclotron radius, and an exact description of the ray would have to include temperature effects. Some work along these lines has been done by Simonutti and Parker.[5] Their results (based on warm-fluid theory) indicate that wave

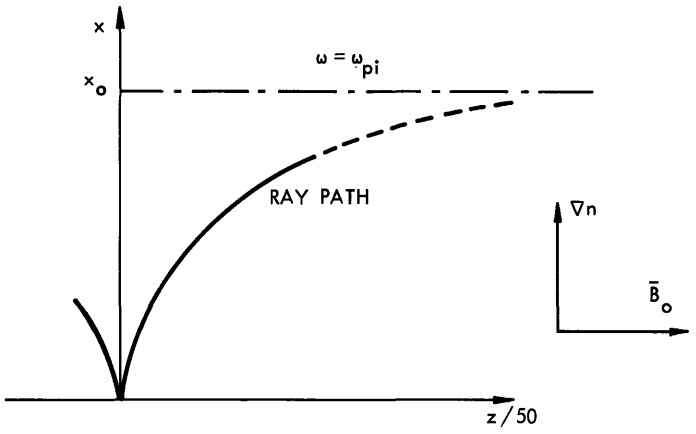

Fig. IX-30. General arrangement for the inhomogeneous plasma and ray path.

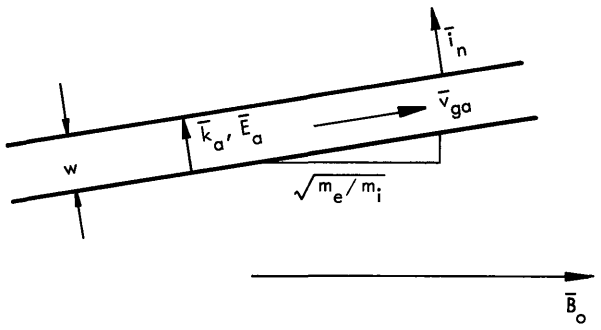

Fig. IX-31.
Segment of a ray at $x \approx x_o/2$.

conversion takes place at some point between $x_o/2$ and x_o for Tokamak plasmas.

Finally, we note that Eq. 1 predicts that as the field penetrates and its shape is distorted, its amplitude increases. The amplification factor for the magnitude of the electric field is approximately

$$\left[\frac{m_i}{m_e}\frac{x}{x_o}\right]^{1/4} (1-x/x_o)^{-3/4}. \tag{6}$$

For a hydrogen plasma, at $x = x_o/2$ ($\omega = \sqrt{2}\ \omega_{pi}$) this factor is approximately 10.

Growth Rates and Thresholds for Uniform Plasma

We shall now refer to results for growth rates that have been given by Karney.[6] In our notation a is the pump, b is the idler, and n is the signal, which is the wave that we are trying to excite. In Fig. IX-32 ω, k, and $\bar{k}$ diagrams are shown for coupling to ion acoustic waves, and in Fig. IX-33 for coupling to electrostatic ion cyclotron or magnetosonic waves.

For coupling to ion acoustic waves the growth rate γ_o in the absence of damping is

$$\frac{\gamma_o}{\omega_n} \approx \frac{v_{ai}}{4(\omega_a/k_a)} \left| \cos 2\alpha + i \frac{\Omega_i}{\omega_a} 5 \sin 2\alpha \sin \beta \right|, \tag{7}$$

where $v_{ai} = eE_a/(m_i\omega_a)$.

For coupling to electrostatic ion cyclotron waves

$$\frac{\gamma_o}{|\omega_b\omega_n|^{1/2}} \approx \frac{\omega_n^2 - \Omega_i^2}{4v_{te}k_{n\perp}\omega_n c_s} \left| v_{ae\parallel} + i \frac{\omega_{pe}}{\omega_a} \sin\psi v_{ae\perp} \right|, \tag{8}$$

where $v_{ae\parallel} = eE_{az}/(m_e\omega_a)$, and $v_{ae\perp} = E_a/B_o$.

Finally, for coupling to magnetosonic waves

$$\frac{\gamma_o}{|\omega_n\omega_b|^{1/2}} \approx \frac{1}{4} \frac{v_{ae\parallel}}{v_{te}}. \tag{9}$$

In the presence of damping the growth rate becomes $\gamma = \left(\gamma_o^2 - \gamma_b\gamma_n\right)^{1/2}$, where γ_b and γ_n are the damping rates of modes b and n. This leads to a threshold for the interaction. We take as an example a hydrogen plasma with parameters $B_o = 30$ kG, $n_o = 2 \times 10^{13}$ cm^{-3}, $T_e = 1$ keV. Then if T_e/T_i is approximately five, we may expect the relative damping of the low-frequency waves to be ~0.1 and that of the lower hybrid waves to be of the order of $10^{-5.7}$. Then the threshold fields (determined from $\gamma_o^2 = \gamma_b\gamma_n$) are approximately as follows.

For Coupling to:	Relative Damping ($T_e/T_i \approx 5$)		Threshold E Field (V/cm)
	Idler	Signal	
Ion acoustic	0.1	0.1	10^6
Electrostatic ion cyclotron	10^{-5}	0.05	10^2
Magnetosonic	10^{-5}	0.1	10^3

These figures should be regarded as rough guides. Note the high threshold for coupling to ion acoustic waves, as compared with the other interactions. The reason for this is that we excite two relatively highly damped modes, whereas in the other cases the idler is very lightly damped.

It should be noted that the threshold fields for a toroidal plasma may be quite different, since the damping rates that we have used are those for modes in a homogeneous,

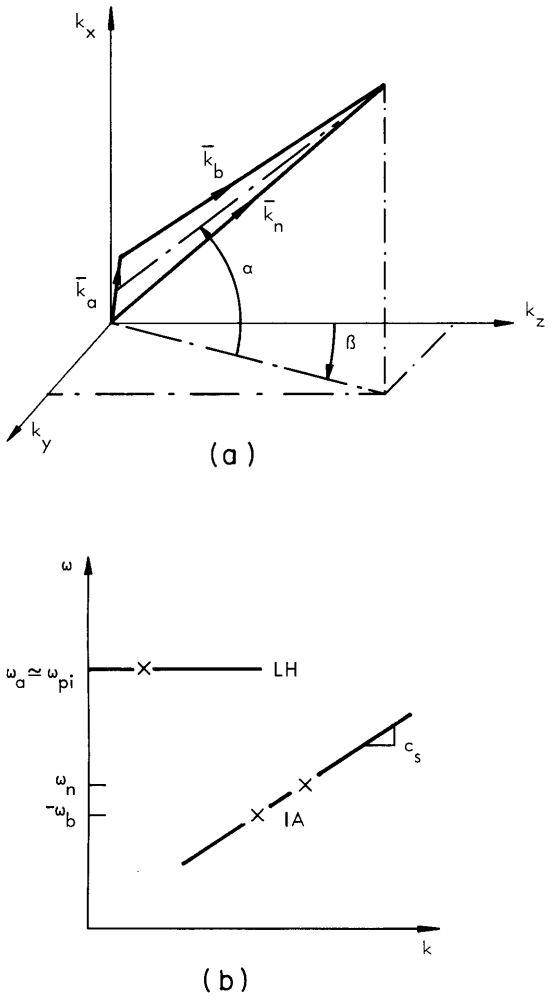

Fig. IX-32.

Coupling to ion acoustic waves: (a) in $\bar{k}$ space; (b) in ω, k space.

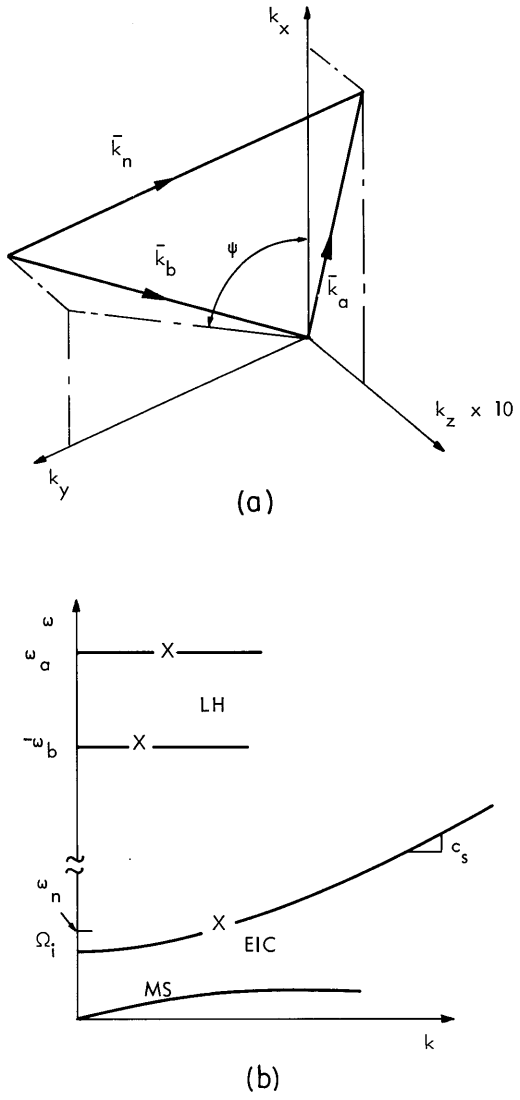

Fig. IX-33.

Coupling to electrostatic ion cyclotron waves: (a) in $\bar{k}$ space; (b) in ω, k space.

infinite-extent Vlasov plasma.

Criterion for Growth with a Finite Pump

We shall examine first the conditions under which we can apply the theory for a spatially infinite pump to the problem with a pump of finite extent in the center (homogeneous region) of a Tokamak plasma such as is shown in Fig. IX-34.

The pump will appear to be of infinite extent to unstable pulses within the pump region if several wavelengths of the excited waves can fit into the pump region. With the plasma parameters given above, the wavelengths of the excited waves are approximately from 1 mm for ion acoustic waves to 10 mm for electrostatic ion cyclotron and magnetosonic waves. Since the width of the pump ray is $\sim w_o(m_e/m_i)^{1/2}$, the required extent of the pump fields at the wall is $w_o \gg 5$–50 cm. (Note that the free-space wavelength at $\omega \sim \omega_{pi}$ is ~10 cm, so the fields would have to be generated from multiple sources.)

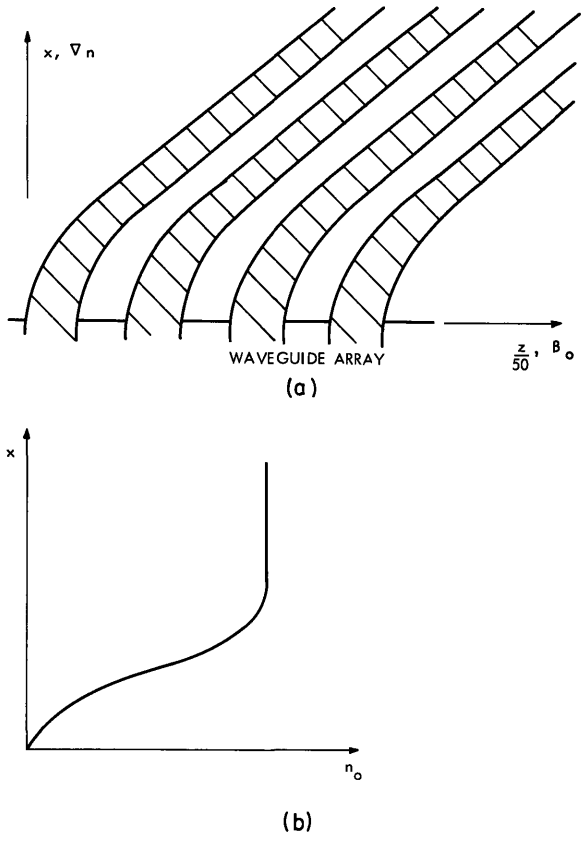

Fig. IX-34. Excitation of plasma with a plateau density. (a) Ray paths with multiple sources. (b) Density profile.

Under this assumption, we form the following picture. An unstable pulse originating from noise begins to grow within the pump region. The behavior of such a pulse in a uniform pump is well understood.[7] It is found that the pulse is confined to a line between two points, $\bar{v}_{gb}t$ and $\bar{v}_{gn}t$, from the point where the pulse started. (Note that these are points moving with the group velocities of the idler and signal.) The center of the pulse grows temporarily at γ_o, in the absence of damping. After a while the edges of the pulse move outside the pump region. We shall assume, however, that the rest of the pulse grows as if the pump were uniform. Some time later, the center of the pulse, which travels at $\frac{1}{2}(\bar{v}_{gb}+\bar{v}_{gn})$ exits the pump region. We arbitrarily call the interaction strong if this part of the pulse has e-folded several times at this point, or

$$\ell \equiv \frac{1}{2}(\bar{v}_{gb}+\bar{v}_{gn}) \cdot \bar{i}_n/\gamma_o \ll w, \tag{10}$$

where ℓ is defined as a "growth length," w is the width of the pump region, and $\bar{i}_n$ is its normal (see Fig. IX-31).

We now focus on the excitation of electrostatic ion cyclotron modes, since this interaction has the lowest threshold, and seems the best candidate for plasma heating. Suppose we take 1 kV/cm as the maximum reasonable field that we can excite at x = 0. Assuming amplification by a factor of 10 as the ray penetrates the plasma, we have fields of the order of 10 kV/cm inside the plasma. For the plasma parameters given, this is considerably above the threshold field and the growth rate γ_o is $\sim 0.1|\omega_b\omega_n|^{1/2}$. We note that we have considerable freedom in two choices of geometry for this interaction because the pump will contain a spectrum in k. Although the growth rate is an insensitive function of geometry, ℓ is strongly dependent on the geometry, because of the dot product in its definition (Eq. 10). For this interaction, $\bar{v}_{gn} \approx k_{nx}c_s^2/\omega_n\bar{i}_x$ and $\bar{v}_{gb} \approx \omega_{pe}/k_b$ and is perpendicular to $\bar{k}_b$. So $|\bar{v}_{gb}| \gg |\bar{v}_{gn}|$. To minimize ℓ, we choose $\bar{k}_a \approx 0$, so that $\bar{k}_a$ and $\bar{k}_b$ can be chosen to be nearly parallel, and $\bar{v}_{gb}$ and $\bar{i}_n$ are nearly perpendicular. In this case $\ell \sim 1$ mm and (10) is satisfied because w » 10 mm (the condition that the pump appear uniform to the nonlinear interaction). With $\bar{k}_a \approx 0$, $\bar{k}_b \approx \bar{k}_n$, and with the limited ranges for which weakly damped modes b and n exist,[1] θ_b and θ_n have to fall in the range ~83-86°. In that case ω_a would have to be approximately four times the local lower hybrid frequency, and we do not expect to encounter wave conversion at this point.

In order to reach the homogeneous region shown in Fig. IX-34, the pump fields have to traverse an inhomogeneous region. Electrostatic ion cyclotron waves will be excited in this region, with a growth rate similar to that for the homogeneous region. As the pulse moves through the density, however, there will be a "detuning" in k_x, since the dispersion relation for lower hybrid waves is a function of density. This phenomenon is important when the k_x mismatch, δ_{kx}, is of the order of the spatial growth rate in

the x direction, ℓ_k, for this detuning and we find

$$\ell_k \sim L\gamma_o/\omega_a, \tag{11}$$

where L is the density gradient scale length. For the parameters that we have been using ℓ_k is ~0.01 L. This will clearly limit the excitation of electrostatic ion cyclotron waves in the inhomogeneous region. Therefore for this case we can expect the main excitation of low-frequency waves to take place in the center of the plasma.

References

1. C. F. F. Karney, A. Bers, and J. L. Kulp, Quarterly Progress Report No. 110, Research Laboratory of Electronics, M.I.T., July 15, 1973, pp. 104-117.
2. C. F. F. Karney and A. Bers, Quarterly Progress Report No. 111, Research Laboratory of Electronics, M.I.T., October 15, 1973, pp. 71-84.
3. R. J. Briggs and R. R. Parker, Phys. Rev. Letters 29, 852 (1972).
4. S. Puri and M. Tutter, Max-Planck-Institut für Plasmaphysik, Report No. IPP IV/59 (1973).
5. M. D. Simonutti and R. R. Parker, Quarterly Progress Report No. 110, Research Laboratory of Electronics, M.I.T., July 15, 1973, p. 79.
6. C. F. F. Karney, "Parametric Coupling to Low-Frequency Plasma Waves," S.M. Thesis, Department of Electrical Engineering, M.I.T. (submitted January 1974).
7. M. S. Tekula, "Low-Frequency Oscillation of a Plasma in a Magnetic Field," S.M. Thesis, Department of Electrical Engineering, M.I.T. (to be submitted).
8. A. Bers, "Theory of Absolute and Convective Instabilities," in G. Auer and F. Cap (Eds.), Survey Lectures, International Congress, Waves and Instabilities in Plasmas, Innsbruck, Austria, April 2-7, 1973, pp. B1-B52.

2. THREE-DIMENSIONAL PULSE EVOLUTION OF COUPLED WAVE-WAVE INTERACTIONS

U.S. Atomic Energy Commission (Contract AT(11-1)-3070)

Abraham Bers, Frank W. Chambers

In a previous report[1] we presented a complete solution for the one-dimensional time-asymptotic pulse shape of coupled wave-wave interactions. In this report we extend our results to describe the time-asymptotic pulse shape in two and three dimensions.

The three-dimensional coupled wave equations resulting from nonlinear interaction are of the following form[2]

$$\left(\frac{\partial}{\partial t} + \vec{v}_2 \cdot \nabla + \gamma_2\right) a_2(\vec{r}, t) = -p_2 K^* a_{10} a_3^*(\vec{r}, t) \tag{1}$$

$$\left(\frac{\partial}{\partial t} + \vec{v}_3 \cdot \nabla + \gamma_3\right) a_3(\vec{r}, t) = -p_3 K^* a_{10} a_2^*(\vec{r}, t), \tag{2}$$

where the notation is the same as in our previous report. The Green's function solution of these equations is

$$G(\vec{r}, t) = \int_L \frac{ds}{2\pi} e^{-ist} \int_{F^3} \frac{d^3\kappa}{(2\pi)^3} e^{i\vec{\kappa}\cdot\vec{r}} \frac{1}{D(\vec{\kappa}, s)}, \tag{3}$$

where the dispersion relation is

$$D(\vec{\kappa}, s) = (s-\vec{\kappa}\cdot\vec{v}_2+i\gamma_2)(s-\vec{\kappa}\cdot\vec{v}_3+i\gamma_3) + \gamma^2 \tag{4}$$

and

$$\gamma^2 = p_2 p_3 |K|^2 |a_{10}|^2 \tag{5}$$

is the maximum possible growth rate (for $p_2p_3 > 0$), which occurs when $\gamma_2 = \gamma_3 = 0$.

The time-asymptotic pulse shape can be found by examining the absolute instability growth rate of $G(\vec{r}, t)$ as seen by an observer[2, 3] with velocity $\vec{V}(\vec{r} = \vec{V}t)$. Thus we seek the absolute instability growth rate for the observer's Green's function

$$G(\vec{V}t, t) = \int_{L'} \frac{ds'}{2\pi} e^{-is't} \int_{F^3} \frac{d^3\kappa}{(2\pi)^3} \frac{1}{D_{\vec{V}}(\vec{\kappa}, s')}, \tag{6}$$

where

$$D_{\vec{V}}(\kappa, s') = D(\vec{\kappa}, s'+\vec{\kappa}\cdot\vec{V}). \tag{7}$$

The absolute instability as seen by the observer is characterized by the complex frequency $s'_o(\vec{V})$ and the complex wave vector $\vec{\kappa}_o(\vec{V})$. These are determined from the simultaneous solution of

$$D_{\vec{V}} = 0 \tag{8}$$

and

$$\frac{\partial D_{\vec{V}}}{\partial \vec{\kappa}} = 0, \tag{9}$$

provided that $\vec{\kappa}_o(\vec{V})$ represents a coincident pinching of the deformed $\vec{F}$ contours as $s'_o(\vec{V})$ is approached from the L contour.

For the dispersion relation (4) we find that the corresponding observer

dispersion relation (7) is

$$D_{\vec{V}} = (s'-\vec{\kappa}\cdot\vec{V}_2+i\gamma_2)(s'-\vec{\kappa}\cdot\vec{V}_3+i\gamma_3) + \gamma^2, \tag{10}$$

where

$$\vec{V}_2 = \vec{v}_2 - \vec{V} \tag{11}$$

$$\vec{V}_3 = \vec{v}_3 - \vec{V}. \tag{12}$$

Equation 9 then gives

$$\vec{V}_2(s'-\vec{\kappa}\cdot\vec{V}_3+i\gamma_3) - \vec{V}_3(s'-\vec{\kappa}\cdot\vec{V}_2+i\gamma_2) = 0. \tag{13}$$

Nontrivial solutions to (13) demand that

$$\vec{V}_2 \times \vec{V}_3 = 0, \tag{14}$$

that is, that $\vec{V}_2$ and $\vec{V}_3$ be collinear, and, by (11) and (12), join in a straight line the tips of the unperturbed group velocity vectors $\vec{v}_2$ and $\vec{v}_3$, as shown in Fig. IX-35.

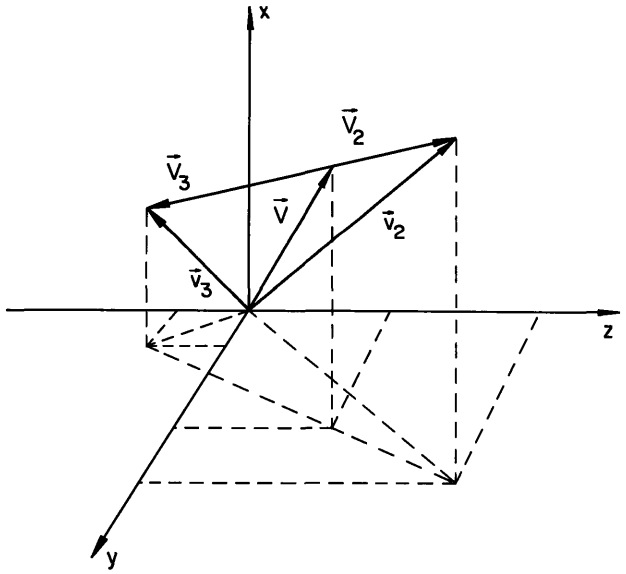

Fig. IX-35. Geometrical constraints between the group velocities $(\vec{v}_2, \vec{v}_3)$ of the interacting waves and the velocity $\vec{V}$ of an observer on the time-asymptotic Green's function pulse. The time-asymptotic, growing pulse extends at most from the arrow tip of $\vec{V}_2$ to the arrow tip of $\vec{V}_3$.

We let $\vec{\kappa} = \vec{\kappa}_{||} + \vec{\kappa}_{\perp}$, respectively, be parallel and perpendicular to either the direction of $\vec{V}_2$ or $\vec{V}_3$, and carry out the κ integration in (6) along these coordinates. By taking $\vec{\kappa}_{||}$ along $\vec{V}_3$, the dispersion relation (10) becomes

$$D_{||} = (s'+\kappa_{||}V_2+i\gamma_2)(s'-\kappa_{||}V_3+i\gamma_3) + \gamma^2, \tag{15}$$

and the pinch-type singularities in the $(s', \kappa_{||})$ integrations, which give the absolute instability as seen by the observer, are determined from the simultaneous solution of

$$D_{||} = 0 \tag{16}$$

and

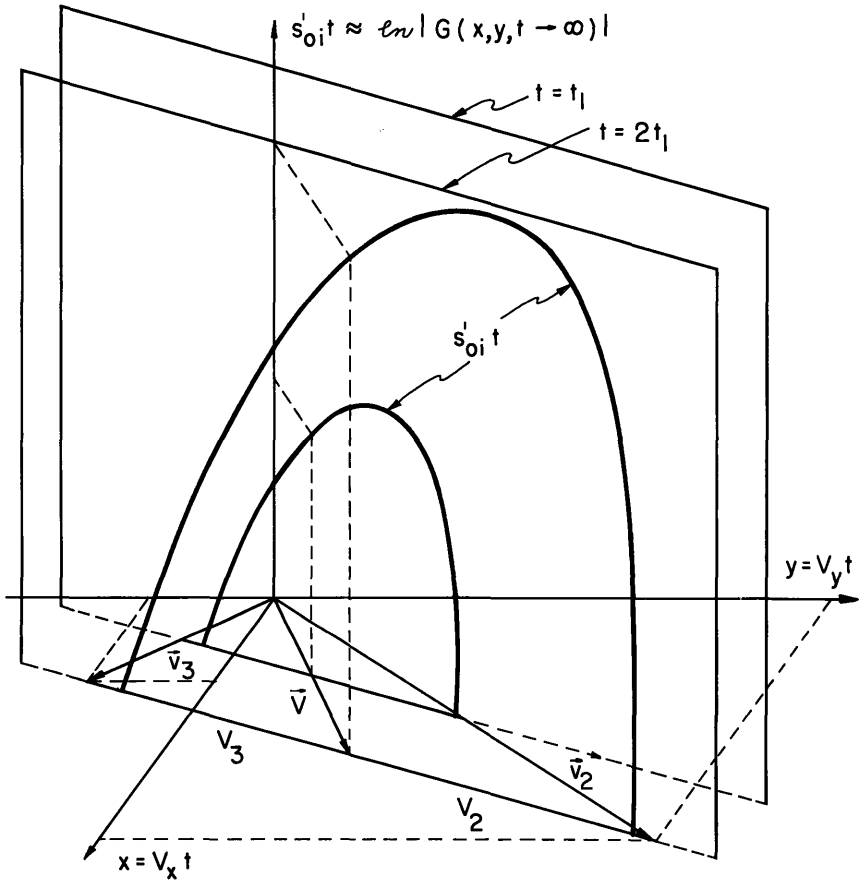

Fig. IX-36. Illustration of the method for constructing the time-asymptotic Green's function pulse for a two-dimensional interaction. In the s_{oi}-$V_{2,3}$ plane the calculation is entirely analogous to the one-dimensional interaction. s_{oi} vs $\vec{V}t$ is shown for two different times, t_1 and $2t_1$.

$$\frac{\partial D_{||}}{\partial \kappa_{||}} = 0. \tag{17}$$

Equations 15-17 are recognized to be analogous to the one-dimensional problem solved in our previous report.[1] Hence, for the three-dimensional problem, the growth rate of the absolute instability as seen by the observer is

$$s'_{oi}(\vec{V}) = \frac{2\gamma(V_2V_3)^{1/2} - (\gamma_2 V_3 + \gamma_3 V_2)}{V_2 + V_3}, \tag{18}$$

where, by (11) and (12), $V_2 = |\vec{v}_2 - \vec{V}|$, and $V_3 = |\vec{v}_3 - \vec{V}|$. A plot of s'_{oi} as a function of $\vec{V}$ gives the time-asymptotic pulse-shape evolution, since $s'_{oi}t \sim \ln |G(t\to\infty)|$ and $\vec{V}t = \vec{r}$. From (18) we find that the unstable ($s'_{oi} > 0$) part of the pulse shape extends at most over the range of $\vec{V}$ from $\vec{V} = \vec{v}_2$ (that is, $V_2 = 0$) to $\vec{V} = \vec{v}_3$ (that is, $V_3 = 0$). As shown in Fig. IX-36, this can be illustrated for the two-dimensional case for a particular set of group velocities $\vec{v}_2$ and $\vec{v}_3$. By applying (18) to interacting waves with group velocities that have all possible spatial directions, and with associated variations in coupling (γ) and damping (γ_2, γ_3), we get the complete time-asymptotic pulse-shape evolution in three dimensions. This is applied to two- and three-dimensional stability analysis for second-order laser-plasma interactions in Section IX-A.1 and to three-dimensional dispersion relations for third-order plasma interactions in Section IX-A.2.

References

1. A. Bers, F. W. Chambers, and R. J. Hawryluk, "Pulse Evolution of Second-Order Wave-Wave Interactions," Quarterly Progress Report No. 111, Research Laboratory of Electronics, M. I. T., October 15, 1973, pp. 31-37.
2. A. Bers, Notes on Lectures: Linear Waves and Instabilities, given at Ecole d'Eté de Physique Théorique, Les Houches, France, July 1972 (Gordon and Breach, New York, in press).
3. A. Bers, "Theory of Absolute and Convective Instabilities," in G. Auer and F. Cap (Eds.), Survey Lectures, International Congress, Waves and Instabilities in Plasmas, Innsbruck, Austria, April 2-7, 1973, pp. B1-B52.

3. THIRD-ORDER NONLINEAR WAVE-WAVE INTERACTIONS: A DIFFERENTIAL-EQUATION APPROACH

National Science Foundation (Grant GK-37979X)

Duncan C. Watson, Abraham Bers

Introduction

The theoretical approach presented here is an outgrowth of the approach used in a previous report.[1] It is therefore useful to recall briefly the earlier work, before sketching the plan to be followed here.

In the earlier report we presented a theory of coherent wave coupling via second- and third-order conductivity in a homogeneous unmagnetized plasma. In the presence of a strong pump, small perturbations separated by multiples of the pump frequency and wavevector are coupled. Three such perturbations were considered. The electric-field polarizations were assumed in advance. The electric-field amplitudes were then related by a set of three coupled linear equations. The consistency condition for this set was a 3×3 determinantal equation:

$$\begin{vmatrix} K_{(1)} + i\left[\dfrac{\vec{e}^{\,*}_{(1)} \cdot \vec{j}^{\,NL(3)}_{(1),\,o,\,-o}}{\epsilon_o \omega_{(1)}}\, u_o u_o^*\right] & i\left[\dfrac{\vec{e}^{\,*}_{(1)} \cdot \vec{j}^{\,NL(2)}_{(o),\,o}}{\epsilon_o \omega_{(1)}}\, u_o\right] & \dfrac{i}{2!}\left[\dfrac{\vec{e}^{\,*}_{(1)} \cdot \vec{j}^{\,NL(3)}_{(-1),\,o,\,o}}{\epsilon_o \omega_{(1)}}\, u_o^2\right] \\ i\left[\dfrac{\vec{e}^{\,*}_{(o)} \cdot \vec{j}^{\,NL(2)}_{(1),\,-o}}{\epsilon_o \omega_{(o)}}\, u_o^*\right] & K_{(o)} + i\left[\dfrac{\vec{e}^{\,*}_{(o)} \cdot \vec{j}^{\,NL(3)}_{(o),\,o,\,-o}}{\epsilon_o \omega_{(o)}}\, u_o u_o^*\right] & i\left[\dfrac{\vec{e}^{\,*}_{(o)} \cdot \vec{j}^{\,NL(2)}_{(-1),\,o}}{\epsilon_o \omega_{(o)}}\, u_o\right] \\ \dfrac{i}{2!}\left[\dfrac{\vec{e}^{\,*}_{(-1)} \cdot \vec{j}^{\,NL(3)}_{(1),\,-o,\,-o}}{\epsilon_o \omega_{(-1)}}\, u_o^{*2}\right] & i\left[\dfrac{\vec{e}^{\,*}_{(-1)} \cdot \vec{j}^{\,NL(2)}_{(o),\,-o}}{\epsilon_o \omega_{(-1)}}\, u_o^*\right] & K_{(-1)} + i\left[\dfrac{\vec{e}^{\,*}_{(-1)} \cdot \vec{j}^{\,NL(3)}_{(-1),\,o,\,-o}}{\epsilon_o \omega_{(-1)}}\, u_o u_o^*\right] \end{vmatrix} = 0 \tag{1}$$

The coupling coefficients in this equation were evaluated by using general formulas derived from the warm-fluid plasma model by the generalized coupling-of-modes formalism:

$$\frac{\vec{e}^{\,*}_a \cdot \vec{j}^{\,NL(2)}_{b,\,c}}{\epsilon_o \omega_a} = \sum_{\text{species}} \frac{im}{\epsilon_o} \sum_{\substack{6 \text{ permutations} \\ \text{of } (-a,\,b,\,c)}} \left\{ \frac{1}{2}\, n_{-a} (\vec{v}_b \cdot \vec{v}_c) + \frac{1}{6}\, \frac{n_{-a} n_b n_c}{n_E^2}\, \gamma(\gamma-2)\, v_T^2 \right\}. \tag{2}$$

$$\frac{\vec{e}_a^{\,*} \cdot \vec{j}^{NL(3)}_{b,c,d}}{\epsilon_o \omega_a} = \sum_{\text{species}} \frac{im}{\epsilon_o} \sum_{\substack{24 \text{ permutations} \\ \text{of } (-a, b, c, d)}} \left\{ \frac{1}{2} n_{-a} \vec{v}_{b+c} \cdot \vec{v}_d + \frac{1}{8} n_E \vec{v}_{-a+b} \cdot \vec{v}_{c+d} \right.$$

$$\left. - \frac{1}{8} \frac{n_{-a+b} n_{c+d}}{n_E} \gamma v_T^2 + \frac{1}{24} \frac{n_{-a} n_b n_c n_d}{n_E^3} \gamma(\gamma-2)(\gamma-3) v_T^2 \right\}. \tag{3}$$

From the determinantal equation (1) we then extracted one-dimensional dispersion relations corresponding to specific instabilities, both modified and unmodified.

In this report we present a theory of coherent wave coupling via second- and third-order conductivity in a homogeneous unmagnetized plasma. Three small perturbations are considered. This time the electric-field polarizations are not specified in advance. The three electric-field components of each of the three perturbations constitute a total of nine unknowns. These nine unknowns are related by a set of nine coupled linear equations. The consistency condition for this set is a 9×9 determinantal equation which we shall derive. This equation can be written to show the analogy with the constrained-polarization case, by using the notation of partitioned matrices.

$$0 = \begin{vmatrix} \vec{\vec{K}}_{(1)} + \vec{\vec{C}}^{NL(3)}_{(1),o,o*} E_o E_o^* & \vec{\vec{C}}^{NL(2)}_{(o),o} E_o & \vec{\vec{C}}^{NL(3)}_{(-1),o,o} E_o^2 \\ \vec{\vec{C}}^{NL(2)}_{(1),o*} E_o^* & \vec{\vec{K}}_{(o)} + \vec{\vec{C}}^{NL(3)}_{(o),o,o*} E_o E_o^* & \vec{\vec{C}}^{NL(2)}_{(-1),o} E_o \\ \vec{\vec{C}}^{NL(3)}_{(1),o*,o*} E_o^{*2} & \vec{\vec{C}}^{NL(2)}_{(o),o*} E_o^* & \vec{\vec{K}}_{(-1)} + \vec{\vec{C}}^{NL(3)}_{(-1),o,o*} E_o E_o^* \end{vmatrix} \tag{4}$$

where, for instance,

$$\left(\vec{\vec{C}}^{NL(3)}_{(1),o,o*}\right)_{AB} \equiv \frac{i}{\epsilon_o \omega_{(1)}} \left(\vec{e}^{\,*}_{(1)A} \cdot \vec{j}^{NL(3)}_{(1)B,o,o*}\right). \tag{5}$$

Now the polarizations and relative amplitudes of the three perturbations can be obtained directly from the relative magnitude of the appropriate entries in the matrix (4).

The coupling coefficients in the determinant may be evaluated by using Eqs. 2 and 3. An alternative method of evaluation is desirable for gaining increased physical understanding and for ease of comparison with other theoretical treatments.[2,3] We have evaluated the coupling coefficients by expanding the warm-fluid plasma equations about the oscillating equilibrium set up by the pump. We obtain directly the differential equations describing the behavior of small perturbations in the pump-modulated medium.

Again we shall extract from the determinantal equation those dispersion relations corresponding to specific instabilities, both modified and unmodified. These dispersion relations are now three-dimensional, and the stability analysis[4-6] (see also Sec. IX-D. 2) may then be applied to find the corresponding three-dimensional time-asymptotic pulse shapes.

Pump-Coupled Perturbations with Arbitrary Polarizations

The initial steps in this discussion are very similar to those in our previous report.[1] Therefore they will be stated briefly.

Let an arbitrary homogeneous medium sustain a monochromatic pump wave

$$\vec{E}_o = E_L \vec{e}_L \exp(i\vec{k}_L \cdot \vec{x} - i\omega_L t) + \text{complex conjugate.} \tag{6}$$

Here $\vec{e}_L$ is a unit vector describing the polarization of the pump. Consider a pump-coupled triplet of linear perturbations

$$\{\vec{E}_+(\vec{k}_+, \omega_+), \vec{E}(\vec{k}, \omega), \vec{E}_-(\vec{k}_-, \omega_-)\}, \tag{7}$$

where

$$(\vec{k}_\pm, \omega_\pm) \equiv (\vec{k} \pm \vec{k}_L, \omega \pm \omega_L). \tag{8}$$

We now depart from the discussion in our previous report by allowing the perturbations to have arbitrary polarizations. We describe each electric-field perturbation in (7) in terms of a (different) basis of unit polarization vectors

$$\left.\begin{aligned} \vec{E}_+ &= E_{M+}\vec{e}_{M+} + E_{N+}\vec{e}_{N+} + E_{S+}\vec{e}_{S+} \\ \vec{E} &= E_M\vec{e}_M + E_N\vec{e}_N + E_S\vec{e}_S \\ \vec{E}_- &= E_{M-}\vec{e}_{M-} + E_{N-}\vec{e}_{N-} + E_{S-}\vec{e}_{S-} \end{aligned}\right\} \tag{9}$$

These bases of unit vectors are unrestricted at present, but will later be restricted in such a way that they acquire immediate physical significance. We denote the second-order nonlinear currents arising

$$\begin{aligned} &\text{from fields } \vec{e}_L \text{ and } \vec{e}_B \text{ by } \vec{j}^{+}_{B}, \text{ from fields } \vec{e}_L \text{ and } \vec{e}_{B-} \text{ by } \vec{j}^{+}_{B-}, \\ &\text{from fields } \vec{e}^{*}_L \text{ and } \vec{e}_B \text{ by } \vec{j}^{-}_{B}, \text{ from fields } \vec{e}^{*}_L \text{ and } \vec{e}_{B+} \text{ by } \vec{j}^{-}_{B+}. \end{aligned} \tag{10}$$

We denote the third-order nonlinear currents arising

from fields $\vec{e}_L, \vec{e}_L^*, \vec{e}_B$ by $\vec{j}_B^{+-}$, from fields $\vec{e}_L, \vec{e}_L^*, \vec{e}_{B\pm}$ by $\vec{j}_{B\pm}^{+-}$,

from fields $\vec{e}_L, \vec{e}_L, \vec{e}_{B-}$ by $\vec{j}_{B-}^{++}$, from fields $\vec{e}_L^*, \vec{e}_L^*, \vec{e}_{B+}$ by $\vec{j}_{B+}^{--}$. (11)

Substituting (9) and (10) in Maxwell's equations, we obtain

$$\left(\sum_B \vec{\vec{K}}_+ \vec{e}_{B+} E_{B+} + E_L E_L^* \sum_B \frac{i\vec{j}_{B+}^{+-}}{\epsilon_o \omega_+} E_{B+}\right) + E_L \sum_B \frac{i\vec{j}_B^{+}}{\epsilon_o \omega_+} E_B + E_L^2 \sum_B \frac{i\vec{j}_{B-}^{++}}{\epsilon_o \omega_+} E_{B-} = 0 \quad (12)$$

$$E_L^* \sum_B \frac{i\vec{j}_{B+}^{-}}{\epsilon_o \omega} + \left(\sum_B \vec{\vec{K}} \vec{e}_B E_B + E_L E_L^* \sum_B \frac{i\vec{j}_B^{+-}}{\epsilon_o \omega} E_B\right) + E_L \sum_B \frac{i\vec{j}_{B-}^{+}}{\epsilon_o \omega} E_{B-} = 0 \quad (13)$$

$$E_L^{*2} \sum_B \frac{i\vec{j}_{B+}^{--}}{\epsilon_o \omega_-} E_{B+} + E_L^* \sum_B \frac{i\vec{j}_B^{-}}{\epsilon_o \omega_-} E_B + \left(\sum_B \vec{\vec{K}}_- \vec{e}_{B-} E_{B-} + E_L E_L^* \sum_B \frac{i\vec{j}_{B-}^{+-}}{\epsilon_o \omega_-} E_{B-}\right) = 0 \quad (14)$$

where $\vec{\vec{K}}_+, \vec{\vec{K}}, \vec{\vec{K}}_-$ are the uncoupled linear dispersion tensors, for instance,

$$\vec{\vec{K}}_+ \equiv \left(\vec{k}_+ \vec{k}_+ - k_+^2\right)\left(c^2/\omega_+^2\right) + 1 + i\vec{\vec{\sigma}}^{\text{LINEAR}}(k_+, \omega_+)/\epsilon_o \omega_+. \quad (15)$$

These three vector equations may be converted into an equivalent set of 9 scalar equations.

We take the dot products of (12) with $\vec{f}_{m+}, \vec{f}_{n+}, \vec{f}_{s+}$, the dot products of (13) with $\vec{f}_m, \vec{f}_n, \vec{f}_s$, and the dot products of (14) with $\vec{f}_{m-}, \vec{f}_{n-}, \vec{f}_{s-}$. Then we have a set of 9 scalar equations linear in the nine unknown field components $E_{M+}, E_{N+}, E_{S+}, E_M, E_N, E_S, E_{M-}, E_{N-}, E_{S-}$. The set of 9 scalar equations is consistent, provided the 9×9 matrix of coefficients of the unknown field components has a zero determinant. This consistency condition may be written by using the partitioned matrix notation.

$$\begin{vmatrix} \vec{\vec{K}}_+ + E_L E_{L+}^* \vec{\vec{C}}_+^{+-} & E_{L+}^+ \vec{\vec{C}}^{+} & E_{L+}^2 \vec{\vec{C}}_-^{++} \\ E_L^* \vec{\vec{C}}_+^{-} & \vec{\vec{K}} + E_L E_L^* \vec{\vec{C}}^{+-} & E_L \vec{\vec{C}}_-^{+} \\ E_{L-}^{*2} \vec{\vec{C}}_+^{--} & E_{L-}^* \vec{\vec{C}}^{-} & \vec{\vec{K}}_- + E_L E_{L-}^* \vec{\vec{C}}_-^{+-} \end{vmatrix} = 0, \quad (16)$$

where the uncoupled linear dispersion tensors have elements typified by

$$(K_+)_{AB} = \vec{f}_A \cdot \vec{\vec{K}}_+ \vec{e}_B \tag{17}$$

and the tensor coupling coefficients have elements typified by

$$\left(C_-^{++}\right)_{AB} = i\vec{f}_{A+} \cdot \vec{j}_{B-}^{++}/\epsilon_o\omega_+. \tag{18}$$

Now we specialize to an unmagnetized plasma. The eigenvectors of $\vec{\vec{K}}$ now lie parallel and perpendicular to k regardless of the value of ω. By taking $\vec{e}_m, \vec{e}_n, \vec{e}_s$ as eigenvectors of $\vec{\vec{K}}$ and $\vec{f}_m, \vec{f}_n, \vec{f}_s$ as eigenvectors of $\vec{\vec{K}}^{\text{transpose}}$, the determinantal equation (16) assumes a form in which $\vec{\vec{K}}$ appears as a 3×3 diagonal matrix. Similarly $\vec{\vec{K}}_+$ and $\vec{\vec{K}}_-$ may be diagonalized. The e-basis vectors for each perturbation now correspond to the polarizations of the uncoupled modes of the plasma having the same propagation vector as the perturbation. This greatly facilitates various simplifications of the determinantal equation.

Coupling Coefficients for Plane-Polarized Electromagnetic Pump

We derive the coupling coefficients appearing in (16) directly from the differential equations describing the plasma model.

We choose the two-species warm-fluid model of an unmagnetized plasma. The equations describing the fluid model are the momentum conservation and the particle conservation equations for each species separately:

$$\left.\begin{aligned} &\frac{\partial\vec{v}}{\partial t} + \vec{v}\cdot\frac{\partial\vec{v}}{\partial t} + \frac{\gamma v_T^2}{n_o}\left(\frac{n}{n_o}\right)^{\gamma-2}\frac{\partial n}{\partial\vec{x}} = \frac{q}{m}(\vec{E}+\vec{v}\times\vec{B}) \\ &\frac{\partial n}{\partial t} + \frac{\partial}{\partial\vec{x}}\cdot n\vec{v} = 0 \end{aligned}\right\} \tag{19}$$

Let the electric field of the laser-light pump be described by (6). Neglect the response of the medium at harmonics of the pump. Then the oscillating equilibrium set up by the pump is described for each species π by

$$\left.\begin{aligned} &\vec{v}_{o\pi} = \vec{v}_{L\pi}\exp\left(i\vec{k}_L\cdot\vec{x} - i\omega_L^t\right) + \text{complex conjugate} \\ &\vec{v}_{L\pi} = iq_\pi E_L\vec{e}_L/m_\pi\omega_L \end{aligned}\right\} \tag{20}$$

Consider the small linear perturbations described by $\vec{E}_1$ and $\vec{B}_1$ and by an n_1 and $\vec{v}_1$ for each species. The equations obeyed by these perturbations are obtained by expanding (19) about (20). They are the linearized momentum conservation equation and the linearized particle conservation equation for each species separately:

$$\left.\begin{aligned}&(\partial\vec{v}_{1\pi}/\partial t)+\vec{v}_{o\pi}\cdot\nabla\vec{v}_{1\pi}+\vec{v}_{1\pi}\cdot\nabla\vec{v}_{o\pi}+\gamma v_{T\pi}^2\nabla(n_{1\pi}/n_\pi)=(q_\pi/m_\pi)(\vec{E}_1+\vec{v}_{1\pi}\times\vec{B}_o+\vec{v}_{o\pi}\times\vec{B}_1)\\&(\partial n_{1\pi}/\partial t)+\nabla\cdot(n_\pi\vec{v}_{1\pi}+n_{1\pi}\vec{v}_{o\pi})=0\end{aligned}\right\}\quad(21)$$

From (21) and Maxwell's equations, after some algebraic manipulations, we may obtain the expressions for nonlinear currents excited by a perturbation field $\vec{E}(\vec{k},\omega)$. This perturbation, together with the positive frequency component of the pump, gives rise to a second-order current at $(\vec{k}+\vec{k}_L,\omega+\omega_L)$:

$$\frac{i\vec{J}^+}{\epsilon_o\omega_+}=-\frac{\omega_p^2}{\omega\omega_+}\left(1+\frac{\gamma v_T^2\vec{k}_+\vec{k}_+}{\omega_+^2-\gamma k_+^2v_T^2}\right)\cdot\left(\frac{\vec{v}_L\vec{k}}{\omega}+\frac{\vec{k}_+\vec{v}_L}{\omega_+}\right)\cdot\left(1+\frac{\gamma v_T^2\vec{k}\vec{k}}{\omega^2-\gamma k^2v_T^2}\right)\cdot\vec{E}.\quad(22)$$

The perturbation $\vec{E}(\vec{k},\omega)$, together with the negative frequency component of the pump field, gives rise to a second-order current at $(\vec{k}-\vec{k}_L,\omega-\omega_L)$:

$$\frac{i\vec{J}^-}{\epsilon_o\omega_-}=-\frac{\omega_p^2}{\omega\omega_-}\left(1+\frac{\gamma v_T^2\vec{k}_-\vec{k}_-}{\omega_-^2-\gamma k_-^2v_T^2}\right)\cdot\left(\frac{\vec{v}_L^*\vec{k}}{\omega}+\frac{\vec{k}_-\vec{v}_L^*}{\omega_-}\right)\cdot\left(1+\frac{\gamma v_T^2\vec{k}\vec{k}}{\omega^2-\gamma k^2v_T^2}\right)\cdot\vec{E}.\quad(23)$$

$\vec{E}(\vec{k},\omega)$ and the positive-frequency pump component acting twice give a third-order current at $(\vec{k}+2\vec{k}_L,\omega+2\omega_L)$:

$$\begin{aligned}\frac{i\vec{J}^{++}}{\omega_{++}\epsilon_o}=-\frac{\omega_p^2}{\omega\omega_{++}}&\left(1+\frac{\gamma v_T^2\vec{k}_{++}\vec{k}_{++}}{\omega_{++}^2-\gamma k_{++}^2v_T^2}\right)\cdot\left[\frac{1}{\omega_+^2-\gamma k_+^2v_T^2}\left(\vec{v}_Lk_+^2\vec{v}_L+\frac{\vec{k}_{++}}{\omega_{++}}\gamma v_T^2(\vec{k}_+\cdot\vec{v}_L)^2\frac{\vec{k}}{\omega}\right.\right.\\&\left.\left.+\vec{v}_L\omega_+(\vec{k}_+\cdot\vec{v}_L)\frac{\vec{k}}{\omega}+\frac{\vec{k}_{++}}{\omega_{++}}\omega_+(\vec{k}_+\cdot\vec{v}_L)\vec{v}_L\right)\right]\cdot\left(1+\frac{\gamma v_T^2\vec{k}\vec{k}}{\omega^2-\gamma k^2v_T^2}\right)\cdot\vec{E}.\end{aligned}\quad(24)$$

$\vec{E}(\vec{k},\omega)$ and the negative-frequency pump component acting twice give a third-order current at $(\vec{k}-2\vec{k}_L,\omega-2\omega_L)$:

$$\begin{aligned}\frac{i\vec{J}^{--}}{\omega_{--}\epsilon_o}=-\frac{\omega_p^2}{\omega\omega_{--}}&\left(1+\frac{\gamma v_T^2\vec{k}_{--}\vec{k}_{--}}{\omega_{--}^2-\gamma k_{--}^2v_T^2}\right)\cdot\left[\frac{1}{\omega_-^2-\gamma k_-^2v_T^2}\left(\vec{v}_L^*k_-^2\vec{v}_L^*+\frac{\vec{k}_{--}}{\omega_{--}}\gamma v_T^2\left(\vec{k}_-\cdot\vec{v}_L^*\right)^2\frac{\vec{k}}{\omega}\right.\right.\\&\left.\left.+\vec{v}_L^*\omega_-\left(\vec{k}_-\cdot\vec{v}_L\right)\frac{\vec{k}}{\omega}+\frac{\vec{k}_{--}}{\omega_{--}}\omega_-\left(\vec{k}_-\cdot\vec{v}_L^*\right)\vec{v}_L^*\right)\right]\cdot\left(1+\frac{\gamma v_T^2\vec{k}\vec{k}}{\omega^2-\gamma k^2v_T^2}\right)\cdot\vec{E}.\end{aligned}\quad(25)$$

$\vec{E}(\vec{k},\omega)$ and the positive- and negative-frequency pump components acting in succession give a third-order current at $(\vec{k},\omega)$ which forms a self-correction to the perturbation:

$$\frac{i\vec{J}^{+-}}{\omega\epsilon_o} = -\frac{\omega_p^2}{\omega^2}\left(1 + \frac{\gamma v_T^2 \vec{k}\vec{k}}{\omega^2 - \gamma k^2 v_T^2}\right)\cdot\left[\frac{1}{\omega_-^2 - \gamma k_-^2 v_T^2}\left(\vec{v}_L k_-^2 \vec{v}_L^* + \frac{\vec{k}}{\omega}\gamma v_T^2(\vec{k}_-\cdot v_L)\left(\vec{k}_-\cdot\vec{v}_L^*\right)\frac{\vec{k}}{\omega}\right.\right.$$

$$\left. + \vec{v}_L\omega_-\left(\vec{k}_-\cdot\vec{v}_L^*\right)\frac{\vec{k}}{\omega} + \frac{\vec{k}}{\omega}\omega_-(\vec{k}_-\cdot\vec{v}_L)\vec{v}_L^*\right)$$

$$+ \frac{1}{\omega_+^2 + \gamma k_+^2 v_T^2}\left(\vec{v}_L^* k_+^2 \vec{v}_L + \frac{\vec{k}}{\omega}\gamma v_T^2\left(\vec{k}_+\cdot\vec{v}_L^*\right)(\vec{k}_+\cdot\vec{v}_L)\frac{\vec{k}}{\omega}\right.$$

$$\left.\left. + \vec{v}_L^*\omega_+(\vec{k}_+\cdot\vec{v}_L)\frac{\vec{k}}{\omega} + \frac{\vec{k}}{\omega}\omega_+\left(\vec{k}_+\cdot\vec{v}_L^*\right)\vec{v}_L\right)\right]\cdot\left(1 + \frac{\gamma v_T^2 \vec{k}\vec{k}}{\omega^2 - \gamma k^2 v_T^2}\right)\cdot\vec{E}. \qquad (26)$$

The nonlinear currents excited by another perturbation $\vec{E}_\pm$ at frequency $(\vec{k}\pm\vec{k}_L, \omega\pm\omega_L)$ can now be obtained simply by raising (lowering) all frequencies in (22)-(26) by $(\vec{k}_L, \omega_L)$.

Next, we substitute (22)-(26) and their frequency-shifted analogues in the expressions for the coupling coefficients (e.g., Eq. 18). The resultant forms depend on the polarization basis vectors f and e only through their dot products with their associated propagation vectors and with $\vec{v}_L$ and $\vec{v}_L^*$. Specializing to a plane-polarized laser, for which $\vec{v}_L, \vec{v}_L^*$ are collinear, we find that the coupling coefficient (25) depends on

$\vec{f}_{A+}$ only through the quantities $\vec{f}_{A+}\cdot\vec{v}_L$, $\vec{f}_{A+}\cdot\vec{k}_+$

and on

$\vec{e}_{B-}$ only through the quantities $\vec{v}_L\cdot\vec{e}_{B-}$, $\vec{k}_-\cdot\vec{e}_{B-}$.

For an unmagnetized, dissipation-free, warm-fluid dispersion tensor the $\vec{f}$ and the $\vec{e}$ may be taken to be identical. We have already chosen $\vec{e}_M$ and $\vec{e}_N$ to be perpendicular to $\vec{k}$, $\vec{e}_{M+}$ and $\vec{e}_{N+}$ perpendicular to $\vec{k}_+$, and $\vec{e}_{M-}$ and $\vec{e}_{N-}$ perpendicular to $\vec{k}_-$. We now demand in addition that $\vec{e}_N$, $\vec{e}_{N+}$ and $\vec{e}_{N-}$ all be perpendicular to $\vec{v}_L$. Then any coupling coefficient involving $\vec{e}_N$, $\vec{e}_{N+}$, $\vec{e}_{N-}$, $\vec{f}_N$, $\vec{f}_{N+}$ or $\vec{f}_{N-}$ is identically zero. Physically this means that we decompose a perturbation field $\vec{E}$ at $(\vec{k}, \omega)$, say, into an electrostatic field $E_S\vec{e}_S$ parallel to $\vec{k}$, an electromagnetic field $E_N\vec{e}_N$ perpendicular to both $\vec{k}$ and $\vec{v}_L$ which takes no part in any coupling, and an electromagnetic field $E_M\vec{e}_M$ perpendicular to both $\vec{e}_S$ and $\vec{e}_N$.

The resultant 9 × 9 determinant (16) will not be reproduced here in full. Instead we shall describe its use for deriving an underlying specific interaction. We shall describe the manner in which specific entries in the 9 × 9 determinant are combined

to give dispersion relations for specific instabilities. The resultant dispersion relations are presented in Section IX-A. 1.

Isolation of Specific Instabilities from the Determinantal Equation

The determinantal equation (16) factors into the three uncoupled electromagnetic roots

$$(K_+)_N = 0, \qquad (K)_N = 0, \qquad (K_-)_N = 0 \tag{27}$$

and a coupled equation formed from (16) by striking out the central row and central column from each 3×3 subdeterminant. We shall focus our attention on the latter.

We find that for very small $|E_L|$ not all of

$$(K_+)_M,\ (K_+)_S,\ (K)_M,\ (K)_S,\ (K_-)_M,\ (K_-)_S \tag{28}$$

can be of order unity simultaneously.

Let $(K)_S, (K_-)_S$ be of order $|E_L|$ and the rest of (28) be of order unity. Then to order $|E_L|^2$

$$(K)_S\,(K_-)_S = |E_L|^2 \left({}_-C^-\right)_{SS} \left(C_-^+\right)_{SS}. \tag{29}$$

This describes either the unmodified plasmon-phonon instability or the unmodified plasmon-plasmon instability, depending on the region of k-ω space that is being considered.

Let $(K_-)_S$ be small and the rest of (28) be of order unity. Then to order $|E_L|^2$

$$(K_-)_S = |E_L|^2 \left\{ \frac{\left({}_-C^-\right)_{SS} \left(C_-^+\right)_{SS}}{(K)_S} + \frac{\left({}_-C^-\right)_{SM} \left(C_-^+\right)_{MS}}{(K)_M} - \left({}_-C_-^{+-}\right)_{SS} \right\}$$

$$\equiv |E_L|^2\, G_-, \quad \text{say.} \tag{30}$$

This describes the modified plasmon-phonon instability. It will soon prove useful to consider also the form obtained by taking $(K_+)_S$ to be small and the rest of (28) of order unity:

$$(K_+)_S = |E_L|^2 \left\{ \frac{\left({}_+C^+\right)_{SS} \left(C_+^-\right)_{SS}}{(K)_S} + \frac{\left({}_+C^+\right)_{SM} \left(C_+^-\right)_{MS}}{(K)_M} - \left({}_+C_+^{+-}\right)_{SS} \right\}$$

$$\equiv |E_L|^2\, G_+, \quad \text{say.} \tag{31}$$

Let $(K)_S, (K_-)_M$ be of order $|E_L|$ and the rest of (28) of order unity. Then to order $|E_L|^2$

$$(K)_S (K_-)_M = |E_L|^2 \left(_-C^-\right)_{MS} \left(C_-^+\right)_{SM}. \tag{32}$$

This describes unmodified stimulated Brillouin or Raman scattering, depending on the region of k-ω space that is being considered.

Let $(K)_S, (K_-)_S, (K_-)_M$ all be of order $|E_L|$ and the rest of (28) of order unity. Then to order $|E_L|$

$$(K)_S = |E_L|^2 \left\{ \frac{\left(C_-^+\right)_{SM} \left(_-C^-\right)_{MS}}{(K_-)_M} + \frac{\left(C_-^+\right)_{SS} \left(_-C^-\right)_{SS}}{(K_-)_S} \right\}. \tag{33}$$

This describes the coalescence of the unmodified Raman and unmodified plasmon-plasmon instabilities.

Let $(K_-)_M$ be small and the rest of (28) be of order unity. Then to order $|E_L|^2$

$$(K_-)_M = |E_L|^2 \left\{ \frac{\left(_-C^-\right)_{MS} \left(C_-^+\right)_{SM}}{(K)_S} + \frac{\left(_-C^-\right)_{MM} \left(C_-^+\right)_{MM}}{(K)_M} - \left(_-C_-^{+-}\right)_{MM} \right\}. \tag{34}$$

This describes modified stimulated Brillouin scattering. It also describes the form of modified stimulated Raman scattering in extremely underdense plasma.

Let $(K)_S$ be small and the rest of (28) be of order unity but with $K_+)_M$ and $(K_+)_S \gg (K_-)_M$ and $(K_-)_S$. Then to order $|E_L|^2$

$$(K)_S = |E_L|^2 \left\{ \frac{\left(C_-^+\right)_{SS} \left(_-C^-\right)_{SS}}{(K_-)_S} + \frac{\left(C_-^+\right)_{SM} \left(_-C^-\right)_{MS}}{(K_-)_M} - (C^{+-})_{SS} \right\}. \tag{35}$$

This describes the form of modified stimulated Raman scattering near the 1/4 critical density surface. Note the close connection between (33) and (35); we shall find that (33) is adequate.

Let $(K_+)_S, (K_-)_S$ be small and the rest of (28) be of order unity. Then to order $|E_L|^4$

$$(K_+)_S (K_-)_S = |E_L|^2 (K_+)_S G_- + |E_L|^2 (K_-)_S G_+$$

$$- |E_L|^4 G_- G_+ + |E_L|^4 H_- H_+, \tag{36}$$

where G_-, G_+ were defined in (30), (31) and

$$H_- \equiv \frac{\left(_-C^-\right)_{SS}\left(C_+^-\right)_{SS}}{(K)_S} + \frac{\left(_-C^-\right)_{SM}\left(C_+^-\right)_{MS}}{(K)_M} - \left(_-C_+^{--}\right)_{SS} \tag{37}$$

$$H_+ \equiv \frac{\left(_+C^+\right)_{SS}\left(C_-^+\right)_{SS}}{(K)_S} + \frac{\left(_+C^+\right)_{SM}\left(C_-^+\right)_{MS}}{(K)_M} - \left(_+C_-^{++}\right)_{SS} \tag{38}$$

Equation 36 describes the so-called nonoscillatory instability. Sometimes we insert for $(K)_S$, $(K)_M$ their values at the wavevector and frequency (k, ω) so that $(K_+)_S = (K_-)_S = 0$. This approximate version is called the unmodified nonoscillatory instability, which was first described by Nishikawa[7] for $k_L = 0$. The version in which $(K)_S$, $(K)_M$ are given their true values is called the modified nonoscillatory instability. Note the close connection among (30), (31), and (36).

Equations (29)-(38) form the basis on which the explicit dispersion relations in Section IX-A. 2 are derived.

References

1. D. C. Watson and A. Bers, Quarterly Progress Report No. 111, Research Laboratory of Electronics, M. I. T., October 15, 1973, pp. 84-98.
2. V. P. Silin, Sov. Phys. – JETP 21, 1127 (1965).
3. D. W. Forslund, J. M. Kindel, and E. L. Lindman, Los Alamos Report LA-UR 73-500 (1973) (unpublished).
4. A. Bers, Notes on Lectures: Linear Waves and Instabilities, given at Ecole d'Eté de Physique Théorique, Les Houches, France, July 1972 (Gordon and Breach, New York, in press).
5. A. Bers, "Theory of Absolute and Convective Instabilities" in G. Auer and F. Cap (Eds.), Survey Lectures, International Congress, Waves and Instabilities in Plasmas, Innsbruck, Austria, April 2-7, 1973, pp. B1-B52.
6. A. Bers and D. C. Watson, Bull. Am. Phys. Soc. 18, 1336 (1973).
7. K. Nishikawa, Phys. Soc. Japan 24, 916 and 1152 (1968).